NASA Contractor Report 4514

Hypersonic Panel Flutter in a Rarefied Atmosphere

Hugo B. Resende

GRANT NGL-05-020-243
MAY 1993

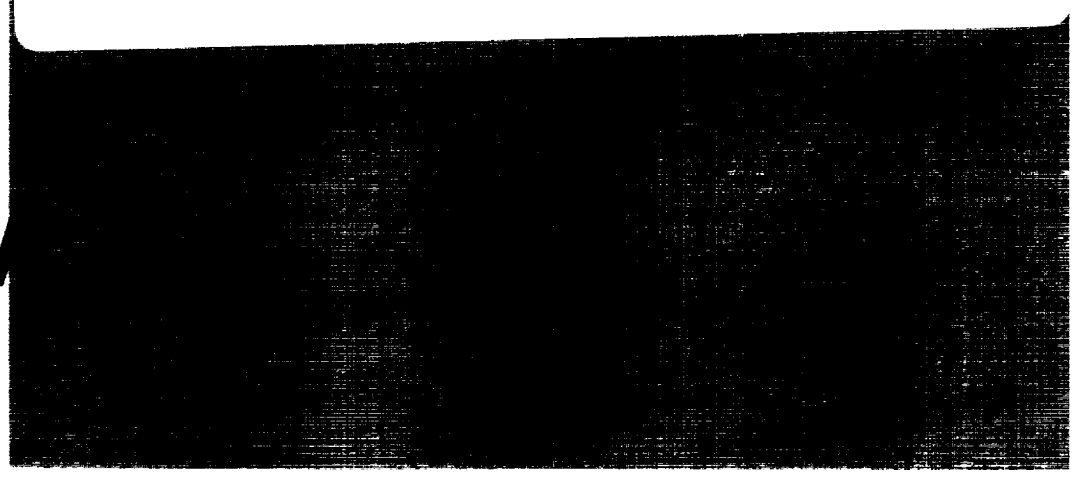

NASA

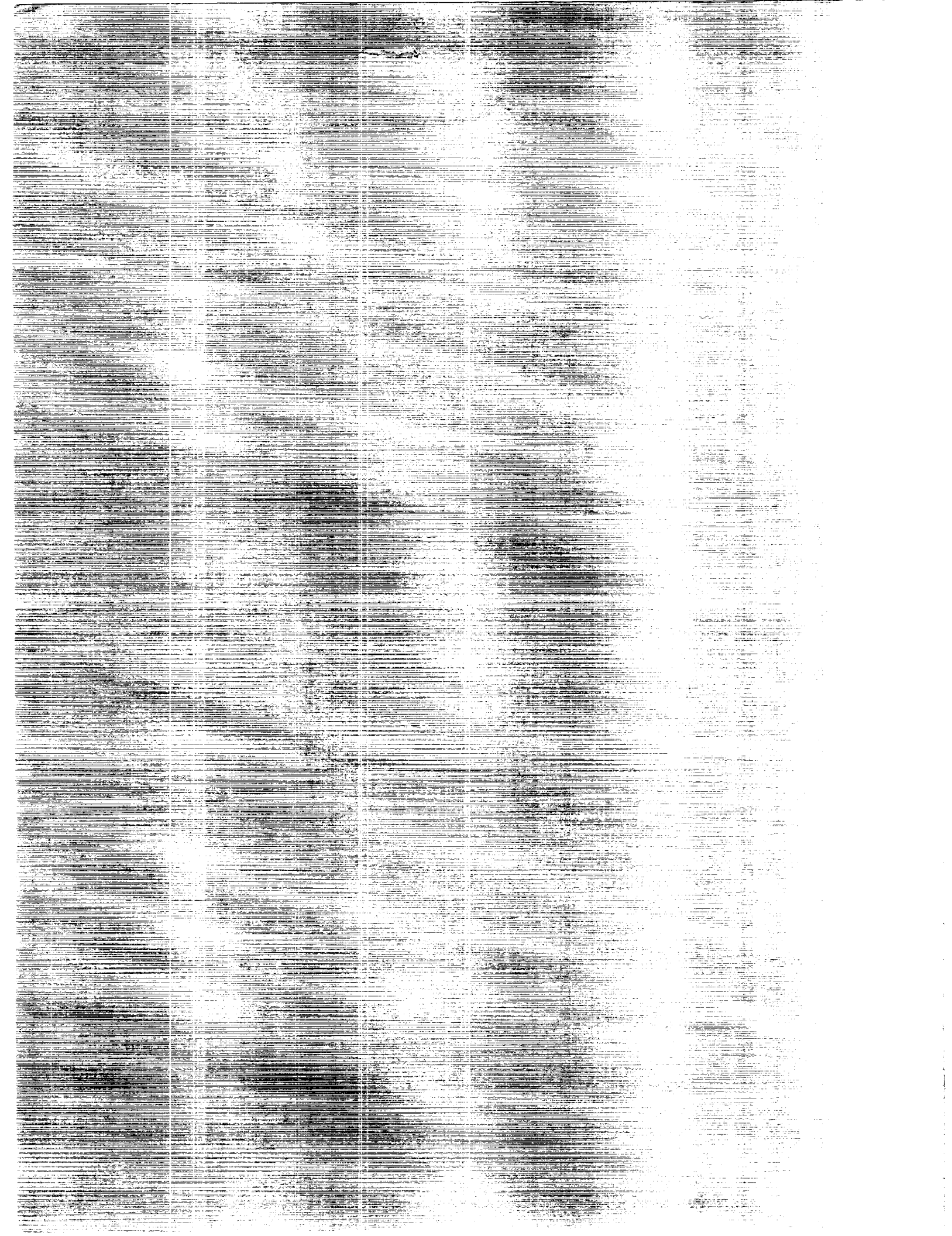

NASA Contractor Report 4514

Hypersonic Panel Flutter in a Rarefied Atmosphere

Hugo B. Resende
Stanford University
Stanford, California

Prepared for
Langley Research Center
under Grant NGL-05-020-243

National Aeronautics and
Space Administration
Office of Management
Scientific and Technical
Information Program
1993

Abstract

Panel flutter is a form of dynamic aeroelastic instability resulting from the interaction between motion of a aircraft structural panel and the aerodynamic loads exerted on that panel by air flowing past one of the faces. It differs from lifting-surface flutter in the sense that it is not usually catastrophic, the panel's motion being limited by nonlinear membrane stresses produced by the transverse displacement. Above some critical airflow condition, the linear instability grows to a limit cycle.

The present investigation studies panel flutter in an aerodynamic regime known as "free molecule flow", wherein intermolecular collisions can be neglected and loads are caused by interactions between individual molecules and the bounding surface. After collision with the panel, molecules may be reflected specularly or reemitted in diffuse fashion. Two parameters characterize this process: the "momentum accommodation coefficient", which is the fraction of the specularly reflected molecules; and the ratio between the panel temperature and that of the free airstream. This model is relevant to the case of hypersonic flight vehicles traveling at very high altitudes and especially for panels oriented parallel to the airstream or in the vehicle's lee. Under these conditions the aerodynamic shear stress turns out to be considerably larger than the surface pressures, and shear effects must be included in the model. This is accomplished by means of distributed longitudinal and bending loads. The former can cause the panel to buckle. In the example of a simply-supported panel, it turns out that the second mode of free vibration tends to dominate the flutter solution, which is carried out by a Galerkin analysis.

Several parametric studies are presented. They include the effects of 1) temperature ratio; 2) momentum accommodation coefficient; 3) spring parameters, which are associated with how the panel is connected to adjacent structures; 4) a parameter which relates compressive end load to its value which would cause classical column buckling; 5) a parameter proportional to the pressure differential between the front and back faces; and 6) initial curvature. The research is completed by an investigation into the possibility of accounting for molecular collisions, which proves to be infeasible given the speeds of current mainframe supercomputers.

Contents

List of Tables

List of Figures

Nomenclature

a	=	panel length
$\boldsymbol{c}$	=	velocity vector
$\mathcal{A}_i$	=	coefficients of nondimensional aerodynamic loads
D	=	$E\,h^3/12\,(1-\nu^2)$ (panel stiffness)
E	=	modulus of elasticity
f	=	frequency (Hz)
f	=	$\mathrm{f}\sqrt{\rho_p\,h\,a^4/D}$ (nondimensional frequency)
f_{MAX}	=	Maxwellian distribution of thermal velocity
h	=	panel thickness
H	=	maximum height of the initially curved panel
k_i	=	spring constants
Kn	=	Knudsen number
m	=	molecule mass
m_x	=	distributed bending moment
M, N, Q	=	bending moment, axial stress force, and shear force resultants
M_∞	=	Mach number
n	=	ρ/m (number density)
N_x	=	applied inplane force
$\mathcal{N}$	=	number flux of molecules
p	=	aerodynamic pressure
p_x , p_z	=	distributed loads in the longitudinal and normal directions
P_x , P_z	=	nondimensional static loads
q	$\equiv$	$\rho_\infty U_\infty^2/2$ (dynamic pressure)

q_n	=	nth generalized coordinate
R	=	gas constant
R_x	$\equiv$	$N_x\, a^2/D$ (compression parameter)
s	$\equiv$	$\sqrt{\gamma/2}\, M_\infty$ (molecular speed ratio)
t	=	time
T	=	temperature
$\mathcal{T}$	$\equiv$	$t\sqrt{D/\rho_p\, h\, a^4}$ (nondimensional time)
th	$\equiv$	h/a (thickness ratio)
u	=	panel longitudinal deflection
U_∞	=	undisturbed flow speed
w	=	panel transverse deflection
w_0	=	initial undeformed shape of the panel midplane surface
W	$\equiv$	w/h
W_n	=	nth nondimensional mode shape
x, z	=	longitudinal and normal coordinates fixed to the undeformed panel
α	=	coefficient of thermal expansion
α_{k_i}	=	$k_i\, a/(k_i\, a + E\, h)$ (spring parameters)
α_k	=	$\alpha_{k_1}\, \alpha_{k_2}/(\alpha_{k_1} + \alpha_{k_2} - \alpha_{k_1}\, \alpha_{k_2})$
α_m	=	momentum accommodation coefficient
β	$\equiv$	$1/2\, RT$
γ	=	ratio of specific heats
Γ_0	=	nondimensional initial curvature of the panel
ε	=	panel midplane strain change
ζ	=	damping ratio
Θ	$\equiv$	T_p/T_∞ (temperature ratio)
κ	=	curvature change of the panel midplane surface
λ	$\equiv$	$2\, q\, a^3/M_\infty\, D$ (dynamic pressure parameter)
λ_Θ , λ^*_Θ	=	normalized parameters: equations (87)
μ	$\equiv$	$\rho_\infty\, a/\rho_p\, h$ (mass ratio)
ν	=	Poisson's ratio
ξ	$\equiv$	x/a

ρ	=	density
τ	=	aerodynamic shear stress
ω	=	frequency

Subscripts

cr	=	critical
i	=	incident property
p	=	panel
peak	=	peak deflection at the position $\xi = 0.75$ of a given limit cycle
r	=	reflected or reemitted property
∞	=	undisturbed flow

Superscripts, etc.

A	=	aerodynamic load
stat	=	static load
$\overline{(\cdot)}$	=	nondimensional aerodynamic load
$(\cdot)_{,}$	=	differentiation with respect to the variable that follows the comma

Chapter 1

INTRODUCTION

The panel flutter phenomenon is a form of dynamic instability resulting from the interaction of the motion of a panel with the aerodynamic loads generated by this motion. It differs from classical flutter in the sense that it is not usually catastrophic, the motion of the panel being limited by a nonlinear membrane stress induced by the transverse displacement. In general the flutter motion corresponds to a limit cycle, which is not necessarily simple harmonic. This subject was intensely studied during the 60's and 70's, and there are several works published in the area. The definitive reference seems to be the 1975 monograph by Dowell [1], while a more recent survey by Reed, Hanson and Alford [2] addresses the requirements directly related to the National Aerospace Plane. Several other comprehensive historical surveys of the liturature are available [3]-[9], including Reference [9] which treats the applications of the methods and results in design practice.

From a historical point of view, the first mention of panel flutter appears to be related with failures that had occurred on the German V2 missile during World War II [10]. The problem was initially regarded as an interesting but not fundamentally different aspect of the general field of aeroelasticity. However, the use of the standard methods for aeroelastic analysis (mainly linear methods at the time) usually resulted in substantial disagreement between theoretical and experimental data. This led to many studies, which disclosed that one of the main difficulties was associated with the rather inaccurate techniques and uncontrolled test conditions

(by present standards) of early experiments. On the other hand, from the theoretical point of view, for some time it was not clear if the fluttering motion should be modeled by "standing" waves or "traveling" waves. This may all have started from the experience that flags, as well as skin panels made of thin paper, flutter at quite low speeds and the motion resembles traveling waves[10].

These early difficulties have been overcome, and it has been demonstrated that the data from theory and experiment are in satisfactory agreement for a wide range of parameters. Among the aspects inherent to panel flutter which are not adequately described by the usual linear, inviscid aeroelastic models are the structural nonlinearities. As the panel bends it also stretches thereby inducing a tension in the panel. As mentioned before, the flutter motion is a limit cycle, representing a balance between the (unstable) linear panel and airloads and that induced tension, which increases the effective panel stiffness. Viscous shear flow effects can also be of importance, one of the reasons being that the boundary layer region next to the panel can significantly modify the effective Mach number and dynamic pressure of the flow. Moreover, the shear stress itself may drastically modify the stability boundary if it is larger or comparable to the pressure, as in the case of hypersonic flow in a rarefied atmosphere.

1.1 Physical Nature of the Problem

There are several types of aeroelastic instabilities which may occur, and these may be classified as static ("divergence") or dynamic ("flutter") instabilities. In the case of panel flutter, divergence is generally associated with subsonic flow[11], while flutter usually only happens for supersonic flows. However, it is possible for flutter to occur in the subsonic regime in the case of a long panel resting on a continuous elastic foundation[12]. In fact, in this case a divergence-like instability sets in first, but it is a very mild one and the panel response only becomes significant when the airspeed approaches that for a flutter-like instability. The much larger number of experimental studies in the supersonic flow regime[13]-[19] reflects this

fact that divergence is normally of less technological importance than flutter. Finally, it is worth pointing out that for flat panels, flutter in the low supersonic flow regime often corresponds to a single-degree-of-freedom instability, while for Mach numbers approximately larger than $\sqrt{2}$ flutter results from coupling between modes ("frequency coalescence"). In the latter case it is clear that any parameter that significantly changes the panel modes and/or frequencies may have a significant effect on the stability boundaries.

To better understand the physical nature of the problem, consider a wind-tunnel experiment for a flat panel at supersonic speeds, with no applied in-plane loads. Once the flow is established at some specified Mach number, the flutter boundary is searched for by increasing the fluid dynamic pressure q (the Mach number is held at the initial value). For small values of q below the flutter boundary, random oscillations may be observed with dominant frequency components near the lower panel natural frequencies: the panel is responding to pressure fluctuations in the turbulent boundary layer, but it acts as a mechanical filter and responds primarily to those frequencies in the pressure field near the structural natural frequencies. The maximum oscillation amplitude is very small. When the flutter boundary is reached at some critical dynamic pressure, q_{cr}, the oscillation becomes essentially periodic, with the amplitude increasing with any further increase in the dynamic pressure. Actually, the experimental value of q_{cr} is more a matter of definition than a result obtained from some precise measurement. An arbitrary but reasonable convention is to define the stability boundary as a flutter band in dynamic pressure[13]. The upper limit can then be taken as the lowest value of q at which a sustained oscillation was observed with an amplitude magnification of 3 to 5 times over that observed at lower values of dynamic pressure. On the other hand, the lower limit may be assumed to correspond to the highest value of q for which no oscillations with regular frequency or with a significant increase in response occurred. The typical error in q_{cr} is of the order of 10%.

There are very few works which tried to investigate failure mechanisms, but at least two such mechanisms can be identified and have occurred in practice. The first one has to do with the stress amplitude due to flutter exceeding the yield stress of the

panel material over a major portion of the structure. In this case the failure can be catastrophic and very rapid. On the other hand, small stress levels can be associated with fatigue failure. Actually, if the stress amplitude and frequency of oscillation are known, one may use a conventional fatigue curve (stress vs. number of cycles to failure) to estimate the fatigue life for the fluttering panel [20,21]. Interesting enough, in a study by Dowell [20] it is shown that whereas a thinner panel will flutter at a lower dynamic pressure than a thicker one, it will be able to exceed its flutter dynamic pressure by a greater amount (on a percentage basis) than a thicker one for a given fatigue life. Another conclusion from the same work is that a significant reduction in panel thickness may be possible if the panel is designed for finite rather than infinite (no flutter) fatigue life. Results obtained by Xue and Mei [21] agree with this finding.

1.2 Methods of Analysis

There are very few exact solutions, as it is always the case in any area, and most of them use the method originally employed by Hedgepeth [22,23]. This method of solution is applicable to isotropic panels, as in the works by Hedgepeth, or to sandwich/orthotropic panels[6],[24]-[26]. Naturally, these analyses are valuable to compare approximate solutions against, but they apply only to the linear problem and were developed only by assuming high supersonic flows.

The most usual approximate method of analysis has been to apply Galerkin's method [27] to the governing partial differential equation(s) of motion. It is worth mentioning that the Galerkin method and the Rayleigh-Ritz method are equivalent in most cases. The main differences are that the latter method involves the stationarity of the total energy of the system, and that the so-called trial functions only need to satisfy the forced boundary conditions, i.e., those conditions directly related to the edges' displacements (deflection and slope). Also, some doubt was initially cast on the use of the Galerkin method since spurious flutter results were obtained for membrane flutter at high supersonic speeds when exact analyses showed no flutter. This problem was studied by Ellen [28], who showed that the instability is

always associated with the coalescence of the two highest eigenvalues. Since only the lower eigenvalues have been determined with any accuracy, it becomes clear that at any stage more terms must be taken to check the instability. Therefore an infinite number of modes is in fact needed. This leads to the conclusion that, although a finite value is found for q_{cr} for a given analysis, it has no meaning because of the manner in which the instability occurs.

Once Galerkin's method is applied to the equation of motion, a system of ordinary differential equations is obtained, which can be solved in several ways:

Characteristic equation: when the system of equations is linear, and in the absence of any structural damping and nonhomogeneous terms as pressurization loads, it is possible to write:[29]–[40]

$$[M]\{\ddot{q}\} + [K]\{q\} + \lambda[A]\{q\} = \{0\} \quad , \tag{1}$$

where $[M]$, $[K]$, and $[A]$ are the inertia, stiffness and aerodynamic matrices, respectively, and λ is a nondimensional parameter proportional to the dynamic pressure. Note that the aerodynamic matrix $[A]$ may depend on Mach number, as well as other parameters, depending on the aerodynamic theory being used. The generalized displacements $\{q\}$ are then assumed to be of the form $\{\phi\}\, e^{i\omega t}$, where the frequency ω is in general complex, i.e., $\omega = \omega_R + i\,\omega_I$. After this substitution, a nontrivial solution of equation (1) is obtained by setting the determinant of the resultant coefficient matrix of $\{\phi\}$ equal to zero. This yields the characteristic equation of the problem, which can be solved for ω if the parameter λ is specified. For $\lambda = 0$ the values of ω can be shown to correspond to the natural frequencies of the panel in a vacuum. Increasing λ changes the frequencies smoothly until a critical value (λ_{cr}) is reached, when two frequencies coalesce. Any further increase in λ makes these frequencies complex conjugate pairs, indicating that at least one of the modes of oscillation is unstable, and thus defining the flutter boundary. Actually, this problem can be looked upon as an eigenvalue problem and solved as such. This approach seems to be numerically more efficient than to solve the characteristic equation

itself if the total number of assumed modes is large. Finally, a traveling wave solution can be obtained in a similar way, as in the papers by Dowell [41,42].

Harmonic balance method: this method is used when the system of equations is nonlinear. It is based on the assumption that the flutter motion consists of a steady periodic vibration, the fundamental harmonic being predominant, that is, [43]–[46]

$$q_n(t) \cong a_n \sin\omega t + b_n \cos\omega t \quad . \tag{2}$$

Substituting this into the system of equations and balancing terms of the first harmonic (terms multiplying $\sin\omega t$ and $\cos\omega t$), one obtains $2N$ algebraic equations for the $2N+2$ unknowns $\{X\} = \{a_1\,,\, b_1\,,\, a_2 \ldots a_N\,,\, b_N\}^T$ plus λ and ω. It should be recalled that neither λ_{cr} nor the relation between λ and ω are known beforehand. One may replace the first two coefficients a_1 and b_1 in $\{X\}$ by λ and ω. Furthermore, since the phase angle is not important in a steady-state solution, one can set $a_1 = 0$ and b_1 equal to a certain small number, which will set the general level of the vibration amplitude corresponding to given values of λ and ω. This reduces the system the equations to a determinate form. It should be said that in the recent work by Yuen and Lau [47] the so-called incremental harmonic balance method is used, with higher harmonics being used to carry out the analyses.

The stability of the solution obtained may be studied by giving a small perturbation to the limit-cycle solution as follows:

$$q_n(t) = [a_n + \xi_n(t)] \sin\omega t + [b_n + \eta_n(t)] \cos\omega t \quad . \tag{3}$$

Substituting this into the system of equations, and then studying the behavior of $\xi_n(t)$ and $\eta_n(t)$, one can find out the stability of the limit-cycle solution. Note that both variables are small perturbed functions, so that one can neglect higher order terms and thus deal only with linear differential equations in $\xi_n(t)$ and $\eta_n(t)$.

Perturbation method: this method obviously applies to nonlinear cases, the solution being studied for values of λ in the vicinity of the linear value λ_{cr}. A very clear application of this method can be found in the work by Morino [48].

Time integration: in this case the generalized coordinates are obtained by direct numerical integration [45],[49]-[61], allowing the study of nonsimple harmonic limit cycle oscillations or even chaotic motion [59]. For a given initial disturbance, the panel motion may decrease with time (if the motion is stable in a linear sense) or may increase with time until a nonlinear but "stable" limit cycle is reached. One drawback of this approach is that if all damping is eliminated from the system the limit cycle cannot be reached. This is a result of treating the problem in the initial value formulation rather than seeking, *a priori*, sustained oscillatory solutions. With regard to convergence, presence experience suggests that at least six modes must be used. However, if in-plane or static pressure loadings induce a significantly large tension in the panel, even more modes may be required. The number of modes required for a given desired accuracy also increases if the panel aspect ratio (length/width) increases.

Another method of analysis which became very common in the last two decades corresponds to the finite element method [62], recognition of the first application usually being given to Olson [63]. The basis of this method is to divide the panel in several discrete elements, the displacement(s) at the nodal points (i.e., points where different elements touch each other) being the unknown variables. One of the biggest advantages of this method is that it can be applied to problems with practically any geometrical boundary conditions on any or all the sides of the panel once the elements are defined. In the case of Galerkin's method a different set of functions must be chosen to represent the deformations which correspond to each set of boundary conditions. One issue regarding convergence in the case of plate elements has to do with the quantities that are taken to be continuous across the interfaces between elements. If the interface compatibility conditions are exactly satisfied the element

is said to be "conforming", this being a desired property. A "non-conforming" element usually implies that normal slopes are discontinuous across the interfaces, while "hyper-conforming" elements use components of the curvature tensor as generalized coordinates. In the latter case a degree of continuity that is not required by compatibility is introduced, slowing down the convergence properties if compared to a solution using the same mesh size and the same degree of polynomial approximation but strictly conforming [69]. Additionally, hyper-conforming elements raise difficulties when elements of different thicknesses or Young moduli meet at a vertex. Two other points that concern only the nonlinear formulation are discussed by Sarma and Varadan [64]. The first one is related to the inclusion of the in-plane displacement term in the strain-displacement relation, since the order of this term is the same as the $(w_{,x})^2$ term. Here $w_{,x}$ represents the derivative of the transverse displacement with respect to a coordinate which runs along the panel. The second point is associated with the applicability of the in-plane boundary conditions at the element level and hence the evaluation of the nonlinear stretching forces. Generally speaking, the nonlinear stretching force is constant along the panel when the in-plane inertia forces are neglected, and there are no distributed in-plane loads. For a two-dimensional panel with immovable edges this force at the system level is proportional to the integral $\int_0^a (w_{,x})^2\, dx$, which is evaluated along the panel length. However, at the element level this is no longer true, since a term related to $u_{,x}$ must be considered. Neglecting to recognize these in-plane displacementes leads to the assumption that they are zero at all nodal points, and that the nonlinear stretching force varies along the panel.

In the linear case [65]-[73] the analysis is very much similar to the one used for Galerkin's method, equation (1), with the difference that the matrices $[M]$, $[K]$, and $[A]$ for the system are arrived at by assembling individual matrices for each element. Also, the generalized coordinates $\{q\}$ represent now the nodal displacement(s). The buckling phenomenon due to in-plane stresses arising from initial and/or thermal effects can be taken into account by introducing the concept of geometrical stiffness [74]. In the nonlinear case [75]-[84] the eigenvalues for a given dynamic pressure specified by λ must be determined iteratively. The most used iterative procedure is

explained in detail in the work by Mei and Rogers [85]. Briefly speaking, for a given λ the linear flutter problem is solved first, yielding a first approximation for the mode shape, $\{\phi\}_0$, which is normalized by its maximum component. Then the first approximate value for the displacement is given by $\{q\}_1 = c\,\Re(\{\phi\}_0\, e^{i\omega t})$, where c is a given amplitude of panel oscillations, and $\Re(\ )$ denotes the real part. It is thereupon possible to evaluate the nonlinear stiffness matrix, which depends on the displacement, and to use this matrix to obtain a new approximation to the mode shape, $\{\phi\}_1$, associated with the amplitude c. The iterative process is repeated until a convergence criterion is satisfied. In many cases it is most efficient and accurate to base the convergence criterion merely on displacement quantities, such as the norms defined by Bergan and Clough [86]:

1. Modified absolute norm:

$$\|\epsilon\|_1 = \frac{1}{N}\sum_{i=1}^{N}\left|\frac{\Delta r_i}{r_{i,\mathrm{ref}}}\right| ,$$

2. Modified Euclidian norm:

$$\|\epsilon\|_2 = \left[\frac{1}{N}\sum_{i=1}^{N}\left|\frac{\Delta r_i}{r_{i,\mathrm{ref}}}\right|^2\right]^{1/2} ,$$

3. Modified absolute norm:

$$\|\epsilon\|_\infty = \max_i\left|\frac{\Delta r_i}{r_{i,\mathrm{ref}}}\right| .$$

Here N is the total number of unknowns components, and Δr_i is the change in the displacement component i during a given iteration cycle. Every such component is scaled by a reference displacement quantity $r_{i,\mathrm{ref}}$, which are, in general, not equal to the corresponding total components because if r_i is close to zero, the ratio $\Delta r_i/r_i$ could be a large number even after convergence has occurred. Instead, every Δr_i is scaled by the largest displacement component of the corresponding "type" (deflections/rotations). A frequency norm, defined as the absolute value of the ratio of the change in eigenvalue during a given iteration cycle and the eigenvalue itself, may

also be useful in the convergence decision. Once the converged values for the eigenvalues are known, the problem is solved as in the linear case, that is, λ_{cr} corresponds to the lowest value of λ for which coalescence occurs (usually for $c = 0$).

Another possible method of analysis is the so-called second method of Liapunov [87]. It has proved useful in a number of stability problems involving ordinary differential equations, but the first application to a panel flutter problem involving a partial differential equation is believed to be given in the work by Parks [88]. Briefly speaking, the Liapunov method involves finding a functional V (defined in phase space) which must possess certain sign properties as prescribed by one of a number of stability and instability theorems [89], and that describes the motion of the panel when it is disturbed from its equilibrium position. For example, if V is a positive definite function and dV/dt can be shown to be a negative semidefinite function along every trajectory, then $V \to 0$ as $t \to \infty$ and the disturbed motion must die out. The fact that such a function cannot be found does not imply that the system is unstable. Indeed, the main drawback of the method is that there is no established procedure for producing a Liapunov function for any given dynamical system.

1.3 Present Application

The present application addresses the issue of the breakdown of continuum fluid mechanics when considering panel flutter in the case of hypersonic flight vehicles traveling at high altitudes, as would occur along the upper trajectory of the National Aerospace Plane. Once the atmosphere becomes very rarefied, one can expect such a breakdown, especially for surfaces parallel to the free stream or in the leeward part of the vehicle. The simplest possible way to deal with the aerodynamics in this case is to neglect the effect of collisions among molecules, which corresponds to assuming that a free-molecule flow exists. Another approach is to use some kind of "particle simulation method" to take the effect of molecules intercollisions into account. The most important drawback in the latter case is related to CPU time requirements, even on the largest supercomputers, as well as memory limitations.

As of today, such applications do not seem to be feasible, although they are possible from a conceptual point of view.

In this dissertation the free-molecule airloads are used in the study of panel flutter in the case of a two-dimensional (beam-like), simply-supported panel. The equations of motion are derived in detail in Chapter 2, allowing for the existence of distributed longitudinal loads, as well as distributed bending moments, along the panel. These kinds of loads are necessary in order to model the aerodynamic shear effects. Linear springs in the longitudinal direction at the panel's leading and trailing edges are also introduced in the structural model. Neglecting rotary and longitudinal inertias, one can reduce the problem to an integro-differential equation in terms of the transverse displacement. The problem is solved using Galerkin's method and direct numerical integration in the time domain.

Chapter 3 deals with the aerodynamic models. The first part consists of a brief summary of existing formulations in the case of continuum flow. Then the free-molecule airloads are obtained using a quasi-steady approximation. This approximation consists of assuming that the angle of attack at a given point in the panel is equal to the local slope, $w_{,x}$, plus the angle induced by the panel normal velocity, $w_{,t}/U_\infty$. It turns out that the aerodynamic shear stress, considering the hypersonic regime, is at least one order of magnitude larger than the pressure. Finally, particle simulation methods are briefly discussed.

Chapter 4 contains the presentation and discussion of numerical results, with the response of the system being analyzed for a wide range of parameters. Finally, Chapter 5 is a summary of conclusions and discussions of possible future work.

Chapter 2

STRUCTURAL MODEL

2.1 Equations of Motion

As discussed in the Introduction, the only case to be considered in this work corresponds to a two-dimensional panel (beam-like panel) with some small initial curvature. A consistent way to obtain the equations of motion in this case is provided by Steele[†], the effect of moderate rotation of the panel midplane surface being accounted for. Actually, the static version of the governing equations in the case of a flat panel are those of the von Kármán plate theory. It should be pointed out that Kirchhoff's hypothesis is assumed to be valid, implying that the effect of the transverse shear deformation is neglected. Roughly speaking, the length/thickness ratio of a isotropic panel should not be less than 15 if results with reasonable accuracy are to be obtained [91]. In the case of composite panels the previous number should read 25.

A complete derivation of the equations of motion is given in this section. Consider then a panel of length a as shown in Figure 1. The displacements from the unstressed state of the panel's midplane surface in the x and z directions are denoted by u and w, and the total transverse displacement of a given midplane surface

[†]This reference corresponds to part of the classnotes provided by Prof. Charles Steele for the course ME 241 at Stanford University, CA (*Moderate Rotation Theory for Beams and Shallow Shells*).

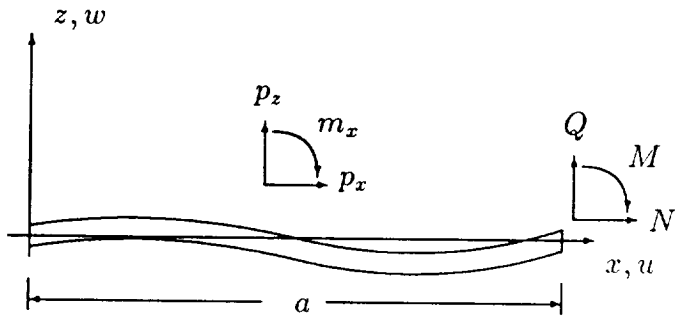

Figure 1: Two-dimensional panel with initial curvature.

point after deformation is given by

$$w_{\text{total}}(x,t) = w_0(x) + w(x,t) \quad . \tag{4}$$

In equation (4) $w_0(x)$ indicates the initial undeformed shape of the midplane surface, while $w(x)$ corresponds to the transverse displacement of the midplane surface relative to its undeformed configuration.

The strain ε of the midplane surface in the x direction is given by

$$\varepsilon = u_{,x} + w_{0,x}\, w_{,x} + \tfrac{1}{2}\, w_{,x}^2 \quad . \tag{5}$$

Note that the subscript $(\,)_{,x}$ denotes differentiation with respect to x. Also, the terms in w in the equation represent the additional stretching of the midplane surface due to moderate rotation.

When following the procedure laid down by Steele (see footnote in page 12), the internal forces in the panel's cross-section are defined as the axial stress resultant N, the bending moment M, and the shear force Q. These resultants, with sign conventions defined as in Figure 1, can be expressed as

$$\begin{aligned} N &= E\,h\,[\varepsilon - \alpha \Delta T(x)] = \\ &= E\,h\,\left[\left(u_{,x} + w_{0,x}\, w_{,x} + \tfrac{1}{2}\, w_{,x}^2\right) - \alpha \Delta T(x)\right] \quad , \end{aligned} \tag{6}$$

$$M = D\,\kappa = -D\,w_{,xx} \quad , \tag{7}$$

$$Q = M_{,x} = -(D\,w_{,xx})_{,x} \quad . \tag{8}$$

Here α is the coefficient of thermal expansion, $\Delta T(x)$ is the temperature difference

between the panel and the supports, h is the panel thickness, D is the panel stiffness, defined as

$$D \equiv \frac{Eh^3}{12(1-\nu^2)} \ ,$$

and κ is the curvature change of the midplane surface, defined by

$$\kappa \equiv -w_{,xx} \ .$$

All other symbols are defined in the Nomenclature table.

The distributed loads p_z and p_x being applied to the panel can be represented as

$$p_z = p_z^+ - p_z^- \ , \tag{9}$$

$$p_x = p_x^+ - p_x^- \ , \tag{10}$$

where the superscripts $(\ )^+$ and $(\ )^-$ correspond, respectively, to the upper and lower surfaces of the panel. It should be noted that the sign convention for $p_z^\pm$ and $p_x^\pm$ is the usual convention for stresses. Then p_z^- corresponds to the stress σ_{zz} on the lower surface and its positive direction is toward the negative z direction. With the above representation for p_x, when $p_x^+ \neq -p_x^-$ there must exist a distributed bending moment, m_x, along the midplane surface. If rotary and longitudinal inertial loads are neglected, and the panel is thin, it is reasonable to take

$$m_x = \frac{h}{2}\left(p_x^+ + p_x^-\right) \ . \tag{11}$$

Finally, the distributed loads, with the sign conventions illustrated in Figure 1, can be expressed as

$$p_z = -\rho_p h\, w_{,tt} + p_z^{\mathrm{A}}(x,t) + \Delta p_z^{\mathrm{stat}}(x) \ , \tag{12}$$

$$p_x = p_x^{\mathrm{A}}(x,t) + \Delta p_x^{\mathrm{stat}}(x) \ , \tag{13}$$

$$m_x = \frac{h}{2}\left[p_x^{\mathrm{A}}(x,t) + \Delta p_x^{\mathrm{stat}}(x)\right] \ . \tag{14}$$

The first term in equation (12) corresponds to the transverse inertial load, while the superscrit $(\ )^{\mathrm{A}}$ indicates an unsteady aerodynamic load and the superscrit $(\ )^{\mathrm{stat}}$

indicates some kind of static load. The kind of aerodynamic load that gives rise to p_x^A is a shear stress. It is assumed that there is no shear stress in the lower surface of the panel in order to write m_x as in equation (14). This last assumption corresponds to the panel being exposed to airflow in its upper surface, and the cavity behind it being filled with fluid at rest.

The equations of motion, as well as the appropriate boundary conditions, can now be obtained from Hamilton's principle:

$$\int_0^a (N\delta\varepsilon + M\delta\kappa)\, dx - \int_0^a (p_x\delta u - p_z\delta w + m_x\delta w_{,x})\, dx + \\ + k_1\, u(0,t)\,\delta u(0,t) + k_2\, u(a,t)\,\delta u(a,t) + \\ - (N^*\delta u + Q^*\delta w - M^*\delta w_{,x})\Big|_0^a = 0 \ . \qquad (15)$$

Here N^*, Q^*, and M^* are the end loads acting at $x = 0$ or $x = a$, while k_1 and k_2 are the spring constants of longitudinal springs attached at the panel ends [the subscript $(\cdot)_1$ corresponds to $x = 0$, with $(\cdot)_2$ corresponding to $x = a$]. It should be emphasized that the first integral term in (15) corresponds to the variation of the strain energy of the panel, while the second integral term is associated with the work done by the external distributed loads. The potential energy of the longitudinal springs is taken into account by the terms in the second line of (15). Finally, the work done by the end loads is associated with the terms in the third line of equation (15).

Using the appropriate expressions for ε and κ, and integrating by parts, one can write the variation terms in the integral portions of equation (15) only in terms of δu and δw. These steps give rise to the following equations of motion:

$$N_{,x} + p_x = 0 \ , \qquad (16)$$

$$M_{,xx} + [N(w_0 + w)_{,x}]_{,x} + p_z + m_{x,x} = 0 \ . \qquad (17)$$

Equations (16) and (17) can be seen to correspond to equations (1-54) and (1-56) of Reference [91], pp. 17, if these are conveniently reduced for the case of cylindrical bending of a flat panel. It is worth mentioning that the equations in the latter case were derived from the nonlinear theory of three-dimensional elasticity, with

the basic assumptions that: (1) linear strains and the squares of angles of rotation are small compared to unity; (2) the rotation about the normal axis to the panel can be neglected in the calculation of strains and stresses; (3) Kirchhoff's hypothesis is valid; and (4) the material is linearly elastic. The appropriate boundary conditions at $x = 0$ or $x = a$ are

$$N = N^* \pm k_i u \qquad \text{or} \qquad u = u^* \tag{18}$$

$$M = M^* \qquad \text{or} \qquad w_{,x} = w^*_{,x} \tag{19}$$

$$M_{,x} + N(w_0 + w)_{,x} + m_x = Q^* \qquad \text{or} \qquad w = w^* \tag{20}$$

The upper sign in front of the ku term in the forced boundary condition (18) corresponds to $x = 0$, while the lower sign to $x = a$.

From equations (16) and (17) it is clearly seen that the resultant force N must be written in terms of w in order to render the equation of motion in the transverse direction complete in itself. By assuming that the distributed load p_x is known, equation (16) can be integrated with respect to x from a generic value x to $x = a$, yielding

$$N(x,t) = N(a,t) + \int_x^a p_x(\eta,t)\,d\eta \ . \tag{21}$$

Also, recall that at the boundaries

$$N = N^* \pm k_i u \ . \tag{18b}$$

Then, if x is taken equal to zero in equation (21), one can obtain a relation between $u(0,t)$ and $u(a,t)$:

$$u(0,t) = \frac{1}{k_1}\left[N^*|_{x=a} - N^*|_{x=0} + \int_0^a p_x(x,t)\,dx - k_2 u(a,t)\right] \ . \tag{22}$$

The next step is to integrate equation (6) from $x = 0$ to $x = a$. It is going to be assumed that the panel is uniform, and $w(0,t) = w(a,t) = 0$. Using the previous

results for $N(x,t)$ and $u(0,t)$ gives

$$N(a,t) = \alpha_k \frac{Eh}{2a} \int_0^a w_{,x}^2 \, dx - \alpha_k \frac{Eh}{a} \int_0^a w \, w_{0,xx} \, dx + \\ - \frac{\alpha_k}{a} \int_0^a \int_x^a p_x(\eta,t) \, d\eta \, dx + \\ + \alpha_k \frac{\alpha_{k_1} - 1}{\alpha_{k_1}} \int_0^a p_x(x,t) \, dx + N_x \ . \tag{23}$$

Here

$$\alpha_{k_1} = \frac{k_1 a}{k_1 a + Eh} \ , \tag{24}$$

$$\alpha_{k_2} = \frac{k_2 a}{k_2 a + Eh} \ , \tag{25}$$

$$\alpha_k = \frac{\alpha_{k_1} \, \alpha_{k_2}}{\alpha_{k_1} + \alpha_{k_2} - \alpha_{k_1} \, \alpha_{k_2}} \ , \tag{26}$$

$$N_x = (1 - \frac{\alpha_k}{\alpha_{k_1}}) \ N^*|_{x=a} - \alpha_k \frac{\alpha_{k_1} - 1}{\alpha_{k_1}} \ N^*|_{x=0} + \\ - \alpha_k \frac{Eh}{a} \alpha \int_0^a \Delta T(x) \, dx \ . \tag{27}$$

Note that $u(0,t) = 0$ is achieved if $\alpha_{k_1} = 1$, that is, $k_1 = \infty$. In this case $\alpha_k = \alpha_{k_2}$. Similarly, $\alpha_{k_2} = 1$ leads to $u(a,t) = 0$ and $\alpha_k = \alpha_{k_1}$. From the definition of N_x, which corresponds to the net applied force at the panel's ends, one can clearly see the influence of different temperature distributions along the panel, $\Delta T(x)$. Given two temperature distributions $\Delta T_1(x)$ and $\Delta T_2(x)$, the effect on the panel response is identical if

$$\int_0^a \Delta T_1(x) \, dx = \int_0^a \Delta T_2(x) \, dx \ .$$

This fact has been previously mentioned in the work by Xue and Mei [21], where the finite element method was used.

The equation of motion in the transverse direction is found to read

$$D w_{,xxxx} + p_x \, (w_0 + w)_{,x} - \left[N(a,t) + \int_x^a p_x(\eta,t) \, d\eta \right] (w_0 + w)_{,xx} + \\ + \rho_p \, h \, w_{,tt} - p_z^{\mathrm{A}} - m_{x,x} = \Delta p_z^{\mathrm{stat}} \ . \tag{28}$$

It is easily seen that, when $p_x \equiv 0$, as well as $w_0(x) \equiv 0$, equation (28) reduces to the form used in classical panel flutter [49]. In this case it is worth emphasizing that the resultant force N is constant along the panel at any given time, contrary to the present case.

One may now assume that both Δp_x^{stat} and Δp_z^{stat} are constant along the panel. If only a flat panel is to be considered, i.e., $w_0(x) \equiv 0$, equation (28) becomes

$$
\begin{aligned}
& D w_{,xxxx} + \rho_p h\, w_{,tt} + \left[p_x^{\text{A}}(x,t) + \Delta p_x^{\text{stat}}\right] w_{,x} - p_z^{\text{A}} - \frac{h}{2}(p_x^{\text{A}})_{,x} + \\
& - \left\{ \alpha_k \frac{Eh}{2a} \int_0^a w_{,x}^2\, dx + \left[\left(1 - \frac{\alpha_k}{\alpha_{k_1}} + \frac{\alpha_k}{2}\right) a - x \right] \Delta p_x^{\text{stat}} + \right. \\
& \quad - \frac{\alpha_k}{a} \int_0^a \int_x^a p_x^{\text{A}}(\eta,t)\, d\eta\, dx + \alpha_k \frac{\alpha_{k_1} - 1}{\alpha_{k_1}} \int_0^a p_x^{\text{A}}(x,t)\, dx + \\
& \quad \left. + \int_x^a p_x^{\text{A}}(\eta,t)\, d\eta + N_x \right\} w_{,xx} = \Delta p_z^{\text{stat}} \, .
\end{aligned}
\tag{29}
$$

The variables in equation (29) are made nondimensional as follows:

$$
\xi = \frac{x}{a} \, , \qquad W = \frac{w}{h} \, ,
$$
$$
\mathcal{T} = t \sqrt{\frac{D}{\rho_p h a^4}} \, . \tag{30}
$$

The result reads

$$
\begin{aligned}
& W_{,\xi\xi\xi\xi} + W_{,\mathcal{T}\mathcal{T}} + \left[\overline{p}_x^{\text{A}}(\xi,\mathcal{T}) + P_x\right] W_{,\xi} - \overline{p}_z^{\text{A}} - \frac{1}{2}(\overline{p}_x^{\text{A}})_{,\xi} + \\
& - \left[6\alpha_k (1-\nu^2) \int_0^1 W_{,\eta}^2\, d\eta + \left(1 - \frac{\alpha_k}{\alpha_{k_1}} + \frac{\alpha_k}{2} - \xi\right) P_x + \right. \\
& \quad - \alpha_k \int_0^1 \int_\xi^1 \overline{p}_x^{\text{A}}(\eta,\mathcal{T})\, d\eta\, d\xi + \alpha_k \frac{\alpha_{k_1} - 1}{\alpha_{k_1}} \int_0^1 \overline{p}_x^{\text{A}}(\eta,\mathcal{T})\, d\eta + \\
& \quad \left. + \int_\xi^1 \overline{p}_x^{\text{A}}(\eta,\mathcal{T})\, d\eta + R_x \right] W_{,\xi\xi} = P_z \, .
\end{aligned}
\tag{31}
$$

The following definitions were also used in equation (31):

$$\begin{aligned} \overline{p}_x^{\mathrm{A}} &= \frac{a^3}{D}\, p_x^{\mathrm{A}} , \qquad P_x = \frac{a^3}{D}\, \Delta p_x^{\mathrm{stat}} , \\ \overline{p}_z^{\mathrm{A}} &= \frac{a^4}{hD}\, p_z^{\mathrm{A}} , \qquad P_z = \frac{a^4}{hD}\, \Delta p_z^{\mathrm{stat}} , \\ R_x &= \frac{a^2}{D}\, N_x . \end{aligned} \tag{32}$$

2.2 Initial Curvature or Imperfections

A quick look at equation (28) may suggest that only the explicit terms in w_0 have to be included in equation (29) in order to obtain the equation of motion which takes into account the effects of initial curvature. However, a more careful examination shows that the inherent geometric curvature of the panel also induces steady aerodynamic loads, which should be included into $\Delta p^{\mathrm{stat}}(x)$. If the aerodynamic loads are assumed to be of the form

$$\overline{p}_z^{\mathrm{A}}(\xi, \mathcal{T}) = \mathcal{A}_1\, W_{,\xi} + \mathcal{A}_2\, W_{,\mathcal{T}} , \tag{33}$$

$$\overline{p}_x^{\mathrm{A}}(\xi, \mathcal{T}) = \mathcal{A}_3\, W_{,\xi} + \mathcal{A}_4\, W_{,\mathcal{T}} , \tag{34}$$

one can write

$$\Delta \overline{p}_x^{\mathrm{stat}}(\xi) = P_x + \mathcal{A}_3\, W_{0,\xi} , \tag{35}$$

$$\Delta \overline{p}_z^{\mathrm{stat}}(\xi) = P_z + \mathcal{A}_1\, W_{0,\xi} . \tag{36}$$

Note that the present definitions of P_x and P_z are similar to the earlier ones, retaining only the constant part of the Δp^{stat} load along the panel.

At least two kinds of initial curvature may be of interest:

1. Constant curvature panel: such a panel was studied by Dowell [52,53] in the late 60's. The initial geometry of the panel may be approximated by the parabola

$$W_0 \equiv \frac{w_0}{h} = \frac{H}{h}\left[1 - 4\left(\xi - \frac{1}{2}\right)^2\right] \ , \tag{37}$$

where H is the maximum height of the curved panel. Then the nondimensional initial curvature of the panel is just

$$\Gamma_0 \equiv -W_{0,\xi\xi} = 8\frac{H}{h} \ . \tag{38}$$

2. Panel with sinusoidal curvature: this case corresponds to take

$$W_0 \equiv \frac{w_0}{h} = \frac{H}{h}\sin p\pi\xi \ , \tag{39}$$

where H is again the maximum height of the curved panel. Then

$$\Gamma_0 \equiv -W_{0,\xi\xi} = \frac{H}{h}(p\pi)^2 \sin p\pi\xi \ . \tag{40}$$

Such a curvature may be of interest when approximating a general initial geometry using a Fourier series.

2.3 Role of Structural Damping

Since this work deals with a rarefied atmosphere, the magnitude of the aerodynamic damping terms, with coefficients $\mathcal{A}_2$ and $\mathcal{A}_4$, may be expected to be very small. This raises the question of how to include more damping, if necessary, into the equation of motion. During numerical integration such damping may be required to yield a converged solution.

Structural damping can significantly modify the panel flutter boundaries, but the modification is extremely dependent on the type of structural damping model employed. If only linear damping is considered, the work by Ellen [92] provides a useful classification of this mechanisms and its influence on the flutter boundaries.

Basically, structural damping can be introduced into the system by adding a term of the form

$$g \frac{\partial^{\jmath+1} w}{\partial t \, \partial x^{\jmath}}$$

to the equation of motion (28), where g is a structural damping coefficient. Two possible mechanisms can be classified as follows:

1. Viscous damping: in this case g is a constant. In its simplest form, $\jmath = 0$, the term is of the same type as the aerodynamic damping term in the case of linear piston theory, as well as the present rarefied formulation. This has the analytical advantage of grouping the structural and aerodynamic damping terms in a single "total" damping quantity. This type of damping is always stabilizing. However, when $\jmath > 0$ the system can be destabilized since the structural damping term may then supply energy to the system instead of dissipating it.

   If a modal solution such as Galerkin's method is used, damping may be taken to vary from mode to mode; this procedure, originally with $\jmath = 0$ terms, is equivalent, on varying g, to the insertion of an appropriate $\jmath > 0$ term with constant g. For example, in Reference [36] a two-mode solution is used to investigate the effects of structural damping with $\zeta_1/\zeta_2 = 1$ and 4. Here ζ_n is the damping ratio of the nth mode and $g = 2\zeta_n \omega_n/\omega_0$, ω_0 being a suitable reference frequency and ω_n the nth natural frequency. Note that $\zeta_1/\zeta_2 = 4$ implies $\zeta_1 \omega_1 = \zeta_2 \omega_2$, that is, $g =$ constant whence $\jmath = 0$. In this case the critical flutter parameter increases with structural damping, although this effect is almost not noticeable for small values of aerodynamic damping, g_A. On the other hand, the case $\zeta_1/\zeta_2 = 1$ can be shown to correspond to $\jmath = 2$, and the effect of increasing the structural damping is destabilizing, especially when g_A is small. Lottati [93] studied the case for $\jmath = 4$ assuming a viscoelastic type of damping, which corresponds to multipling the panel stiffness D by a factor equal to $1 + g \frac{\partial}{\partial t}$. His conclusion is that this kind of damping has a strong destabilizing effect for all values of $g \neq 0$. One point that is worth emphasizing after all this discussion is that the assumption of $\zeta_n \omega_n = \zeta_1 \omega_1$,

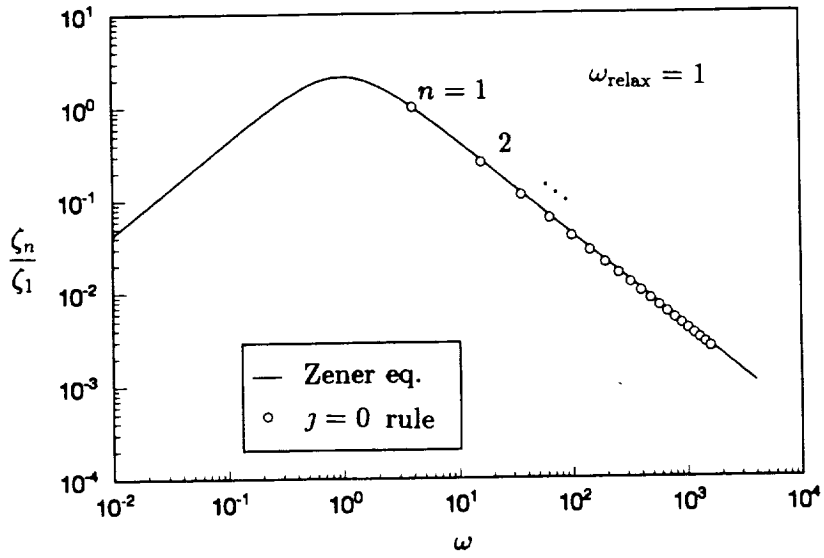

Figure 2: Correlation of predicted damping ratio for $j = 0$ with Zener equation.

corresponding to $j = 0$, yields values of ζ_n/ζ_1 that follow closely the results obtained if the "Zener equation" described in Reference [94],

$$\zeta \sim \frac{\omega/\omega_{\text{relax}}}{1 + (\omega/\omega_{\text{relax}})^2},$$

is used for values of frequency at least four times larger than the relaxation frequency ω_{relax} defined there, see Figure 2. This may be significant since the Zener equation is based on a very basic physical assumption, i.e., that the mechanism which causes energy dissipation in metals is heat flow due to strain-induced temperature gradients. Experimental data obtained for aluminum panels correlate well with the theoretical results.

2. Hysteretic damping: it can be shown that the viscous type of structural damping just discussed results in a dissipation of energy per cycle which is proportional to the frequency of oscillation. As structural hysteresis loops appear experimentally to be frequency independent, the previous damping expressions need to be modified to include this mechanism. This can be done by taking $g = \hat{g}/|\omega|$, where $\hat{g}$ is a constant parameter and $|\omega|$ is the modulus of the complex frequency of the motion, which makes this definition applicable

to nonharmonic oscillations. The drawback of this kind of formulation is that, for a real frequency of vibration, this term becomes $i\,\hat{g}\,\partial^{j}w/\partial x^{j}$ for the positive frequency spectrum, a form that is strictly valid only at neutral stability.

2.4 Galerkin's Solution

As discussed in the Introduction, one of several ways to solve the integro-differential equation (31) is to use Galerkin's method, where a expansion of the form

$$W(\xi,\mathcal{T}) = \sum_{m=1}^{\infty} q_m(\mathcal{T})\, W_m(\xi) \tag{41}$$

is adopted. Here $W_m(\xi)$ are assumed modes and only a few modes are used in practice, that is, the series is truncated. In the case of a simply supported panel it is possible to take

$$W_m(\xi) = \sin m\pi\xi \ . \tag{42}$$

By applying Galerkin's method, one converts the integro-differential equation (31) into a system of ordinary differential equations in time. The number of equations equals the number of assumed modes taken in equation (41). For the case of modes (42), the nth equation is given by

$$\begin{aligned} a_n\, q_n + \sum_r \left(a^{*}_{nr}\, q_r^2 + a^{**}_{nr}\, q_r + a^{***}_{nr}\, \dot{q}_r\right) q_n + \\ + \sum_m b_{nm}\, q_m + \sum_m \left(\sum_r b^{*}_{nmr}\, q_r + \sum_r c^{*}_{nmr}\, \dot{q}_r\right) q_m \ + \\ + \sum_m b^{**}_{nm}\, q_m^2 + c_n\, \dot{q}_n + \sum_m c_{nm}\, \dot{q}_m + \frac{1}{2}\,\ddot{q}_n = d_n \ . \end{aligned} \tag{43}$$

The definitions of the various coefficients are listed in Appendix A. Note that the introduction of viscous structural damping with $\jmath = 0$ in the present case amounts to add the term

$$\pi^2\,\zeta_1\,\dot{q}_n \tag{44}$$

to the term $c_n\,\dot{q}_n$.

Chapter 3

AERODYNAMIC MODELS

3.1 Continuum Flow

In the study of panel flutter in this regime, the aerodynamic shear loading is usually neglected compared to the aerodynamic pressure. Also, the latter may be considered as the sum of two parts: 1) one given by the pressure fluctuations on the panel in the absence of any panel motion, e.g., due to turbulent boundary layer fluctuations, and 2) the other due to the panel motion itself. Inherent to this superposition is the assumption that the panel motion and the consequent portion of the aerodynamic pressure are sufficiently small so that the turbulent pressure fluctuations themselves are not substantially modified [1]. This means that this last contribution can be taken as prescribed from experiment or separate analysis. On the other hand, the aerodynamic pressure due to the panel motion may be related to w in general by an expression of the form (two-dimensional case): [1]

$$p_z^{\mathrm{A}}(x,t) = -\rho_\infty U_\infty^2 \left\{ \frac{1}{M_\infty} \left[w_{,x} + \frac{1}{U_\infty} w_{,t} \right] + \right.$$

$$\left. + \int_0^t \int_0^a A(x-x', t-t') \left[w_{,x'} + \frac{1}{U_\infty} w_{,t'} \right] dx'\, dt' \right\} . \qquad (45)$$

Here A is an "indicial" function which depends parametrically on the freestream Mach number, $M_\infty \equiv U_\infty / a_\infty$, where a_∞ is the freestream speed of sound. Note that this term describes the effects of spatial and temporal memory, i.e., the pressure at

a particular point x, at a particular time t, is influenced by the motion at all points, $0 < x' < a$, at all previous times, $0 < t' < t$. The neglect of the memory effect leads to the so-called linear "piston theory" approximation [95,4]

$$p_z^{\mathrm{A}}(x,t) = -\frac{\rho_\infty U_\infty^2}{M_\infty}\left[w_{,x} + \frac{1}{U_\infty} w_{,t}\right] = \tag{46a}$$

$$= -\rho_\infty a_\infty \left[U_\infty w_{,x} + w_{,t}\right] . \tag{46b}$$

This result is accurate enough for large values of M_∞ (high supersonic-hypersonic regime) and can be recognized as the relation between the motion of and pressure on a piston in a tube. The total piston velocity includes both a convection term, $U_\infty w_{,x}$, as well as the direct velocity, $w_{,t}$. Here the panel is the equivalent piston and the fluid "tube" is perpendicular to the undeformed panel.

By nondimensionalizing according to expressions (30), one modifies equation (46a) into

$$\overline{p}_z^{\mathrm{A}}(\xi,\mathcal{T}) = -\lambda\left[W_{,\xi} + \sqrt{\frac{\mu}{\lambda M_\infty}}\, W_{,\mathcal{T}}\right] , \tag{47}$$

where:

$$\lambda = \frac{2qa^3}{M_\infty D} , \qquad \mu = \frac{\rho_\infty a}{\rho_p h} ,$$
$$q = \frac{1}{2}\rho_\infty U_\infty^2 . \tag{48}$$

Note that the parameter μ can be identified as a mass ratio. Also, q is the familiar dynamic pressure.

Another level of approximation can be obtained if simple harmonic motion is assumed and equation (45) is expanded as a power series in frequency, ω, that is,

$$\tilde{p}_z^{\mathrm{A}}(x,\omega) = -\frac{\rho_\infty U_\infty^2}{\sqrt{M_\infty^2 - 1}}\left[\tilde{w}_{,x} + \frac{M_\infty^2 - 2}{M_\infty^2 - 1}\frac{i\omega}{U_\infty}\tilde{w}\right] + \mathcal{O}(\omega^2) . \tag{49}$$

In the time domain this corresponds to the so-called "quasi-steady" approximation, and it is clear that it reduces to the linear piston theory result for $M_\infty \gg 1$. At low supersonic Mach number the second term between the brackets gives rise to negative damping when $M_\infty^2 < 2$, which can lead to single-degree-of-freedom flutter.

All the remarks regarding the applicability of piston theory results also apply to this approximation.

For the sake of completness, it should be noted that second-order piston theory introduces nonlinearity in the aerodynamic model by adding the term

$$-\frac{\rho_\infty U_\infty^2}{M_\infty}\left[\frac{\gamma+1}{4}M\left(w_{,x}+\frac{1}{U_\infty}w_{,t}\right)^2\right]$$

to the linear expression (46a). This nonlinearity may become important for hypersonic speeds because of the Mach number factor multiplying the term between parentheses, but Eastep and McIntosh[45] emphasize that only the terms

$$-\frac{\rho_\infty U_\infty^2}{M_\infty}\left\{\frac{\gamma+1}{4}M_\infty\left[(w_{,x})^2+\frac{2}{U_\infty}w_{,x}\,w_{,t}\right]\right\} \tag{50}$$

are relevant for parameter ranges anywhere near those found in practice. In fact, the term proportional to $(w_{,x})^2$ produces an overpressure, tending to push the panel into the cavity, for any excursion of the panel from its flat undisturbed state.

If "external" aerodynamic pressure contributions independent of the panel motion are not considered, and linear piston theory is used, the values for the $\mathcal{A}_i$ coefficients in equations (33) and (34) are

$$\begin{aligned} \mathcal{A}_1 &= -\lambda\,, \quad & \mathcal{A}_2 &= \mathcal{A}_1\sqrt{\frac{\mu}{\lambda M_\infty}}\,, \\ \mathcal{A}_3 &= 0\,, & \mathcal{A}_4 &= 0\,. \end{aligned} \tag{51}$$

3.2 Rarefied Flow

As a spacecraft or aircraft gains altitude, the air becomes increasingly less dense. At a sufficiently high altitude the atmosphere becomes so rarefied that one can expect the breakdown of the continuum hypothesis. When this happens, the discrete molecular nature of the gas surrounding the spacecraft can no longer be ignored. At this point methods from kinetic theory[96]-[98] must be used to predict the aerodynamic

behavior. It is useful to mention that the analysis of such flow fields is included in the field of rarefied gas dynamics. The available literature in this subject is very extensive, but the proceedings of the biannual series of International Symposia on Rarefied Gas Dynamics form a unique record of the field. More especifically, the recent survey by Muntz [99] is a very enlightening work.

The basic parameter for specifying the degree of rarefaction of a low-density flow is the Knudsen number, Kn, which is the ratio of the molecular mean free path of the gas to a characteristic dimension of the flowfield. Continuum flow theory is assumed to apply when this parameter is much smaller than one. On the other hand, a large Knudsen number (usually $\mathrm{Kn} \geq 1$) characterizes the so-called free molecule flow in which intermolecular collisions are neglected. The region between these limits is generally referred to as the transition flow regime.

3.2.1 Free-Molecule Regime: Quasi-Steady Approximation

The estimate of the aerodynamic loads due to the panel's motion in the free-molecule flow regime is based on the previous development made by Ashley [96]. In this study the steady values of the pressure and shear stress exerted on a surface element at an arbitrary orientation with respect to the mean flow were obtained through a general procedure. Note that only a simple gas (i.e., the gas is composed of a single chemical species) is considered. Assuming $|w_{,x}| \ll 1$, one sees that at any instant the "steady" slope of a surface element of the panel to the mean stream U_∞ is $w_{,x}$. The "quasi-steady" approximation implies that the surface element normal velocity $w_{,t}$ induces a further inclination relative to the mean flow, such that the total slope of a surface element becomes $w_{,x} + w_{,t}/U_\infty$. Inherent to the use of this approximation in the procedure described by Ashley is the assumption that enough molecules strike the surface element during an interval Δt, and that both $w_{,x}$ and $w_{,t}$ do not change *appreciably* during this time interval.

Following the development by Ashley, the normal and shear stresses are separated into those due to the incoming stream of molecules (p_i and τ_i) and those due to the reflected or reemitted stream (p_r and τ_r). The total pressure and shear stress

are then given by

$$\tau = \tau_i + \tau_r \ . \tag{52}$$

$$p = p_i + p_r \ , \tag{53}$$

The incident values can be obtained by considering first a reference frame $x'y'z'$ fixed relative to the mean motion of the gas. Then the number of molecules of class $\boldsymbol{c}'$ (i.e., molecules having velocities in the range $\boldsymbol{c}'$ to $\boldsymbol{c}' + d\boldsymbol{c}'$) per unit volume is given by[98]

$$\begin{aligned} dn &= n_\infty f_{\mathrm{MAX}}\, dc_1'\, dc_2'\, dc_3' = \\ &= n_\infty \left(\frac{\beta_\infty}{\pi}\right)^{3/2} e^{-\beta_\infty (c_1'^2 + c_2'^2 + c_3'^2)}\, dc_1'\, dc_2'\, dc_3' \ , \end{aligned} \tag{54}$$

where $n_\infty = \rho_\infty / m$ is the number density of the flow, β_∞ is defined by

$$\beta_\infty = \frac{1}{2RT_\infty} \ ,$$

m is the mass of one molecule, and R is the gas constant. Note that the Maxwellian distribution of thermal velocity, f_{MAX}, was used to characterize the velocity distribution function of the undisturbed flow.

Consider now a surface element moving with velocity components $e_1 U_\infty$, $e_2 U_\infty$, $e_3 U_\infty$ in the directions x', y', z' respectively. A new reference frame $x_s y_s z_s$ is instantaneously fixed to the surface element, parallel to the $x'y'z'$ system and such that x_s is the outward normal to the surface, as shown in Figure 3. Then any molecule has velocity components in the x_s, y_s, z_s directions given by

$$\boldsymbol{c} = \boldsymbol{c}' - \boldsymbol{e}\, U_\infty \ . \tag{55}$$

Hence the distribution of molecular velocities, which was initially given by equation (54), can be rewritten in terms of c_1, c_2, and c_3:

$$dn = n_\infty \left(\frac{\beta_\infty}{\pi}\right)^{3/2} e^{-\beta_\infty \left[(c_1 + e_1 U_\infty)^2 + (c_2 + e_2 U_\infty)^2 + (c_3 + e_3 U_\infty)^2\right]}\, dc_1\, dc_2\, dc_3 \ . \tag{56}$$

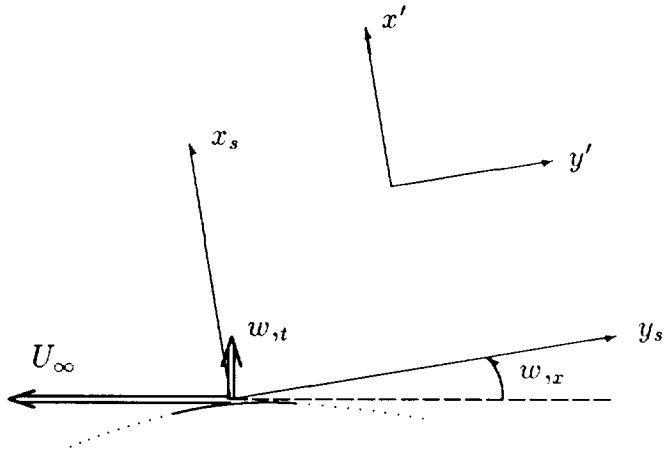

Figure 3: Reference frames for the quasi-steady approximation.

The flux of molecules of class $\boldsymbol{c}$ arriving at the surface element is given by $-c_1\,dn$ [98], that is,

$$-\,n_\infty c_1 f_{\mathrm{MAX}}\,dc_1\,dc_2\,dc_3\ . \tag{57}$$

The minus sign in the above expression is necessary because only molecules with velocities in the x_s direction in the negative range $-\infty < c_1 < 0$ can strike the surface. If this expression is integrated in each velocity range, one can find the number of molecules $\mathcal{N}_i$ striking unit area of the surface element per unit time:

$$\begin{aligned}
\mathcal{N}_i &= -n_\infty \left(\frac{\beta_\infty}{\pi}\right)^{3/2} \int_{-\infty}^{0} c_1\, e^{-\beta_\infty (c_1+e_1U_\infty)^2}\,dc_1 \times \\
&\qquad \times \int_{-\infty}^{\infty} e^{-\beta_\infty (c_2+e_2U_\infty)^2}\,dc_2 \int_{-\infty}^{\infty} e^{-\beta_\infty (c_3+e_3U_\infty)^2}\,dc_3 = \\
&= n_\infty \left\{ \frac{e^{-\beta_\infty e_1^2 U_\infty^2}}{2\sqrt{\pi\beta_\infty}} + \frac{e_1U_\infty}{2}\left[1+\mathrm{erf}\left(e_1U_\infty\sqrt{\beta_\infty}\right)\right]\right\} = \\
&= \frac{n_\infty U_\infty}{2}\,\Phi_3(e_1)\ .
\end{aligned} \tag{58}$$

In equation (58) the following functions were used:

$$\Phi_3(\varsigma) = \Phi_1(\varsigma) + \frac{\varsigma}{s}\Phi_2(\varsigma) \ , \tag{59a}$$

$$\Phi_1(\varsigma) = \frac{e^{-\varsigma^2}}{\sqrt{\pi}\, s} \ , \tag{59b}$$

$$\Phi_2(\varsigma) = 1 + \mathrm{erf}(\varsigma) \ . \tag{59c}$$

Here $\mathrm{erf}(\varsigma)$ represents the conventional error function of statistical theory, defined by

$$\mathrm{erf}(\varsigma) \equiv \frac{2}{\sqrt{\pi}} \int_0^{\varsigma} e^{-\eta^2}\, d\eta \ .$$

The parameter $s = U_\infty / c_{mp}$ is the so-called molecular speed ratio or the "Mach number" based on the most probable molecular speed, $c_{mp} = 1/\sqrt{\beta_\infty}$. It should be noted that for a perfect gas $s = \sqrt{\gamma/2}\, M_\infty$.

The forces on the surface can be found by considering first the total momentum I of the mass stream $m\mathcal{N}_i$ in some arbitrary direction specified by the direction cosines ℓ_1, ℓ_2, ℓ_3. This is found by integrating the momenta of molecules, $-(c_1\ell_1 + c_2\ell_2 + c_3\ell_3)\, c_1\, dn$, in each velocity range, yielding

$$I_{(\ell_1,\ell_2,\ell_3)} = -q \left\{ (e_1\ell_1 + e_2\ell_2 + e_3\ell_3)\,\Phi_1(e_1) + \right.$$

$$\left. + \left[\frac{\ell_1}{2s^2} + e_1 (e_1\ell_1 + e_2\ell_2 + e_3\ell_3) \right] \Phi_2(e_1) \right\} \ . \tag{60}$$

The pressure p_i is then obtained by setting $\ell_1 = -1$, $\ell_2 = \ell_3 = 0$, while the shear stress τ_i corresponds to $\ell_2 = 1$, $\ell_1 = \ell_3 = 0$.

In the case of a two-dimensional, rigid surface inclined with respect to the undisturbed flow by an angle θ, one has $e_1 = \sin\theta$, $e_2 = -\cos\theta$, and $e_3 = 0$. For the corresponding panel flutter case it is reasonable to take $|\theta| \ll 1$, such that $\sin\theta \approx \theta$ and $\cos\theta \approx 1$. The quasi-steady approximation then calls for setting $\theta = w_{,x} + w_{,t}/U_\infty$, where it is important to point out that $w_{,t}/U_\infty \ll 1$ because the flow is considered

to be hypersonic. With these results, the incident pressure and shear stress are given by

$$\tau_i = q\,\Phi_3(\epsilon) \ , \tag{61}$$

$$p_i = q\left\{\frac{\epsilon}{s}\,\Phi_3(\epsilon) + \frac{1}{2s^2}\,\Phi_2(\epsilon)\right\} \ , \tag{62}$$

where

$$\epsilon = s\left(w_{,x} + \frac{w_{,t}}{U_\infty}\right) \ .$$

Note that in the case of a steady tangent stream ($w_{,x} = w_{,t} = 0$) the previous equations reduce to

$$\tau_{i_{\text{steady}}} = \frac{q}{\sqrt{\pi}\,s} = \frac{\rho_\infty U_\infty}{2\sqrt{\pi\beta_\infty}} \ , \tag{63}$$

$$p_{i_{\text{steady}}} = \frac{q}{2s^2} = \frac{\rho_\infty}{4\beta_\infty} \ . \tag{64}$$

Before turning to the problem of finding the reemitted pressure and shear stress, it is important to comment on the gas-surface boundary conditions. Despite a great deal of theoretical and experimental study on this subject [100,103], there is still no general consensus about what kind of model should be used when treating gas-surface interactions. The two most simple models are those of specular and diffuse reflection [104].

The specular model assumes perfectly elastic collisions between molecules and the surface, that is, the molecular velocity component normal to the surface is reversed, while that parallel to the surface remains unchanged. Thus

$$\tau_{r\,\text{spec}} = -\tau_i \ , \tag{65}$$

$$p_{r\,\text{spec}} = p_i \ . \tag{66}$$

This is a useful model for analytical studies but it is not physically meaningful in real gas-surface interactions.

In diffuse reflection the velocity of each molecule after reflection is independent of its incident velocity. In fact, it is assumed that the molecules are brought to rest relative to the surface and then reemitted with the equilibrium distribution corresponding to a temperature T_r, which may differ from the temperature T_p of the surface. Thus the values of τ_r and p_r correspond to expressions (63) and (64) applied for a stationary gas at temperature T_r, that is,

$$\tau_{r_{\text{diff}}} = 0 \ , \tag{67}$$

$$p_{r_{\text{diff}}} = \frac{\rho_r}{4\beta_r} = \frac{n_r m}{4\beta_r} \ . \tag{68}$$

In the absence of adsorption or emission effects at the surface, the incident number flux of molecules $\mathcal{N}_i$ to a surface element must be balanced by the reflected number flux $\mathcal{N}_r$. Therefore, using equation (58),

$$\frac{n_\infty U_\infty}{2} \Phi_3(\epsilon) = \frac{n_r}{2\sqrt{\pi\,\beta_r}}$$

$$\Rightarrow \quad p_{r_{\text{diff}}} = \frac{\rho_\infty R\, s}{2} \sqrt{\pi T_\infty T_r}\ \Phi_3(\epsilon) \ .$$

Actually, the factor multiplying the function Φ_3 in the above expression can be reduced to a more suitable form if the definition of the speed of sound for a perfect gas is used, and the relationship between M_∞ and s is recalled. Doing this

$$p_{r_{\text{diff}}} = \sqrt{\frac{\pi}{2\gamma}}\, \frac{q}{M_\infty} \sqrt{\frac{T_r}{T_\infty}}\, \Phi_3(\epsilon) \ . \tag{69}$$

Note that in the case of a steady tangent stream the expression for $p_{r_{\text{diff}}}$ becomes

$$p_{r_{\text{steady}}} = \frac{q}{\gamma M_\infty^2} \sqrt{\frac{T_r}{T_\infty}} = \frac{\rho_\infty}{4\beta_\infty} \sqrt{\frac{T_r}{T_\infty}} \ . \tag{70}$$

The extent to which the reflected molecules have their temperature adjusted toward that of the surface may be indicated by the "energy accommodation coefficient" α_e, defined by

$$\alpha_e = \frac{\mathcal{E}_i - \mathcal{E}_r}{\mathcal{E}_i - \mathcal{E}_p} \ . \tag{71}$$

In expression (71) $\mathcal{E}_i$ and $\mathcal{E}_r$ are respectively the incident and reflected total energy fluxes, while $\mathcal{E}_p$ is the total energy flux for the case of complete diffuse reflection, i.e., $T_r = T_p$. Some experiments with engineering surfaces in contact with gases indicate that the reflection process approximates complete diffuse reflection. However, Hurlbut [102] mentions that recent measurements made in the Shuttle Orbiter, as well as the study of the decay of rotational frequency of the spin stabilized satellite Explorer VI, rule out the complete diffusive process as the predominant scattering mode of molecules interacting with surfaces. Alternative empirical reemission models have been proposed in past years. An example is the Nocilla model studied by Hurlbut and Sherman [105], as well as Pandolfi and Zavatarro [106]. The inclusion of some arbitrary fraction of specular reflection appears,however, to remain the most practical way of allowing for departures from complete diffuse reflection. This approach is going to be followed here, such that a fraction α_m of the molecules is considered to reflect specularly, while the remaining fraction $(1 - \alpha_m)$ reflects diffusively with $T_r = T_p$. Note that the coefficient α_m can be viewed as a "momentum accommodation coefficient". According to the foregoing convention, and using equations (52) and (53), the total shear stress and pressure exerted on unit area of the surface element can be written as

$$\tau = (1 - \alpha_m)\,\tau_i \ ,$$

$$p = (1 + \alpha_m)\,p_i + (1 - \alpha_m)\,p_{r_{\text{diff}}} \ .$$

With the use of equations (62), (61), and (69) the final expressions for τ and p are

$$\frac{\tau}{q} = (1 - \alpha_m)\,\Phi_3(\epsilon) \ , \tag{72}$$

$$\frac{p}{q} = \left[(1 + \alpha_m)\,\frac{\epsilon}{s} + \frac{1 - \alpha_m}{M_\infty}\sqrt{\frac{\pi}{2\gamma}\,\frac{T_p}{T_\infty}}\right]\Phi_3(\epsilon) + \frac{1 + \alpha_m}{2s^2}\,\Phi_2(\epsilon) \ . \tag{73}$$

These relations are still nonlinear in the motion $w(x,t)$, but they may be linearized if one recognizes that the parameter ϵ may be reasonably taken to be small.

Expanding the exponential and "erf" functions in Φ_1 and Φ_2, assuming that $\epsilon \ll 1$, and retaining only terms of up to first order in ϵ gives

$$\frac{\tau}{q} = \frac{1-\alpha_m}{\sqrt{\pi}\,s} + (1-\alpha_m)\left(w_{,x} + \frac{w_{,t}}{U_\infty}\right) , \tag{74}$$

$$\frac{p}{q} = \frac{1}{2s^2}\left[1 + \alpha_m + (1-\alpha_m)\sqrt{\frac{T_p}{T_\infty}}\right] + \\ + \frac{1}{2\sqrt{\pi}\,s}\left[4(1+\alpha_m) + \pi(1-\alpha_m)\sqrt{\frac{T_p}{T_\infty}}\right]\left(w_{,x} + \frac{w_{,t}}{U_\infty}\right) . \tag{75}$$

Note that both expressions have a steady part that does not depend on the panel motion, as should be expected. Also, the ratio of p/τ for both the steady and unsteady parts is of order of $1/s$. Since the regime considered is hypersonic ($M_\infty > 10$) and $M_\infty/s = \mathcal{O}(1)$, the results indicate that the pressure is much smaller than the shear stress. It must be pointed out that equations (74) and (75) correspond to equations (2.55) and (2.56) of Reference [107], pp. 43, where the parameter $\theta = 1 - \alpha_m$.

In order to find p_x^{A} and p_z^{A} it is necessary to decompose both τ and p along the x and z axes of the structural model, and take only the unsteady part. Thus,

$$p_x^{\mathrm{A}} = (1-\alpha_m)\,q\left(w_{,x} + \frac{w_{,t}}{U_\infty}\right) , \tag{76}$$

$$p_z^{\mathrm{A}} = -\frac{q}{\sqrt{\pi}\,s}\left\{\left[2(1+\alpha_m) + \frac{\pi}{2}(1-\alpha_m)\sqrt{\frac{T_p}{T_\infty}}\right]\left(w_{,x} + \frac{w_{,t}}{U_\infty}\right) + \right. \\ \left. - (1-\alpha_m)w_{,x}\right\} . \tag{77}$$

Note that the term $[(\cdots)/s^2]\,w_{,x}$ due to the contribution of the steady part of the pressure p to the load p_x^{A} has been neglected. On the other hand, the corresponding contribution of the steady part of the shear stress τ to p_z^{A} was retained because it is of the same order of magnitude as the other terms due to the unsteady part of p.

If equations (76) and (77) are nondimensionalized according to definitions (30) and (32), the final result reads

$$\overline{p}_x^{\mathrm{A}}(\xi,\mathcal{T}) = \frac{\lambda M_\infty}{2}\,\mathrm{th}\,(1-\alpha_m)\left[W_{,\xi}+\sqrt{\frac{\mu}{\lambda M_\infty}}\,W_{,\mathcal{T}}\right] , \tag{78}$$

$$\overline{p}_z^{\mathrm{A}}(\xi,\mathcal{T}) = -\frac{\lambda}{\sqrt{2\pi\gamma}}\left\{\left[2(1+\alpha_m)+\frac{\pi}{2}(1-\alpha_m)\sqrt{\Theta}\right]\left[W_{,\xi}+\sqrt{\frac{\mu}{\lambda M_\infty}}\,W_{,\mathcal{T}}\right]+ - (1-\alpha_m)W_{,\xi}\right\} , \tag{79}$$

where:

$$\mathrm{th}=\frac{h}{a} , \qquad \Theta=\frac{T_p}{T_\infty} . \tag{80}$$

Note that three more parameters are added to the problem when the effects of shear stress and rarefied flow are introduced: th, α_m, and Θ. In fact, th is inherently built into the definition of P_x if it is to be compared to P_z, and the ratio T_p/T_∞ can be taken as a variable of the system if the heat transfer problem between the plate and the flow is to be considered. In this work T_p, and consequently Θ, is assumed to be held constant.

If equations (78) and (79) are considered, the values of the $\mathcal{A}_i$ coefficients are

$$\mathcal{A}_1 = -\frac{\lambda}{\sqrt{2\gamma\pi}}\left[2(1+\alpha_m)+(1-\alpha_m)\left(\frac{\pi}{2}\sqrt{\Theta}-1\right)\right] , \tag{81}$$

$$\mathcal{A}_2 = -\frac{\lambda}{\sqrt{2\gamma\pi}}\left[2(1+\alpha_m)+\frac{\pi}{2}(1-\alpha_m)\sqrt{\Theta}\right]\sqrt{\frac{\mu}{\lambda M_\infty}} , \tag{82}$$

$$\mathcal{A}_3 = \frac{\lambda M_\infty}{2}\,\mathrm{th}\,(1-\alpha_m) , \tag{83}$$

$$\mathcal{A}_4 = \mathcal{A}_3\sqrt{\frac{\mu}{\lambda M_\infty}} . \tag{84}$$

Note that the relation $\mathcal{A}_2 = \mathcal{A}_1 \sqrt{\mu/\lambda M_\infty}$ holds if the shear stress effects are neglected, as in the case of linear piston theory. Therefore,

$$\frac{\mathcal{A}_{1\text{f-mol (no shear)}}}{\mathcal{A}_{1\text{pist}}} = \frac{1}{\sqrt{2\gamma\pi}} \left[2(1+\alpha_m) + \frac{\pi}{2}(1-\alpha_m)\sqrt{\Theta} \right] .$$

In practice $\Theta > 1$, with the result that the previous ratio becomes always larger than approximately 4, irrespective of the value of α_m. This suggests that piston theory estimates of panel stability are unconservative with respect to free molecule results when shear stress contributions are not considered. Actually, the same kind of relation between $\mathcal{A}_2$ and $\mathcal{A}_1$ is also true for the case of pure specular reflection ($\alpha_m = 1$). Again piston theory airloads are unconservative.

Finally, note that the value of P_x corresponding to the steady value of τ is given by

$$\tau_{\text{steady}} = q \frac{1-\alpha_m}{\sqrt{\pi}\, s}$$

$$\Rightarrow \qquad P_x = \frac{a^3}{D} \tau_{\text{steady}} = \lambda \frac{1-\alpha_m}{\sqrt{2\pi\gamma}} . \tag{85}$$

3.2.2 Transition Regime: Particle Simulation Methods

If intermolecular collisions are to be taken into account, there are basically two approaches: 1) try to solve the Boltzmann equation [108], which is the fundamental equation of kinetic theory if only two-body collisions are important, or 2) model the gas flow at the molecular level [104],[109]-[115].

The Boltzmann equation is written in terms of the velocity distribution function, with the independent variables being those of phase space (coordinates and velocities). One of the major difficulties in obtaining solutions for nontrivial gas flow problems in the transition regime in this case lies in the complicated structure of the so-called collision integral. One way to overcome this problem is to linearize the collision term for flows where the average speed and temperature exhibit little variations. Another approach consists of using alternative, simpler expressions for the collision integral, i.e., collision models. A somewhat different method consists

in expanding the velocity distribution function in terms of a small parameter. If this parameter is taken as the Knudsen number, such an expansion is known as the Chapman-Enkosg expansion. Both the Euler and Navier-Stokes equations of fluid mechanics can be derived in this way by retaining terms of up to zeroth and first order, respectively. The natural extension of the Chapman-Enskog theory is to carry the expansion to higher powers of Kn, which should provide formulations applicable further and further into the transition regime. The so-called Burnett equations correspond to carrying the Chapman-Enskog expansion to second-order accuracy, and there has been a major effort at Stanford University to calculate hypersonic Burnett shock solutions [116].

The alternative, as stated before, is to use some kind of particle simulation method, where the gas is modeled by some thousands or even millions of simulated molecules in a computer. The memory requirements are very large in this case since the velocity components, internal states, and position coordinates of the particles must be stored as the solution is advanced in time. On the other hand, such phenomena as dissociation and chemical reactions can be readily incorporated into the program as long as the physics of the processes can be described at the molecular level. The calculations are always unsteady, with the molecules being followed through representative collisions and boundary interactions. However, most applications up to the time of this writing have been restricted to obtaining steady state solutions as the large-time limit of the unsteady flow. One of the main reasons for this is the necessity to use some kind of averaging to obtain accurate macroscopic properties such as pressure and density. If the solution is assumed to be approaching a steady state, time averaging can be used. A cell network is necessary only in physical space, and then mainly to facilitate the sampling of properties and the choice of collision pairs. Usually the algorithms are described in such a way that the computation time is directly proportional to the number of molecules and cells in the simulated flow. This means that solutions are also very computationally intensive because of the large number of simulated particles.

The most widely used particle simulation method is the direct simulation Monte Carlo (DSMC) method, as introduced by G. A. Bird [104] in the 1960s. This method

has been constinuously advanced to the state where it is reliable, quite accurate and can handle complex problems [117]. In principle, three-dimensional problems are not conceptually different from two- or one-dimensional cases since the collisions are always treated as a three-dimensional phenomenon. However, the CPU time and memory requirements for a typical three-dimensional application may be up to two orders of magnitude larger than those for a two-dimensional problem. One of the major drawbacks of the DSMC method is that the collision algorithm employed does not allow one to make effective use of supercomputers having a vector and/or parallel architecture. This can be better realized if it is known that an efficiently vectorized code is over an order of magnitude faster on a vector machine than the same code when limited to scalar execution. Therefore, the development of a selection rule governing collisions which is compatible with parallel decomposition would greatly improve the performance of such a method. This was accomplished by Baganoff and McDonald [112], leading to the theses of McDonald [113], applicable to the Cray vector computer architecture (initially the Cray-2 and afterwards the Cray-YMP), and Dagum [114], who used a 32k processor Connection Machine.

Chapter 4

RESULTS

The general solution for the system of equations (43) in free molecule flow is obtained following the procedure described by Dowell[49]. Thus, all the parameters (λ, μ, M_∞, α_m, Θ, γ, th, P_z, R_x, α_{k_i}, the kind of curvature and H/h) are specified, with the q_n being determined as functions of time $\mathcal{T}$ by numerical integration. The numerical integrator used is an adaptive-stepsize, fifth-order Runge-Kutta algorithm[118], with monitoring of local truncation error to ensure accuracy. Actually, the code is implemented in such a way to allow the user to specify a maximum value for the time step, with a default value of 9.95×10^{-3} in terms of the nondimensional time $\mathcal{T}$. No results are going to be shown, but several studies were made regarding the maximum size of the time step. If the default value is used, the actual time step usually remains close to 8×10^{-4}. For a maximum value of the order of 10^{-5} or smaller, there is basically no change in the time step, while the final solutions remain the same. Therefore, it may be assumed that there are no mathematical instabilities associated with the numerical integration. Usually the interesting kinds of solutions which are sought are limit cycles, with the value of λ being varied for a given set of parameters until such solutions are found.

Some aspects of the problem can be discussed before any actual numerical results are shown. First, it is useful to take a closer look at the integro-differential equation (31), especially the terms involving $\overline{p}_x^{\mathrm{A}}$. Now recall that this distributed

load has a contribution proportional to $W_{,\xi}$. Then the term

$$\left(\overline{p}_x^{\mathrm{A}} + P_x\right) W_{,\xi}$$

leads to a contribution of the form $(W_{,\xi})^2$, which is similar to the one present in the second-order piston theory formulation, equation (50). As explained before, this produces an overpressure, tending to push the panel into the cavity, i.e., the limit-cycle motion may be expected to be asymmetric with respect to its maximum and minimum amplitudes. This having been said, one may conclude that the minimum amplitude (in absolute value) is going to be larger than the maximum amplitude in the case of a flat panel. As will be seen, this is not the case, most probably because of the integral terms involving $\overline{p}_x^{\mathrm{A}}$ which multiply $W_{,\xi\xi}$. As a matter of fact, these terms can be written as

$$\alpha_k \int_0^1 W(\xi,\tau)\, d\xi \; - \; W(\xi,\tau) \; + \; \text{terms involving } W_{,\tau} \quad ,$$

meaning that the total membrane stress for a given deflection does not equal the one for the same deflection with a sign change. This further indicates an asymmetry in the limit-cycle motion.

Second of all, an analysis of the contribution of the airloads to the coefficient a_n of the generic equation (43) can give some hints about the variation of the frequency of flutter (or the main harmonic of a limit-cycle solution). Looking at the definition of a_n in Appendix A, one can see that the presence of the term $\mathcal{A}_3/2 > 0$ indicates that the frequency of flutter is going to be larger than the one corresponding to the same problem when shear stress effects are neglected. If the influence of initial curvature is considered, an increase in the initial amplitude of the panel ($H/h > 0$) may be expected to lead to an increase in the main harmonic in the case of sinusoidal curvature. The behavior should be the opposite for a constant curvature (parabolic) panel.

Thirdly, suppose that the panel is fixed horizontally at both ends. It can be shown that, in the case of a uniform distributed longitudinal load like the one corresponding to P_x, half of the panel is under tension while the other half is under compression. Then a large enough load may cause the panel to buckle. When

this happens, the buckling mode shape has a considerable contribution from the second mode, in contrast to classical buckling. In the latter case the buckling mode shape corresponds to the first mode solely. It should be recalled that only a simply-supported panel is being considered here. If a six-mode representation is used $P_{x\text{buck}} = 83.16$, and the ratio between the contributions of the second and first modes to the buckling mode shape equals 0.2615.

Finally, regarding a general solution q_n, one can note from equation (43) that $-q_n$ is not a solution. This should be borne in mind when considering stable static deformation solutions, such as a buckled solution. Mathematically speaking this effect is associated with "quadratic" terms like $a^{**}_{nr}\, q_r\, q_n$ or $b^{**}_{nm}\, q^2_m$. By looking at the definition of the coefficients of equation (43) in Appendix A, it is clear that all such quadratic terms appear because of the unsteady shear stress and/or initial curvature.

4.1 Nominal Configuration

Regarding the numerical results to be presented in this chapter, the nominal configuration is specified by the following parameter values:

$$\begin{aligned} M_\infty &= 25\,, & \mu &= 2.37 \times 10^{-9}\,, \\ \Theta &= 3.5\,, & \text{th} &= 0.005\,, \\ \alpha_m &= 0\,, & \gamma &= 1.4\,, \\ \alpha_{k_1} &= 1\,, & \alpha_{k_2} &= 1\,, \\ R_x &= 0\,, & P_x &= 0\,, \\ H/h &= 0\,, & \nu &= 0.3\,. \end{aligned}$$

The environmental parameters correspond to a standard altitude of 110 km [119], while the material is taken to be Réne 41. The value of $\Theta = 3.5$ is associated with a panel temperature of approximately $840\,^\circ\text{K} \approx 1050\,^\circ\text{F}$. It is worth pointing out that these are realistic values corresponding to a point in the National Aerospace Plane (NASP) flight envelope [120,121] which approaches orbiting motion.

The first interesting observation when solving the problem is associated with the extremely small value for μ due to the low density. In this case, as mentioned in Reference [49], it is not possible to achieve a limit-cycle solution through time integration. Whatever motion is excited by the specified initial conditions, it continues "forever" in the computation [Figure 4a)]. In order to achieve a limit-cycle solution, and thus define the flutter boundary, it was decided to introduce structural damping of the viscous type into the formulation. This was accomplished by following the rule discussed in Section 2.3, in which $\zeta_n = \zeta_1 \omega_1 / \omega_n$. As may be noted by comparing Figures 4a) and 4b), this indeed introduces enough damping into the system to allow the limit cycle to be achieved. The final limit cycle amplitude has clearly not been reached at $\mathcal{T} \approx 8$, but the solution is changing toward it. The influence of the magnitude of this kind of damping on the flutter boundary is going to be discussed later.

Next, it is also interesting to analyze the shear stress effects in the panel flutter phenomenon. Figure 5 shows the bifurcation diagram (limit-cycle amplitude versus dynamic pressure) for three different free-molecule models: FM_p indicates that only the pressure is considered, FM_{us} that unsteady shear stress effects are also included, while FM corresponds to the complete free-molecule model. One point to be mentioned here is that all values of the panel deflection to be shown in this chapter are associated with the coordinate $\xi = 0.75$. This is approximately the location where the panel assumes its maximum deflection amplitude in a given cycle. It should be said that a six mode representation is being used here; further comments on the number of modes and convergence of the solution are given later in this section. It can be seen from Figure 5a) that the introduction of shear stress effects stabilizes the panel. There is not a large difference if the steady part of the shear stress is considered or not, although its inclusion slightly destabilizes the system for small values of the limit-cycle amplitude. It is not shown here, but this is not true for an incompletely-converged two-mode solution, since the curve for the FM (complete) model is significantly shifted to the right with respect to that for the FM_{us} model. Another point to emphasize is that the limit-cycle peak amplitudes are slightly asymmetric due to the unsteady longitudinal load $\overline{p}_x^{\mathrm{A}}$, as expected. This

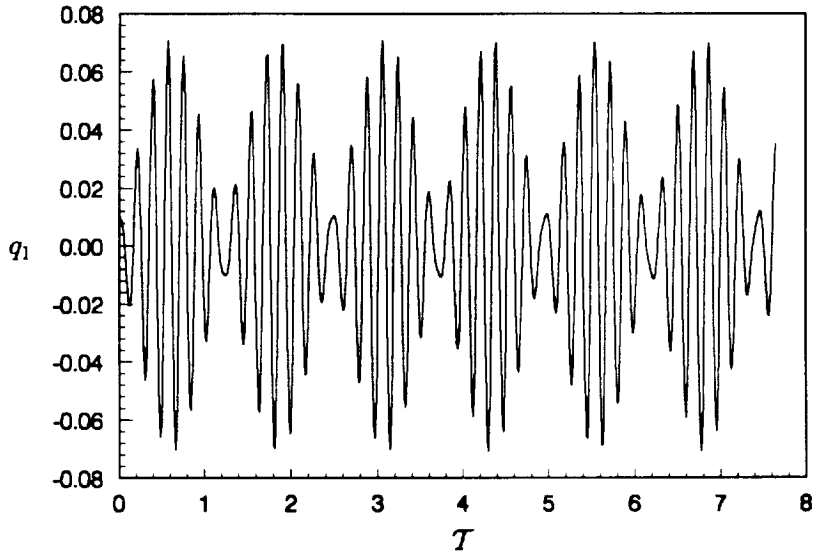

a) No structural damping.

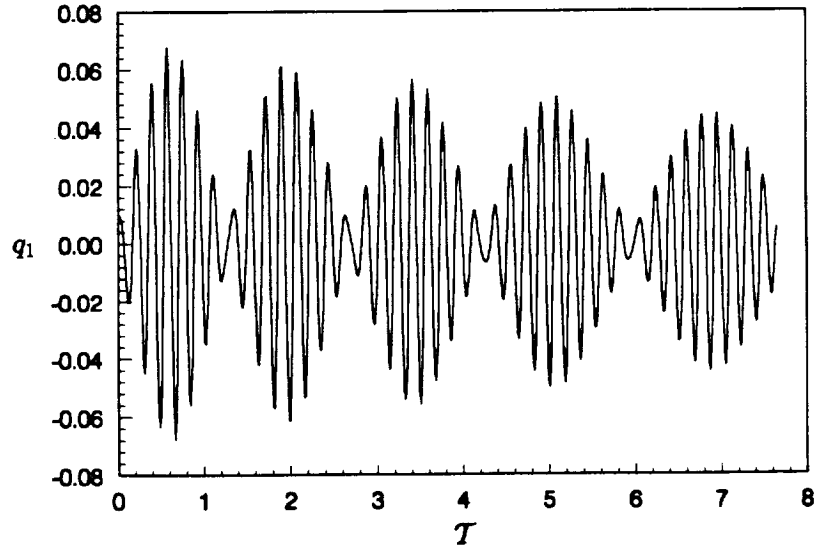

b) Structural damping included: $\zeta_1 = 0.01$.

Figure 4: Time history of the first generalized coordinate q_1: nominal configuration, six-mode solution, $\lambda = 312.3$ and $q_1(0) = 0.01$ [six mode representation, with all zero initial conditions except for $q_1(0)$].

effect becomes more noticeable as the amplitude increases. In general the negative peak (in absolute value) is smaller than the positive peak.

The variation of the limit-cycle main harmonic is shown in Figure 5b) for the different free-molecule models. Actually, all q_n are essentially simple harmonic in the present case, although this may not be true in general. It should be noted that the frequencies used are made dimensionless in the same way as time. The usual natural frequencies for the linear panel correspond to the relation $f_n = n^2 \pi/2$. As expected, the inclusion of shear stress effects causes the frequencies to increase. A curious point is that the curves corresponding to the models FM_p and FM_{us} seem to be parallel, with the steady longitudinal load causing a sharper increase in frequency as the limit-cycle amplitude increases. In dimensional terms, the values of the frequencies in Hz are given by

$$\mathrm{f} = \sqrt{\frac{D}{\rho_p\, h\, a^4}}\, f = \frac{\mathrm{th}}{a} \sqrt{\frac{E}{12\,\rho_p\,(1-\nu^2)}}\, f \quad . \tag{86}$$

For René 41 $E \approx 1.8 \times 10^{11}$ N/m^2 and $\rho_p \approx 8.2 \times 10^3$ kg/m^3, such that for the nominal configuration $\mathrm{f} \approx 7\, f/a$. Assuming a panel 60 cm long, this means that a value of $f = 6$ corresponds to a frequency of 70 Hz.

Once it is understood how the inclusion of the aerodynamic shear stress affects the phenomenon, all remaining calculations were obtained using the most realistic FM or complete free-molecule model. The natural next step consists of a convergence study, illustrated in Figure 6 through the use of a bifurcation diagram. The numbers close to the solid curves indicate the numbers of modes used in each solution. It is clearly seen that six modes will ensure converged solutions, which compare very well with solutions obtained using up to twelve modes. The linear flutter parameter λ_{cr}, corresponding to a zero limit-cycle amplitude, can be determined with a relative error of approximately 15% when using only two modes, but this error increases for a given limit-cycle amplitude. For the six-mode solution $\lambda_{cr} = 312.296$ and $f_{cr} = 5.6140$. Other examples have been carried out which further verify these conclusions.

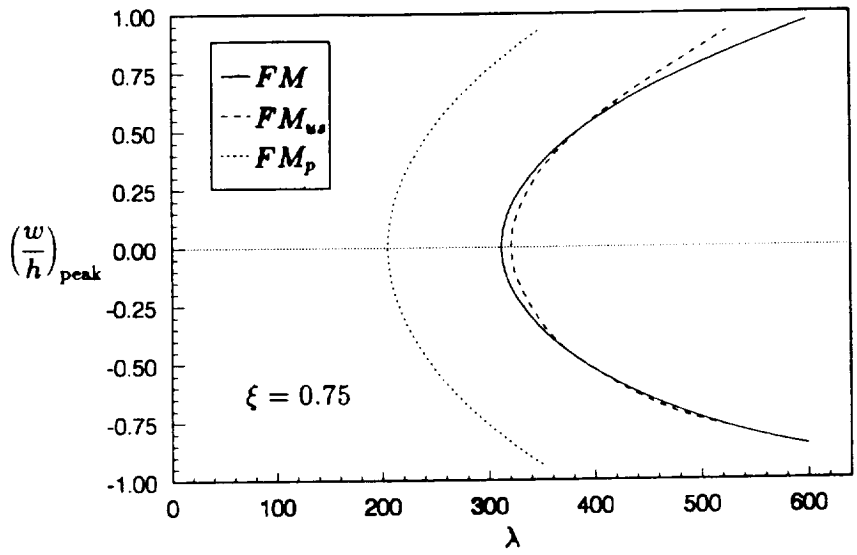

a) Limit-cycle amplitude.

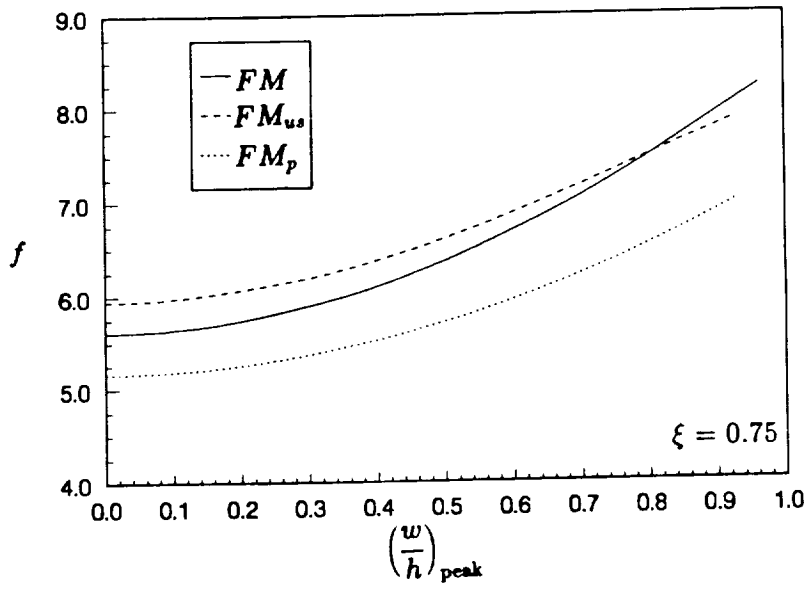

b) Limit-cycle main harmonic.

Figure 5: Variation of limit cycle characteristics for different free-molecule models: nominal configuration and six-mode solution (see text for label definitions).

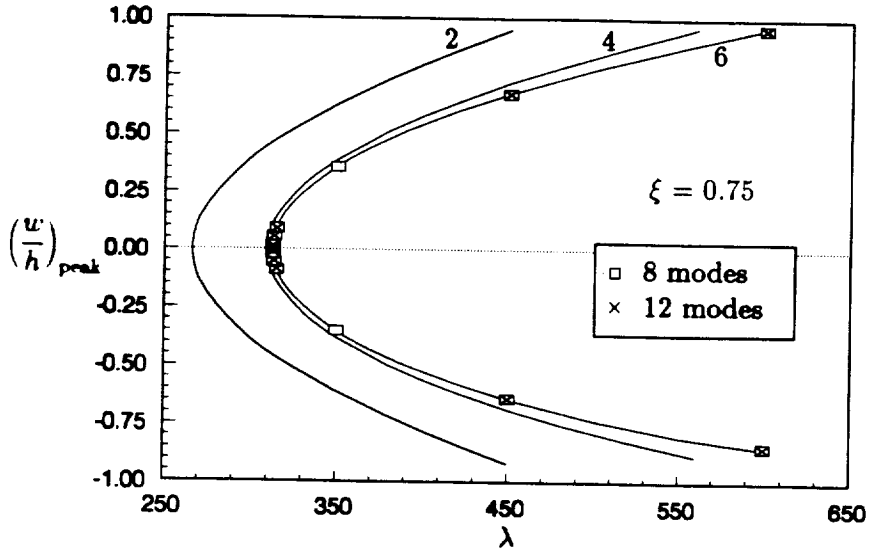

Figure 6: Bifurcation diagram: convergence study for nominal configuration.

Figure 7 shows phase portraits for the two- and six-mode solutions, respectively. The numbers close to each curve indicate the generalized coordinates. The positive peak amplitudes in both cases are similar, and one can see how the higher modes influence the results. The arrows in the figures indicate the direction of motion, as well as points corresponding to a given time instant. From this last information, it is clear that even modes are practically in phase with each other, as well as odd modes. On the other hand, even modes are essentially out of phase relative to odd ones. Finally, it is worth emphasizing the initially unexpected result that the second mode is the dominant one, instead of the first mode. This is believed to occur due to the buckling of the panel under the uniform distributed load P_x. In fact, if the value of $P_{x\text{buck}}$ given in the introduction of this chapter is used, the buckling load in the present case corresponds to a value of $\lambda \approx 247$. This means that the panel is inside the buckling region when it starts fluttering. Although it is not shown because it is physically unrealistic, a phase portrait corresponding to Figure 7 but including only unsteady shear stress effects leads to a dominant first mode. From now on, all results to be presented correspond to a six-mode solution, unless stated otherwise.

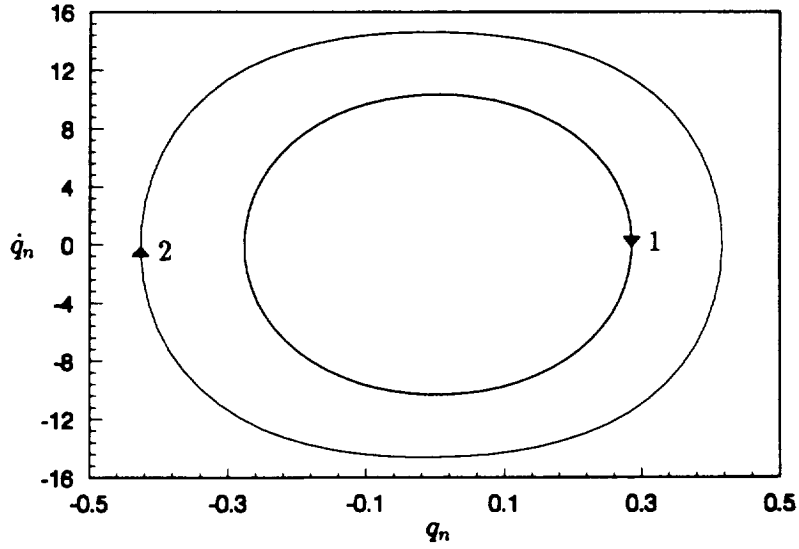

a) two-mode solution: $\lambda = 350$ and $\left(\frac{w}{h}\right)_{\text{peak}} = 0.629$.

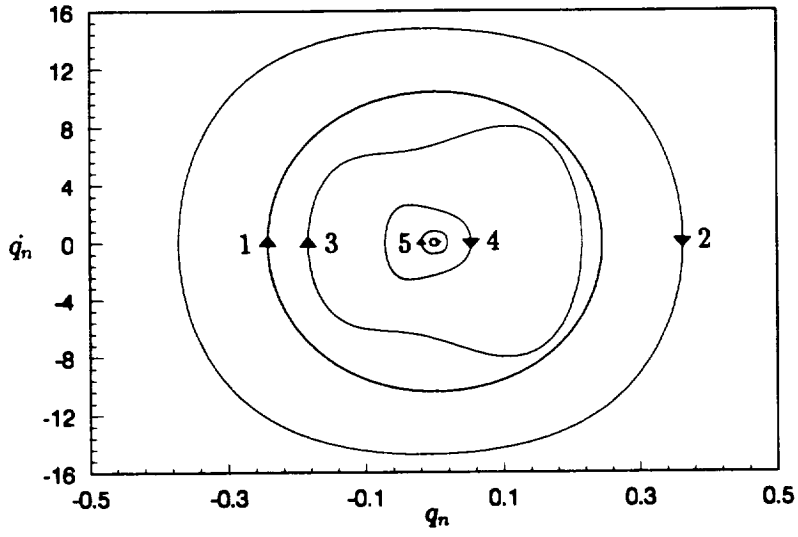

a) six-mode solution: $\lambda = 450$ and $\left(\frac{w}{h}\right)_{\text{peak}} = 0.677$.

Figure 7: Phase portrait of generalized coordinates: convergence study for nominal configuration (numbers identify the trajectories of different degrees of freedom).

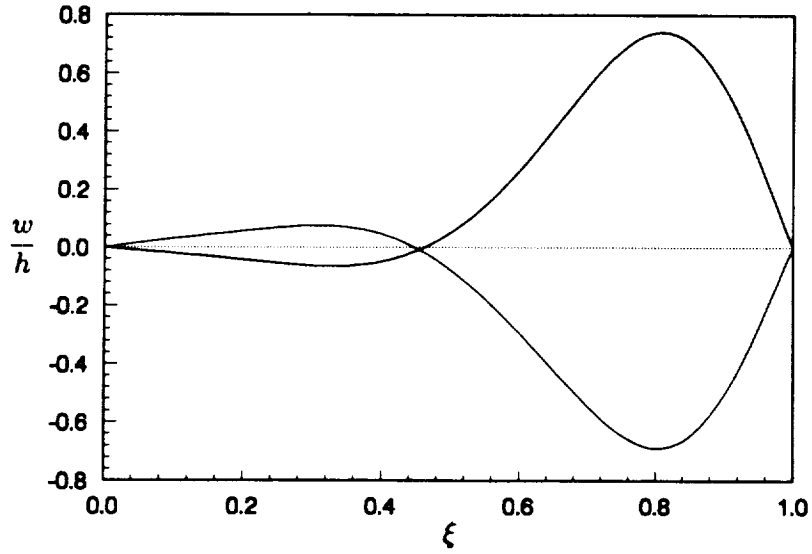

Figure 8: Panel displacement at the points in time of maximum deflections: nominal configuration, six-mode solution and $\lambda = 450$.

The panel motion is illustrated in Figure 8 at two different times for the case of Figure 7b), that is, $\lambda = 450$. The points in time correspond to the maximum deflections (positive and negative) of the limit cycle. The motion resembles classical panel flutter, Reference [49], with the distinguishing difference that the point of zero deflection is closer to the center of the panel. This is obviously due to the contribution of the second mode, which also moves the point of maximum deflection farther back ($\xi \approx 0.8$). It should be emphasized that, due to the amplitude asymmetry, the points of maximum deflection along the panel for the positive and negative peaks are slightly different.

4.2 Initial Conditions: Nonuniqueness

Before any further analysis of the phenomenon, it is necessary to say something about the dependence of the solutions on the initial conditions. If $q_1(0) \neq 0$, with all the other initial conditions set to zero, this dependency can be partially seen by analyzing the time histories for different values of $q_1(0)$, Figure 9. Note that the

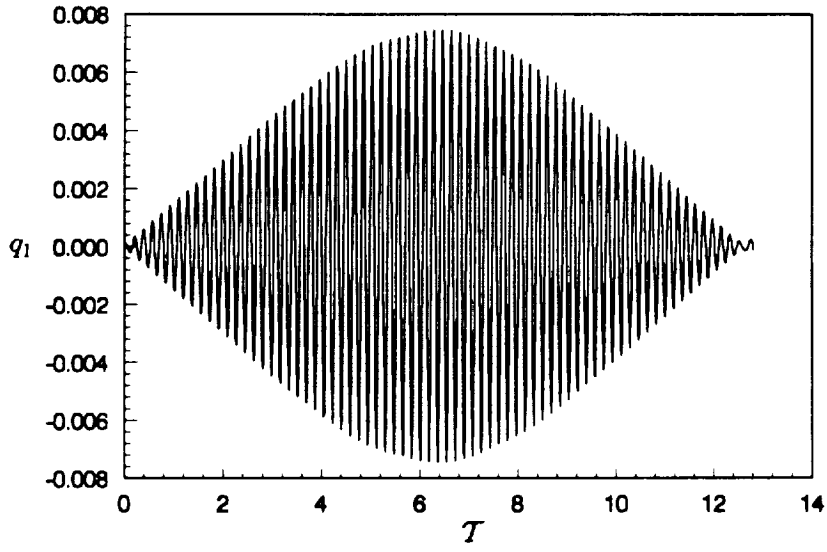

a) $q_1(0) = 0.0001$.

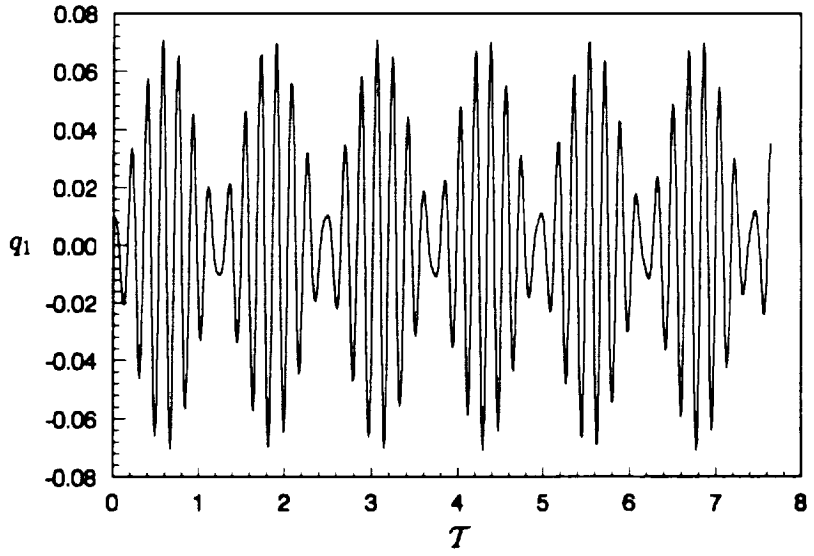

b) $q_1(0) = 0.01$.

Figure 9: Time histories of the first generalized coordinate q_1: nominal configuration, $\lambda = 312.3$ and zero structural damping.

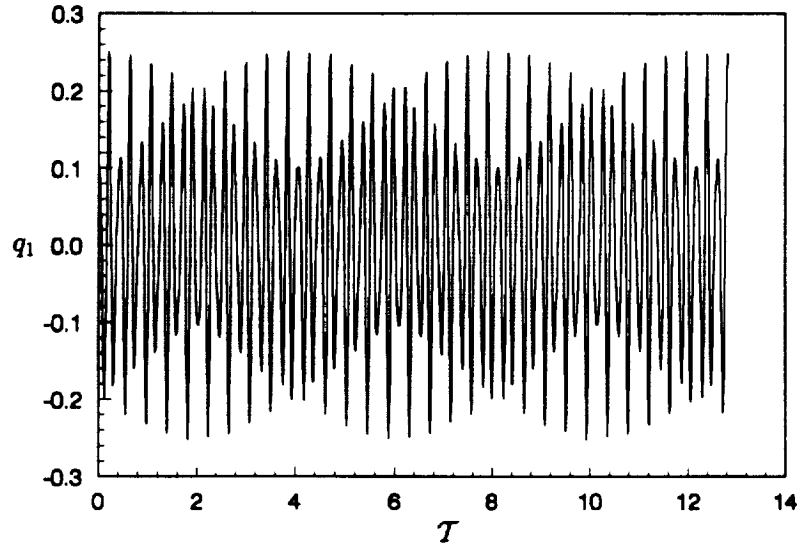

c) $q_1(0) = 0.1$.

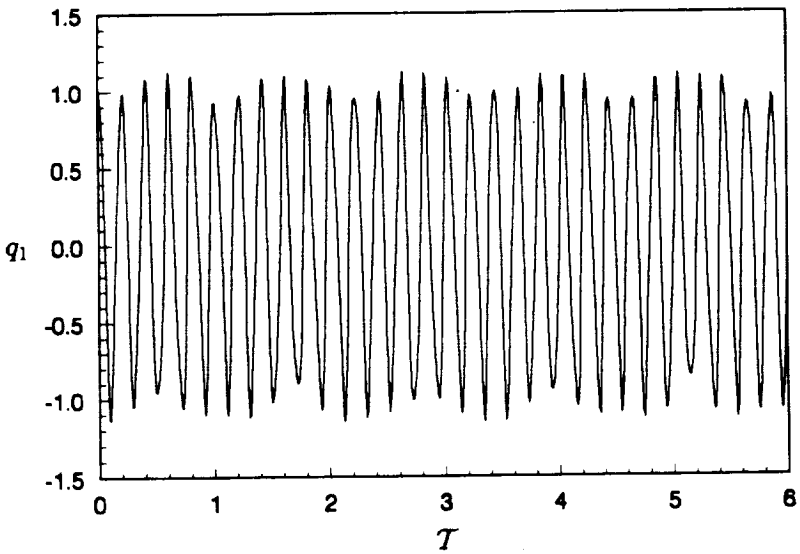

d) $q_1(0) = 1.0$.

Figure 9: (cont.) Time histories of the first generalized coordinate q_1: nominal configuration, $\lambda = 312.3$ and zero structural damping.

solutions were computed with zero structural damping in order to permit a better visualization. Also, $\lambda = 312.3$ corresponding to a value just above the linear flutter boundary. In spite of the quite different nature of the time histories, it can be seen that some kind of modulation exists, especially for the cases of $q_1(0) = 0.0001$ and 0.01. If the frequency content of these curves is analyzed, one finds that the power spectra of the generalized coordinates have very distinct peaks for two different values of frequency, which get closer together as $q_1(0)$ decreases. The first peak is generally greater than the second one, with the difference between them increasing for larger values of $q_1(0)$. Actually, for the cases of $q_1(0) = 0.0001$ and 1 there is essentially just one peak in the power spectra of q_1 if they are not plotted using a logarithm scale. For $q_1(0) = 0.0001$ this happens because the peaks are too close together, corresponding to a nondimensional frequency of 5.596 ($\Delta f = 0.098$). For $q_1(0) = 1$ the second peak is much smaller (two orders of magnitude) than the first one at $f = 4.958$. The dependency on the initial conditions is revealed even better, however, if the corresponding phase portraits are examined (Figure 10). It is important to point out that these results get much more complex as λ is further increased, with a FFT analysis of the motion showing an increasingly broad spectrum of frequencies.

The next step consists of ascertaining the influence of structural damping on the flutter boundary, as well as on the limit-cycle solutions. Regarding the latter, once structural damping is introduced in the system solutions for the various initial conditions (with the dynamic pressure parameter being hold constant), all converge to the same limit cycle, except for the case $q_1(0) = 1$. Figure 11 shows the phase portraits of the generalized coordinates for the two kinds of limit cycles obtained. The different values of λ correspond to solutions that yield approximately the same value of the maximum positive deflection at $\xi = 0.75$. Again the numbers close to the curves indicate the generalized coordinates. Solution type I corresponds to the basic solution discussed in the last section. Solution type II represents a much more complex limit cycle, with the panel attaining much larger deflections: a maximum positive deflection at $\xi = 0.75$ of 0.3100 versus 0.0024 for the other solution when $\lambda = 312.3$. Also, this second kind of solution has a frequency content richer than the

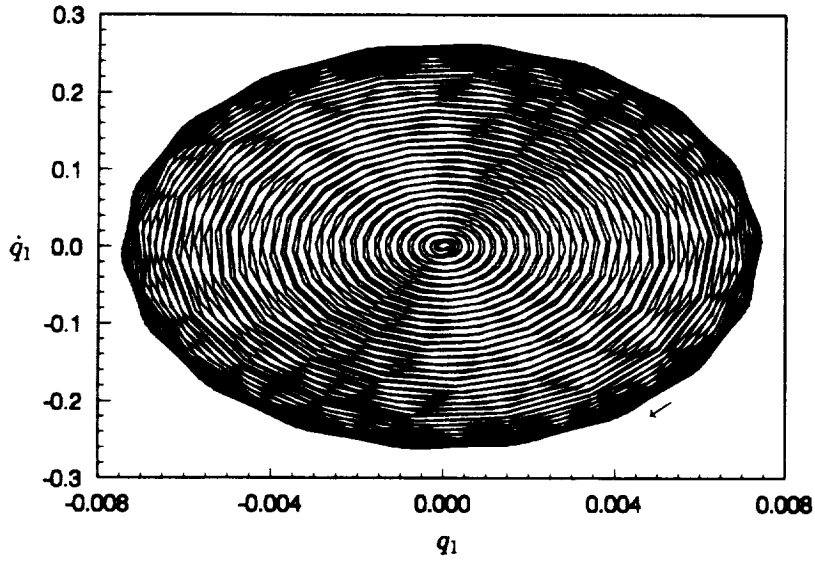

a) $q_1(0) = 0.0001$.

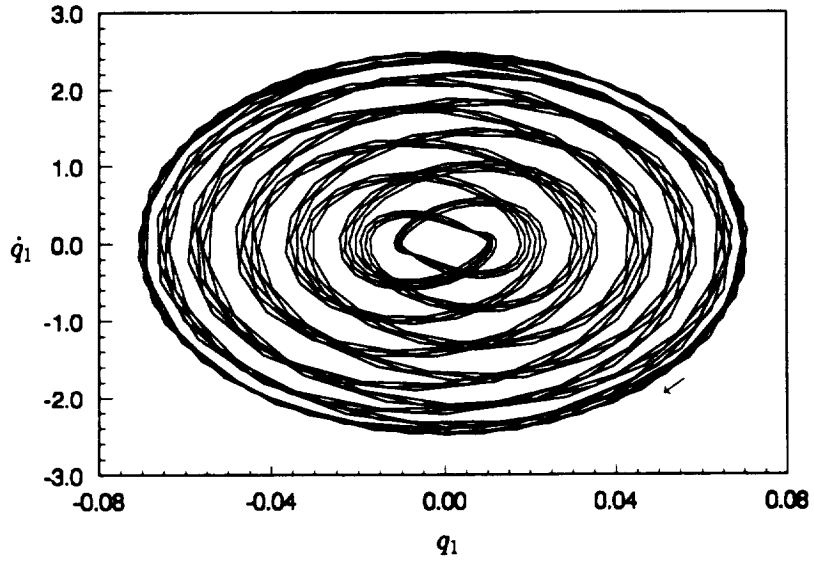

b) $q_1(0) = 0.01$.

Figure 10: Phase portraits of the first generalized coordinate q_1: nominal configuration, $\lambda = 312.3$ and zero structural damping.

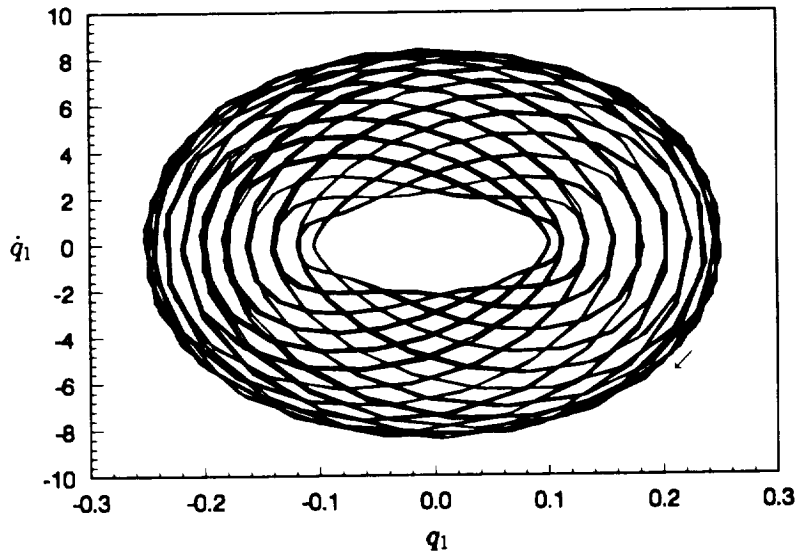

c) $q_1(0) = 0.1$.

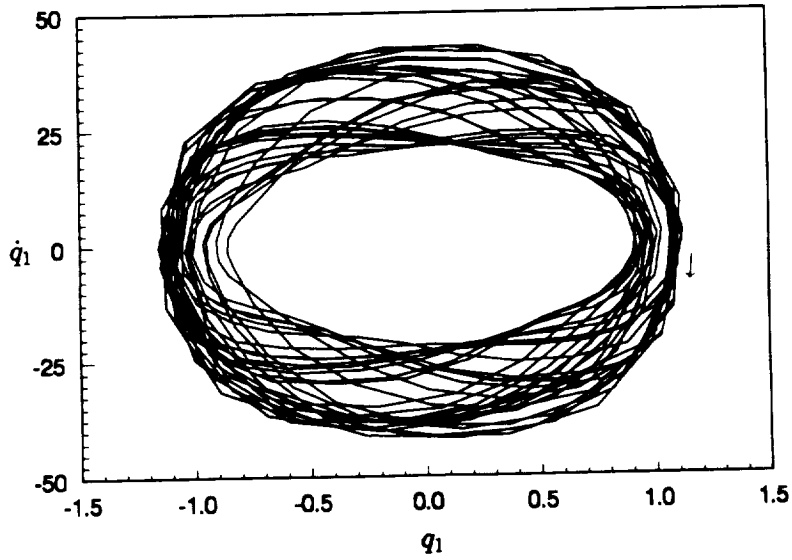

d) $q_1(0) = 1.0$.

Figure 10: (cont.) Phase portraits of the first generalized coordinate q_1: nominal configuration, $\lambda = 312.3$ and zero structural damping.

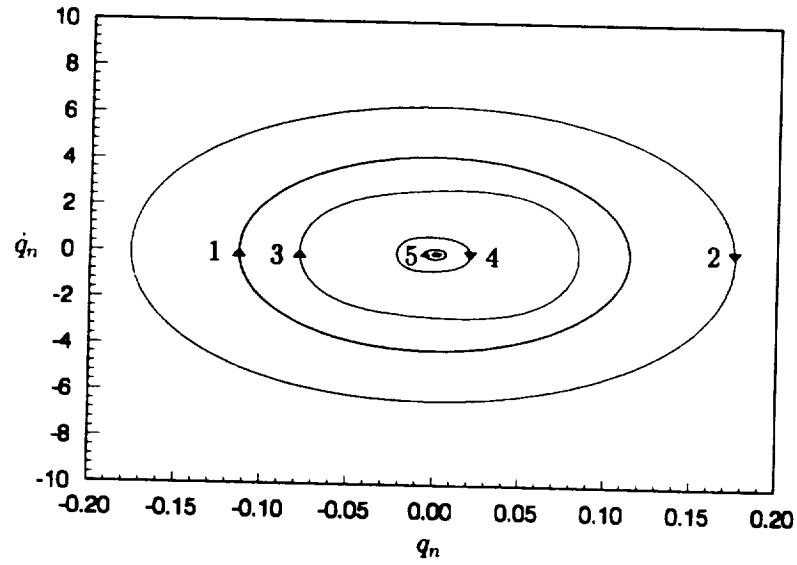

a) Solution type I: $\lambda = 340.2697$.

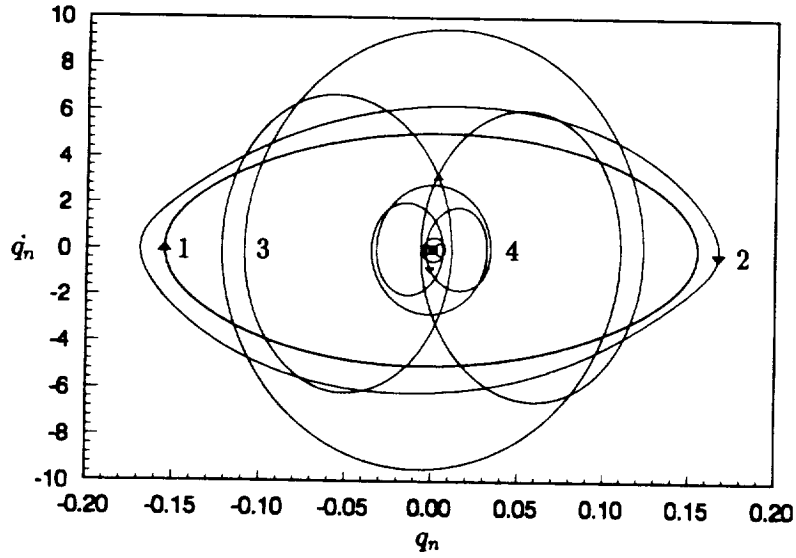

b) Solution type II: $\lambda = 312.3$.

Figure 11: Phase portraits of the generalized coordinates: nominal configuration and $\zeta_1 = 0.01$ (numbers identify the trajectories of different degrees of freedom).

first one. Interesting to note is that the main harmonics are at 5.614 and 5.003 for solution types I and II, respectively. They compare very nicely with the frequencies obtained for the cases $q_1(0) = 0.0001$ and 1 when the structural damping was taken as zero. For the rest of the analysis in this chapter it is going to be assumed that the type-I limit cycle is the significant solution. This decision was based on two facts: 1) $q_1(0) = 1$ is quite a large "disturbance", and 2) the type-II limit-cycle solution is not "robust" in the sense that such a solution cannot always be obtained for a given λ if the initial conditions are the ones corresponding to the same kind of solution for a different value of the dynamic pressure parameter in the neighborhood of λ. The type-I limit cycle is robust in this sense.

Going back to the question of how the flutter boundary is affected by the magnitude of the structural damping, Figure 12 shows that this influence is minimal for values of $\zeta_1 \leq 0.01$. This is interesting because physically one would expect the actual structural damping ζ_n to be of order 0.001 or smaller. A value of $\zeta_1 = 0.01$ was used in all the results to be shown in this chapter in order to make the numerical calculations converge faster. It is worth pointing out that larger values of ζ_1 lead to larger values of λ_{cr}, as discussed in Section 2.3. For example, $\lambda_{cr,\zeta_1=0.0005} = 312.286$ as compared to the value of 312.296 given previously.

4.3 Effects of Aerodynamic Parameters

There are basically three aerodynamic parameters in the present problem: 1) the Mach number M_∞, 2) the temperature ratio Θ, and 3) the momentum accommodation coefficient α_m. The mass ratio μ could also have been included, but in the case of free-molecule flow it is too small to be of significance. The Mach number and mass ratio only appear as the combination μ/M_∞ when piston theory is used. This is no longer true for free molecule flows, with the coefficient $\mathcal{A}_3$ being proportional to the Mach number, equation (83).

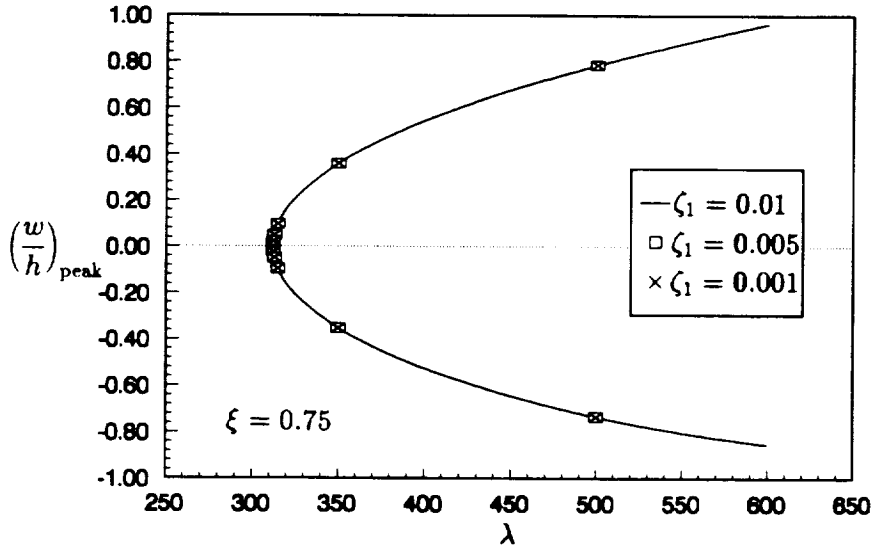

a) Limit-cycle amplitude.

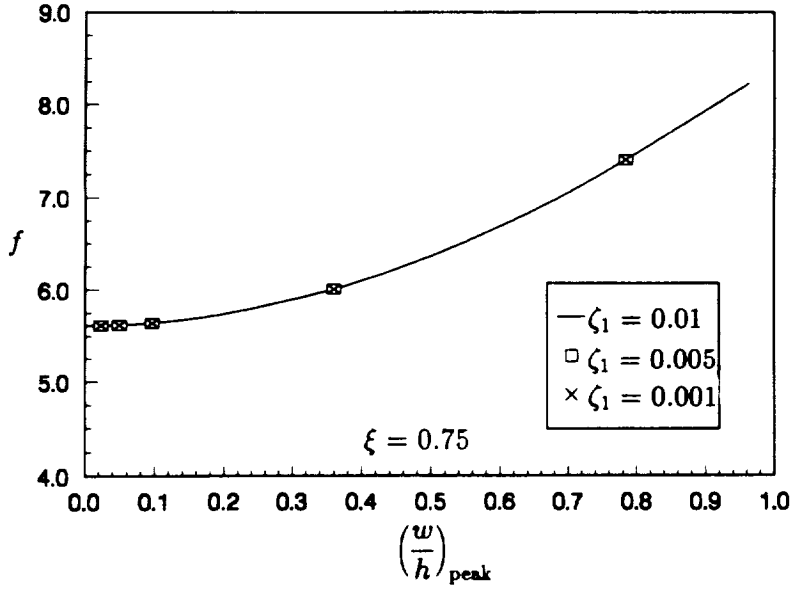

b) Limit-cycle main harmonic.

Figure 12: Effect of structural damping on the flutter characteristics: nominal configuration.

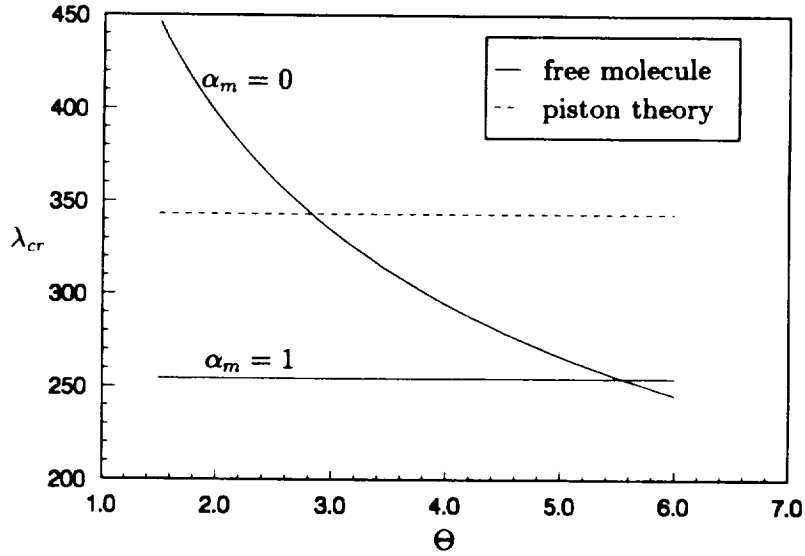

Figure 13: Influence of the temperature ratio Θ on the linear flutter parameter λ_{cr}, and comparison with piston theory results.

Comparison with piston theory results are shown in Figure 13 for the linear flutter parameter. The figure also shows how the free-molecule λ_{cr} varies with the temperature ratio for the two limiting cases of $\alpha_m = 0$ and 1. Note that in the latter case, when all the molecules are reflected specularly from the panel, the flutter condition is independent of Θ. It is clear that the comparison between piston theory results and those obtained using the present rarefied formulation is highly dependent on the values of Θ and α_m specified. The fact that λ_{cr} decreases with Θ for $\alpha_m < 1$ should have been expected, since an increase in the temperature ratio implies an increase in the pressure load, as indicated by the expressions for $\mathcal{A}_1$ and $\mathcal{A}_2$, equations (81) and (82).

The effect on the linear flutter parameter of varying α_m is shown in Figure 14. The first thing that strikes one is that the curves are nearly straight lines for high enough values of the temperature ratio. This means that it may sufficiently accurate during a design process to only compute two points in the curve, and use them to estimate λ_{cr} for different values of α_m. It is suggested in the literature that values in the vicinity of 0.2 lead to better agreement with experimental results. Another

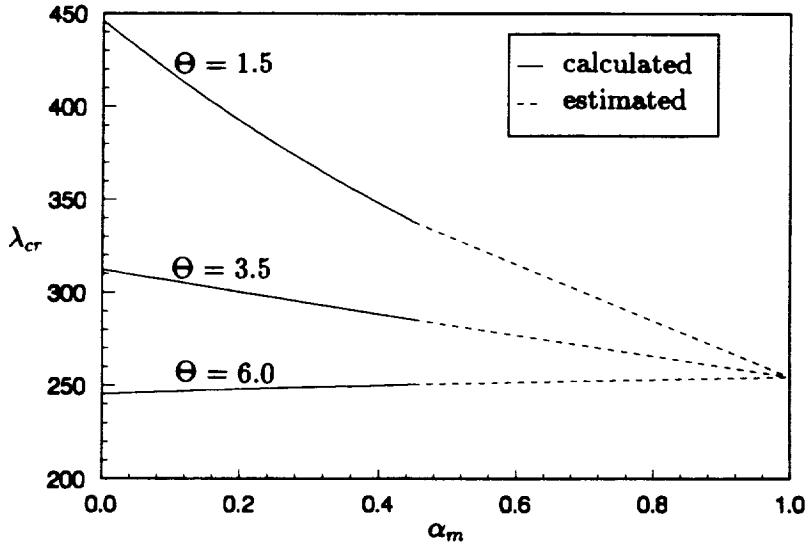

Figure 14: Influence of the momentum accomodation coefficient α_m on the linear flutter parameter λ_{cr}.

point is that the slopes of the curves in Figure 14 depend on the value of Θ which is assumed. In fact, this could have been realized from Figure 13 since the free-molecule curves shown there represent limiting cases; that is, given a value of Θ, λ_{cr} for an arbitrary value of α_m must lie between the curves for $\alpha_m = 0$ and $\alpha_m = 1$. This gives rise to a curious observation: there is a value of the temperature ratio ($\Theta \approx 5.6$) for which λ_{cr} is independent of α_m.

Finally, Figure 15 gives the variation of the linear flutter parameter with Mach number. It is seen that λ_{cr} monotonically decreases with decreasing M_∞. If the effect of the terms associated with $\mathcal{A}_2$ and $\mathcal{A}_4$ is neglected, which is a reasonable assumption due to the small value of the mass ratio, this trend makes sense in view of the fact that $\mathcal{A}_3$ decreases with a decrease of the Mach number, and that the shear stress stabilizes the system. In the case of linear piston theory, λ_{cr} increases when M_∞ decreases for a fixed value of the mass ratio, that is, the trend is the opposite one.

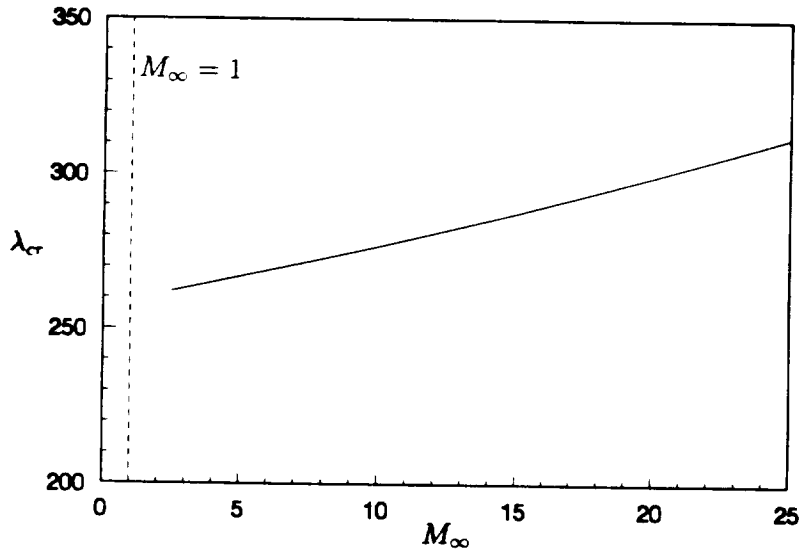

Figure 15: Influence of the Mach number M_∞ on the linear flutter parameter λ_{cr}.

4.4 Effects of Structural Parameters

Three set of parameters are included in this category: 1) the "spring support parameters" α_{k_i}, 2) the applied compression parameter R_x, and 3) the pressure differential parameter P_z.

In the first case, it is assumed that the panel is supported at leading and trailing edges by springs oriented longitudinally, such as to idealize flexibility in adjacent panels or the underlying structure. In classical panel flutter the presence of such springs alters the limit-cycle amplitude but not the linear flutter parameter. That is, only the supercritical characteristics of the panel are modified. In the present case the behavior is quite different because of the distributed tangential loads, especially P_x. Under such a uniform distributed load, and for both ends fixed in the x direction, half of the panel is under tension (front), while the other half is under compression (back). When the trailing edge is supposed to have a spring attached to it ($\alpha_{k_1} = 1$, $\alpha_{k_2} < 1$), the smaller the spring constant, the larger the tension region along the panel. This appreciably stabilizes the system, as can be seen from Figure 16. On the other hand, when only the leading edge spring exists ($\alpha_{k_1} < 1$, $\alpha_{k_2} = 1$) the behavior

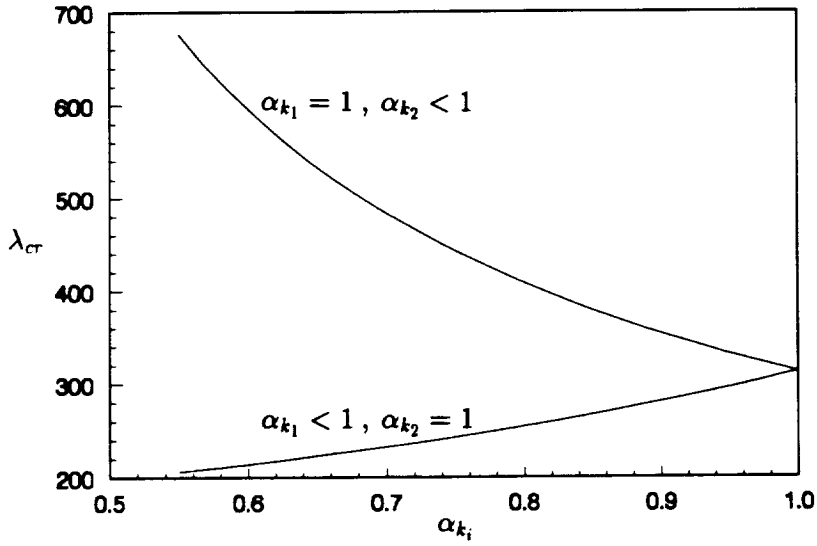

Figure 16: Influence of the spring support parameters α_{k_i} on the linear flutter parameter λ_{cr}.

changes. Now the smaller the spring constant, the larger the compression region, and the system is destabilized. However, the rate of decrease of λ_{cr} is much smaller than the rate of increase of λ_{cr} in the first case. Finally, it is shown in Appendix B that the value of the linear flutter parameter for an arbitrary combination α_{k_1}, α_{k_2} can be found by considering the appropriate case where only the front spring or the back spring exists, depending whether $\alpha_{k_1} > \alpha_{k_2}$ or not.

Before commenting on the influences of other parameters, it is interesting to analyze the behaviors of the system when the α_{k_i} are varied for different values of the temperature ratio Θ. In order to do this it is useful to define two new variables:

$$\lambda_\Theta = \frac{\lambda - \lambda_{\text{nom},\Theta}}{\lambda_{\text{nom},\Theta\,=\,3.5}} + 1 \qquad \text{and} \qquad \lambda^*_\Theta = \frac{\lambda}{\lambda_{\text{nom},\Theta}} \ , \tag{87}$$

where $\lambda_{\text{nom},\Theta}$ corresponds to the value of λ_{cr} for the nominal configuration but a given value of Θ. Note that the second variable corresponds to a *normalization* of the dynamic pressure parameter for each different temperature ratio. On the other hand, the first variable is nothing more than a *translation* in the origin of the λ scale, plus a normalization with respect to the nominal configuration. This last normalization is done only to make it possible to plot the flutter boundaries using

the same scale for both λ_Θ and λ^*_Θ. One should realize that $\lambda^*_{\Theta=3.5}$ and $\lambda_{\Theta=3.5}$ are the same variable. Figure 17 shows how the linear flutter parameter varies with the spring support parameters using these variables as the ordinate. Three values of the temperature ratio were investigated, $\Theta = 1.5$, 3.5, and 6.0. It is very clear that the use of λ^*_Θ brings the flutter boundaries closer together, especially the lower curves corresponding to $\alpha_{k_1} < 1$, $\alpha_{k_2} = 1$. Also, note that the flutter boundaries are steeper for smaller values of the temperature ratio.

The behavior of the system in the presence of applied compressive loads, $R_x < 0$, is illustrated in Figure 18. It resembles very much the kind of results obtained in classical panel flutter, with a distinguishing difference associated with the buckling boundary. As mentioned before, for a given set of parameters in the case of a static deflection, if q_n is a solution, $-q_n$ is not. Computations show that the positive-static solution corresponding to a given λ is smaller than the negative one (in absolute value). Also, as $-R_x$ increases beyond π^2 this difference increases, with the static-positive solution approaching zero earlier than the corresponding negative solution. Both these effects are illustrated in Figure 19. Then for large enough values of $-R_x$ the solution becomes noticeably "unstable" for values of the negative static deflection close to zero (Figure 20). The meaning for "unstable" here is that the solution seems to be converging with time to a finite value, but it then goes to zero in a relatively short interval. The interpretation of this result is that the system tries to approach a negative deflection when the corresponding positive solution has already become zero. Some disturbance then makes it "jump" from the former to the latter. It should be mentioned that the behavior of the first generalized coordinate (Figure 20) is typical of the entire motion.

Another interesting feature related to the action of compressive loads is illustrated in Figure 21, which is representative of points close to the intersection between the buckling and flutter boundaries, $R_x \approx -33$. The case shown in the figure corresponds to a value of R_x slightly smaller than the one associated with the intersection between boundaries. Again the solution seems to be converging to a finite value, but it then begins to vary rapidly. In this case it eventually would converge to zero if the calculation were allowed to run for a longer time. However, if values

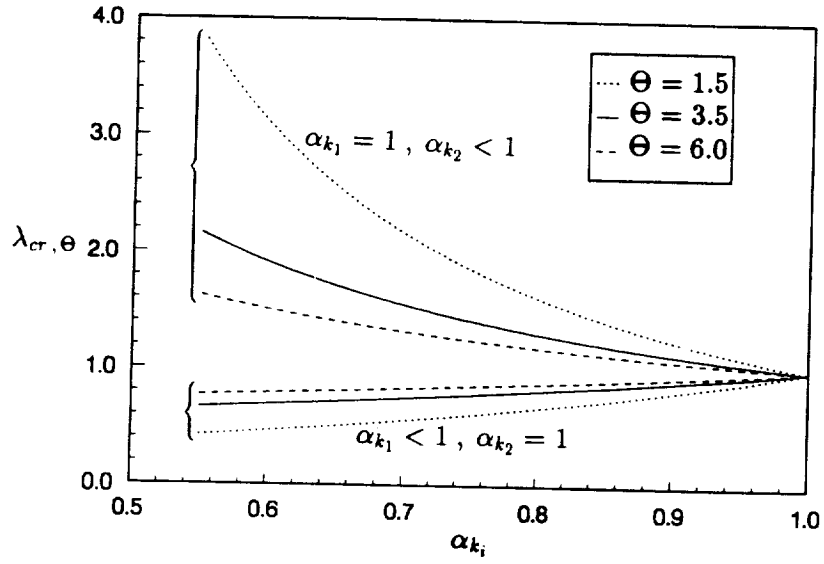

a) Shifted variable.

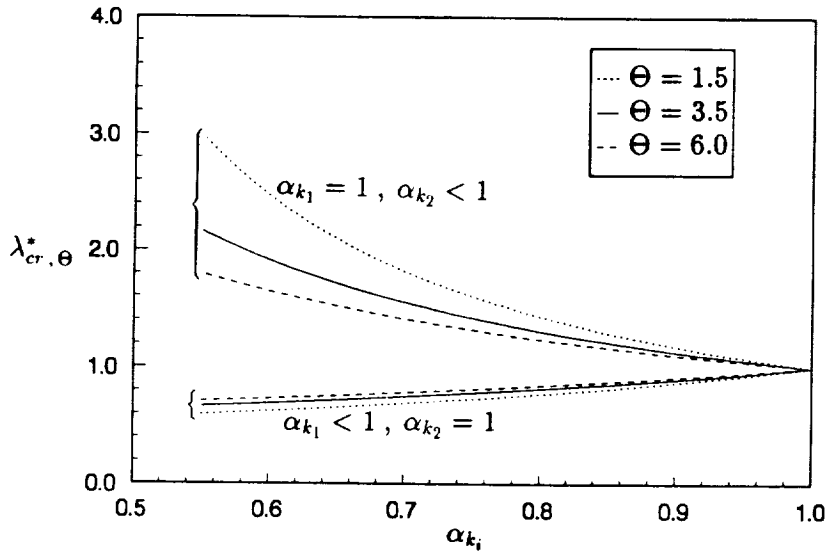

b) Normalized variable.

Figure 17: Influence of the temperature ratio Θ in the flutter boundaries when the spring support parameters α_{k_i} are varied.

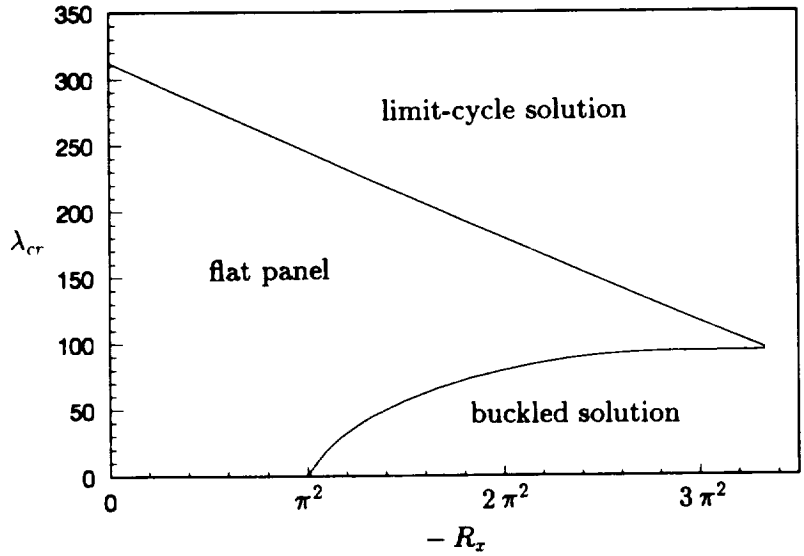

Figure 18: Influence of the applied compression parameter R_x on the linear flutter parameter λ_{cr}.

of $-R_x$ larger than the one corresponding to the intersection between boundaries are used, a similar behavior can be noticed with the further complication that the motion does not seem to subside. This failure to converge to rest can also happen in the limit-cycle solution region, which was not the case for smaller values of $-R_x$. As discussed by Dowell and Ilgamov [59] there is the possibility that this motion is an example of chaos.

The influence of the temperature ratio on the flutter boundaries is again investigated in Figure 22. As in the previous case (Figure 17) the stability boundaries come close together when the variable λ^*_Θ is used to plot the curves. In fact, the stability boundaries for $\Theta = 3.5$ and 6.0 practically coincide. Another interesting point is that the slope of the limit-cycle boundary, which is essentially linear, increases as the temperature ratio increases in this case [Figure 22b)]. On the other hand, this same slope *decreases* as Θ increases when λ is used [Figure 22a)]. Basically this means that one obtains conservative results if λ^{cr} for any specified temperature ratio is estimated using the value of $\lambda^*_{cr,\Theta}$ for the largest temperature ratio being considered. In other words, the value of the linear flutter parameter for a given Θ

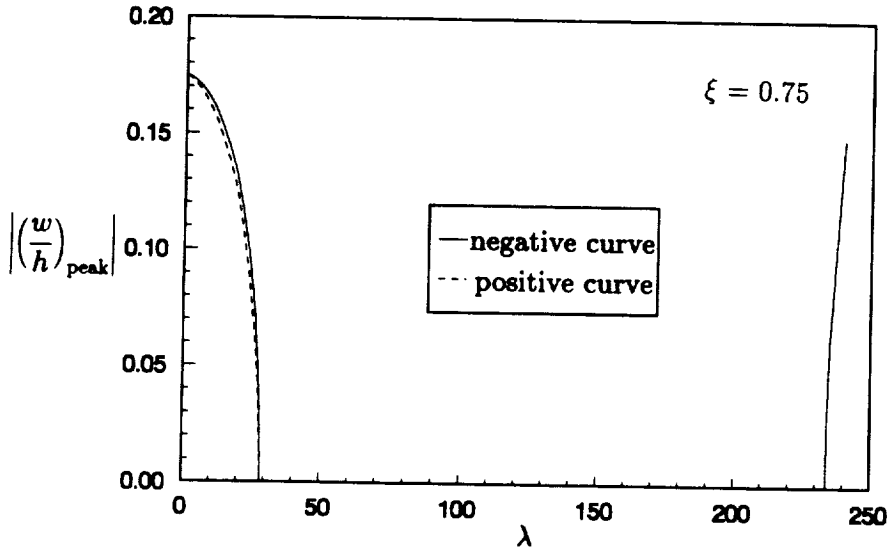

a) $R_x = -7\pi^2/6$.

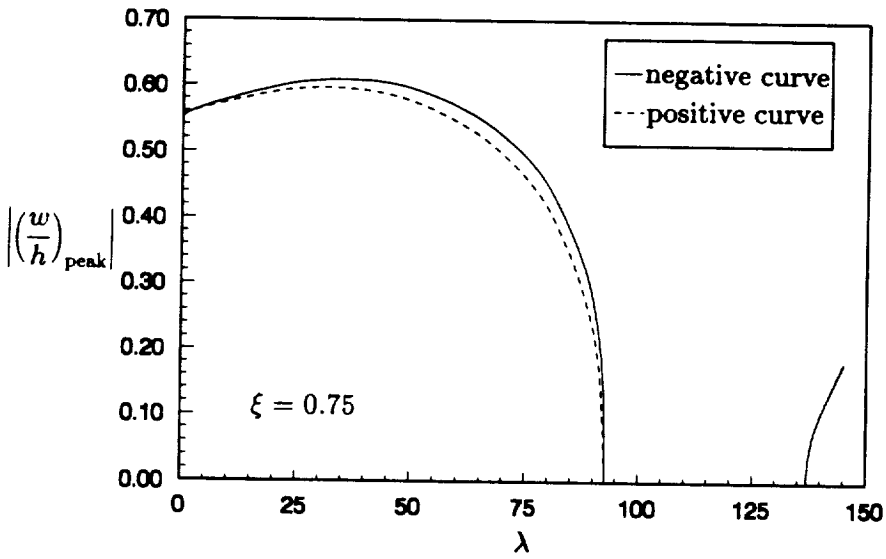

b) $R_x = -8\pi^2/3$.

Figure 19: Influence of the applied compression parameter R_x in the amplitude of the solution.

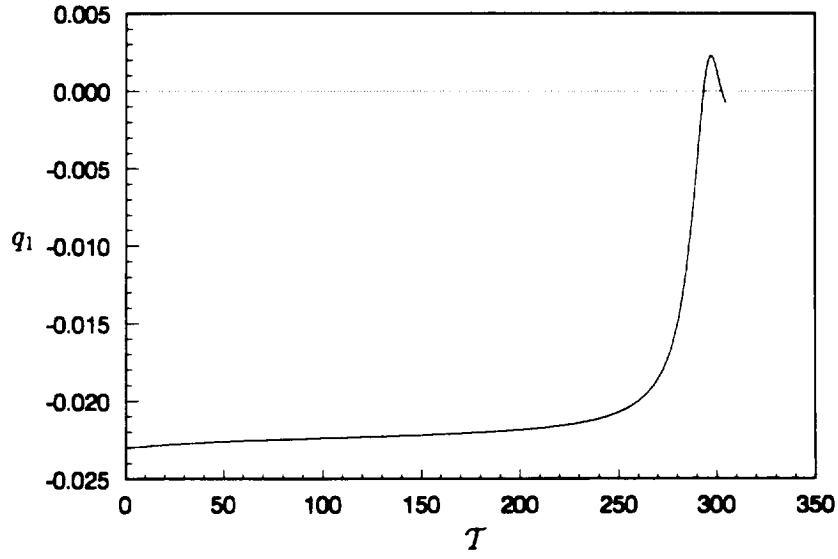

Figure 20: Time history of the first generalized coordinate q_1 for $R_x = -8\pi^2/3$ and $\lambda = 92.656$.

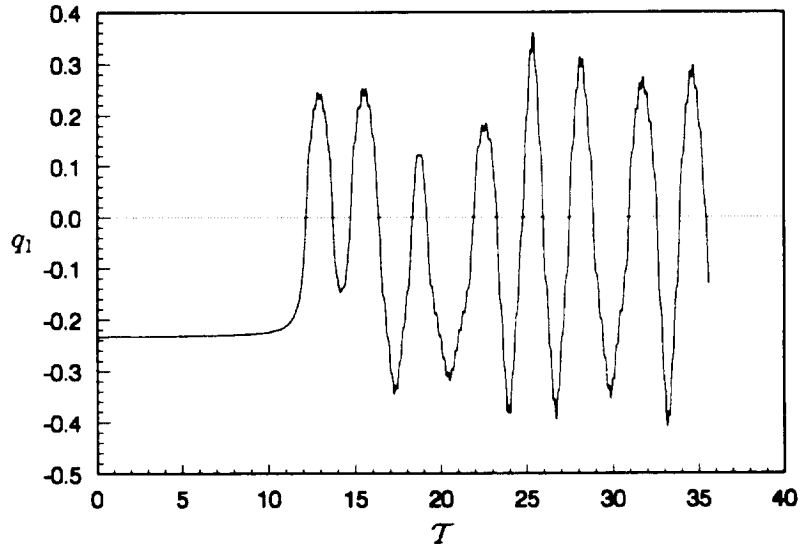

Figure 21: Time history of the first generalized coordinate q_1 for $R_x = -10\pi^2/3$ and $\lambda = 93.704$.

obtained using as an estimate $\lambda^*_{cr,\Theta}$ for a larger temperature ratio is smaller than the correct value.

Pressure differentials are specified by the parameter P_z. A positive value corresponds to a uniform static pressure difference between the panel sides in the positive z direction, i.e., excess pressure in the interior. It can be seen from Figure 23 that the flutter boundaries again approach each other if they are plotted using λ^*_Θ, i.e., their curvature are more nearly the same. As in the case of applied compressive loads, a large temperature ratio yields smaller values of $\lambda^*_{cr,\Theta}$ when compared with the same results for a smaller temperature ratio. A new feature of the free-molecule case compared to classical panel flutter is that the flutter boundary is no longer symmetrical about its location for $P_z = 0$. An upward pressure ($P_z = 0$) causes a somewhat lower increase in the linear flutter parameter than a downward pressure. Finally, it should be recalled that in the presence of a pressure differential the limit-cycle solution is "superimposed" upon a nonzero static deflection. At the linear flutter condition Figure 24 shows that the deflection increases in absolute value with increasing values of P_z. It can also be seen that the static deflection is essentially antisymmetric with respect to the line $P_z = 0$.

Finally, Figure 25 shows how the amplitude of the limit-cycle solution varies for different values of the temperature ratio. In order to understand the plots in the figure, it should be emphasized that none of the curves have the same value of $\lambda_{cr,\Theta}$ or $\lambda^*_{cr,\Theta}$, as seems to be implied by the plots. This feature was arrived at by appropriately translating the origins of the horizontal axes of the diagrams for the different values of Θ in order to obtain a better visualization. This accounts for the fact that there is no numbering in those axes. It can be seen from Figure 25 that the limit-cycle amplitude increases faster with λ_Θ the higher the temperature ratio is, the difference in curvature being easily verified. However, if λ^*_Θ is used instead the curves are much closer together, especially for larger values of Θ. The same kinds of results are obtained if values of $P_z \neq 0$ and $\alpha_{k_i} \neq 1$ are used.

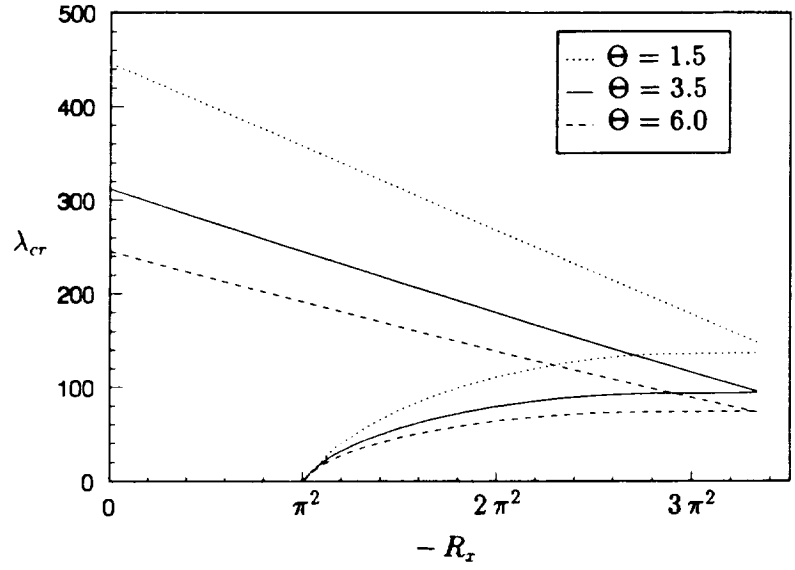

a) Nonmodified variable.

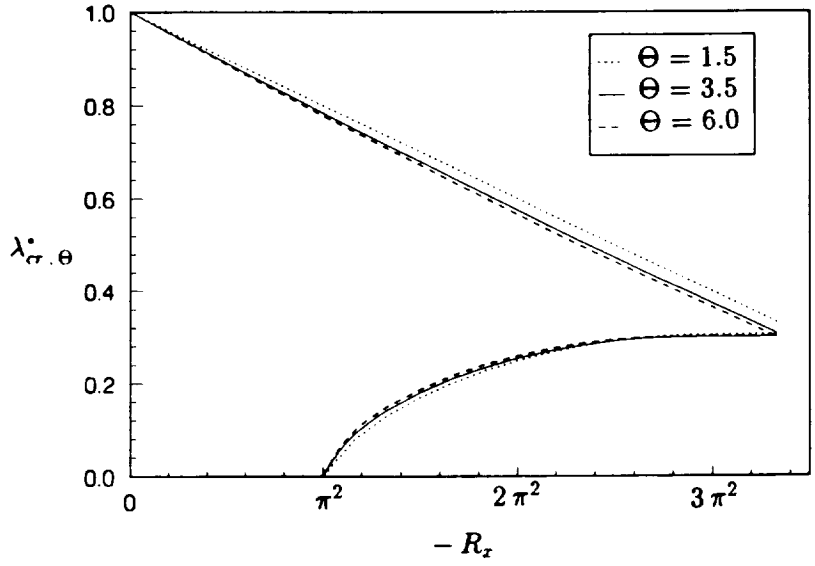

b) Normalized variable.

Figure 22: Influence of the temperature ratio Θ in the stability boundaries when the applied compression parameter R_x is varied.

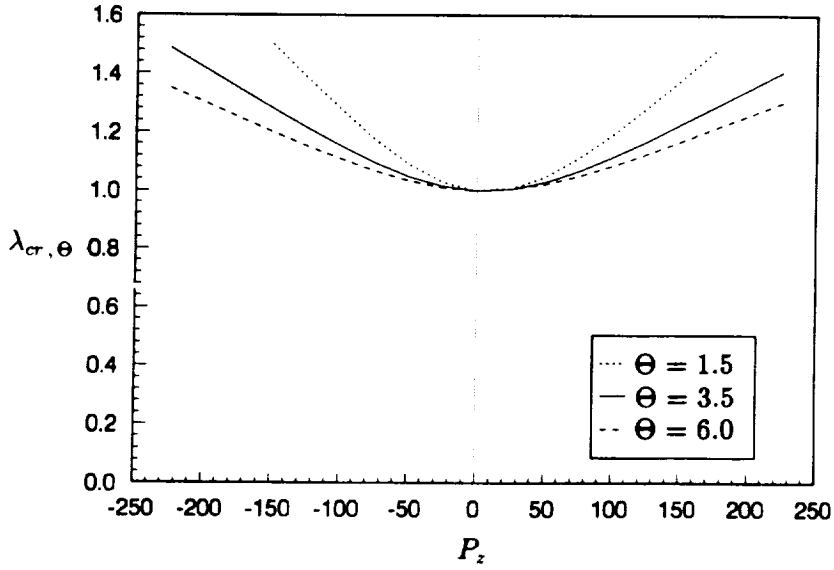

a) Shifted variable.

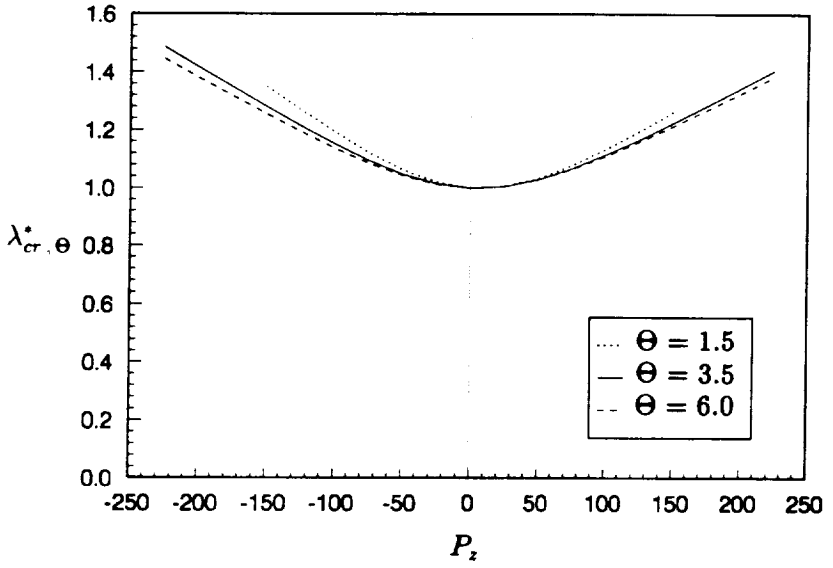

b) Normalized variable.

Figure 23: Influence of the temperature ratio Θ in the flutter boundaries when the pressure differential parameter P_z is varied.

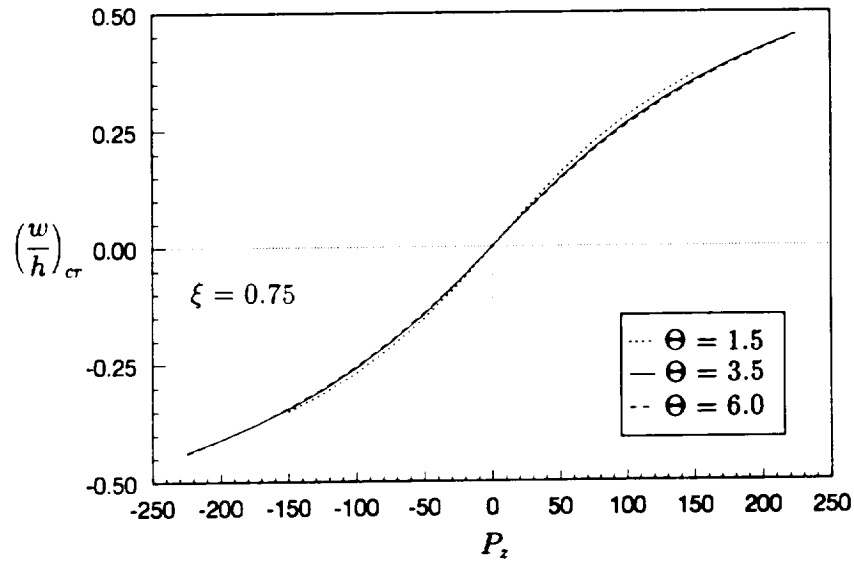

Figure 24: Influence of the pressure differential parameter P_z on the static deflection at the linear flutter condition.

4.5 Initial Curvature Effects

When incorporating the effects of initial curvature into the code, a comparison with the results by Dowell [52] was performed to ensure the correct implementation of the coefficients in the general equation of motion (43). As a direct result of this effort, it was established that the problem becomes very sensitive to the initial conditions as the maximum height of the panel, H, increases. Furthermore, the motion also tends to be what Dowell called a "heavily modulated oscillating function" for large values of the panel height. Most probably these motions constitute yet another example of chaos. Because of this fact, the present study was limited to relatively small values of the parameter H/h.

Only results for two kinds of initial curvature are analyzed here: 1) constant curvature, and 2) half-sinusoidal curvature ($w_0 = H \sin \pi\xi$). In these cases the undeformed shapes of the panel are not markedly different from each other. Accordingly, the bifurcation diagrams for both cases when $H/h = 0.5$ are similar, with values of λ_{cr} close to each other (Figure 26). It should be noted that in both cases the system is destabilized with respect to the flat panel problem. This is the same

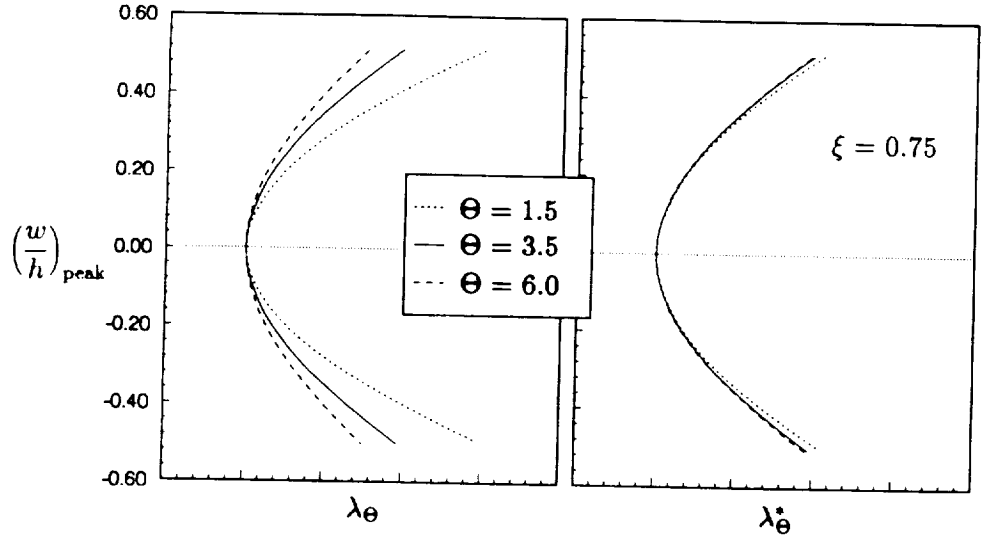

a) $R_x = -7\pi^2/6$.

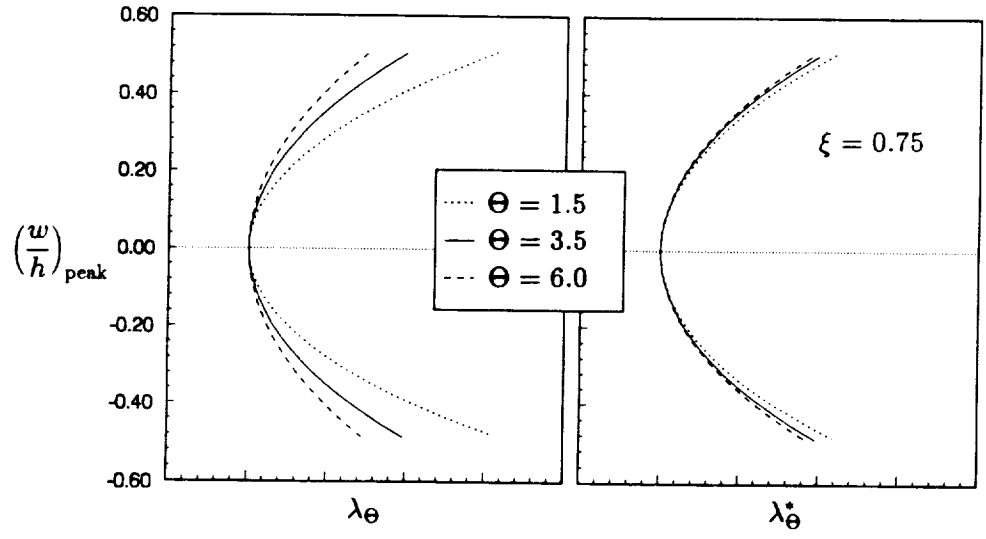

b) $R_x = -8\pi^2/3$.

Figure 25: Influence of the temperature ratio Θ in the limit-cycle amplitude for different values of R_x: $P_z = 0$ and $\alpha_{k_1} = 1$.

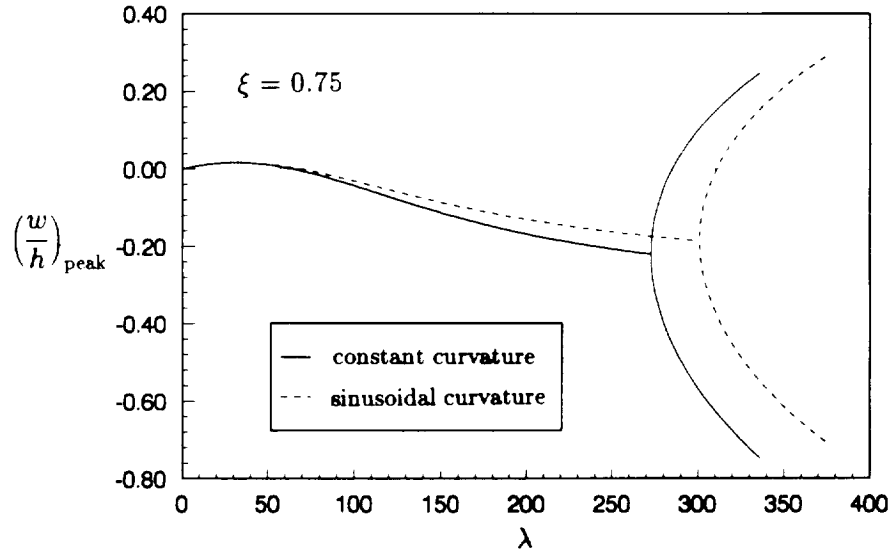

Figure 26: Bifurcation diagrams for $H/h = 0.5$.

trend obtained when linear piston theory is used. For small values of λ the solution corresponds to a static deflection due to the steady airloads caused by the panel curvature. The deflection (from the initial curved shape) at the point $\xi = 0.75$ is initially positive but then becomes negative. The panel deformation is illustrated in Figures 27 and 28 for two different values of λ in each case. It can be seen from part a) of the figures that a large portion of the panel is deflected downward (relative to the initial curved shape) even for small values of the dynamic pressure parameter, and that this deformation approaches a half-sine shape as λ is increased. On the other hand, if the deformation is superimposed to the initial shape [part b) of the figures], it becomes clear that the panel starts fluttering when it is deformed to a relatively flat geometry. In these conditions the compressive loads acting on the panel are, most probably, considerable.

When the maximum height is further increased to a value of $H/h = 1.0$, the behaviors of the system for the different cases of initial curvature are no longer very similar, with the constant curvature panel having a much smaller value for λ_{cr} (Figure 29). The static-deformation behavior of the panel resembles the one discussed for $H/h = 0.5$. One complication now is that, once the panel starts fluttering,

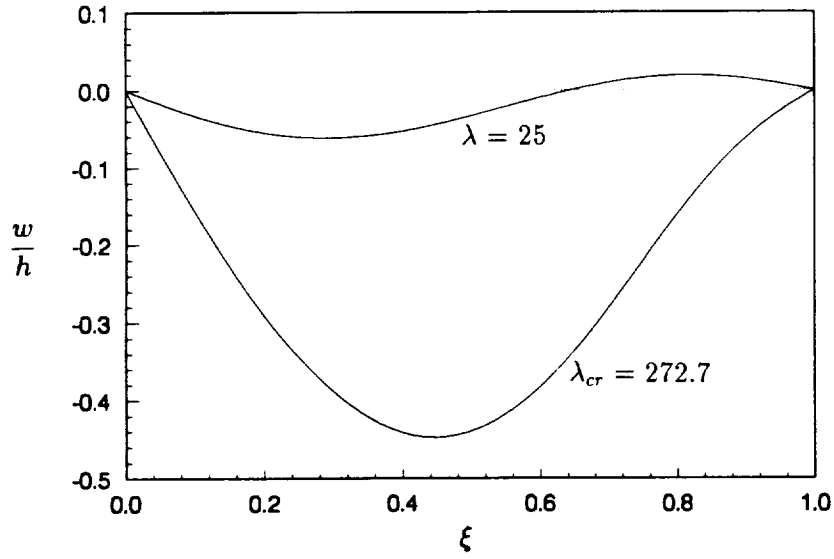

a) Perturbed deflection.

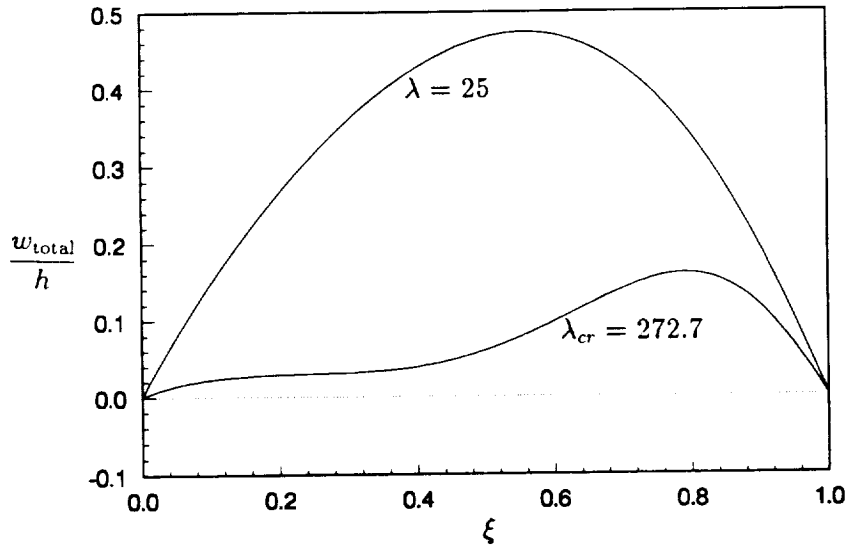

b) Total deflection.

Figure 27: Static deflection of parabolic panel for $H/h = 0.5$.

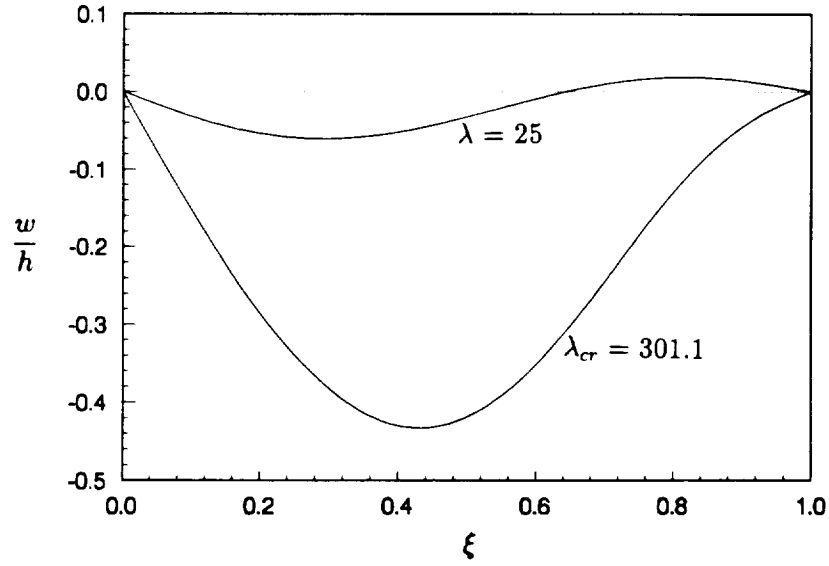

a) Perturbed deflection.

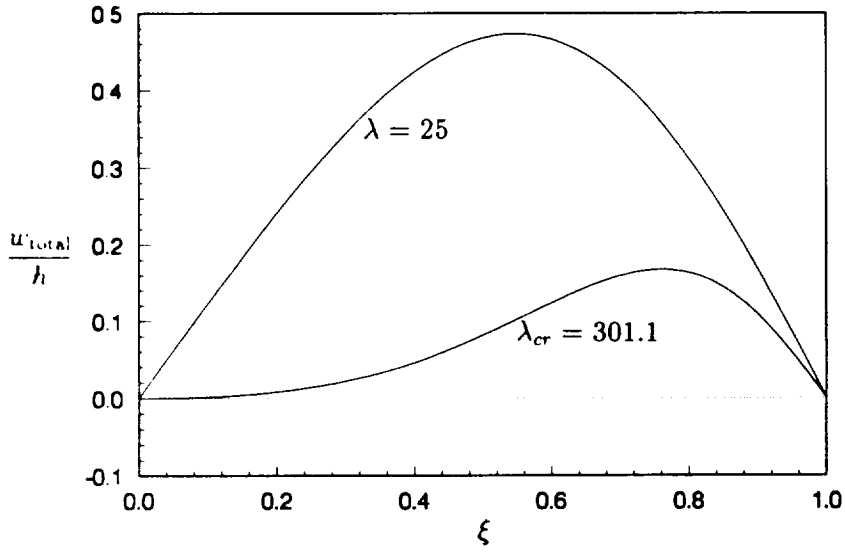

b) Total deflection.

Figure 28: Static deflection of sinusoidal panel for $H/h = 0.5$.

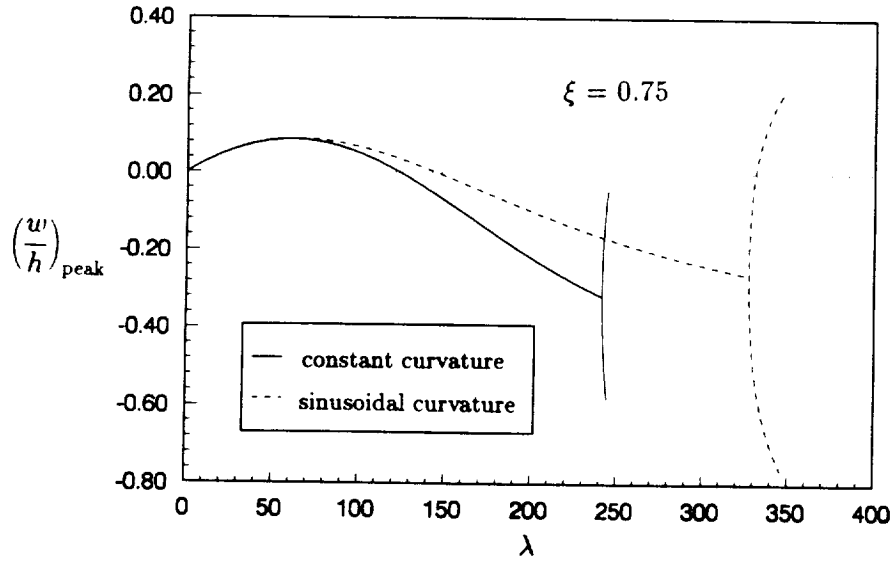

Figure 29: Bifurcation diagrams for $H/h = 1.0$.

the solution becomes very sensitive to the initial conditions. Eventually there is a change in the kind of the limit cycle achieved, even if λ is increased through very small increments.

The behavior of the system for a value of $H/h = 2.0$ is similar to the previous case of $H/h = 1.0$, with a further separation between the values of λ_{cr} for the two initial curvature cases discussed. It is interesting to observe, however, that the linear flutter parameter has increased for both cases relative to the values corresponding to the problem when $H/h = 1$.

In view of the foregoing results, any actual analysis in a design process should be done assuming a parabolic shape, since this would give smaller values for the linear flutter parameter, leading to conservative results. On the other hand, due to the sensitivity of the results to the initial curved shape, one may wonder whether there really is some meaning in doing this kind of analysis, especially because of manufacturing restrictions on the panel final shape.

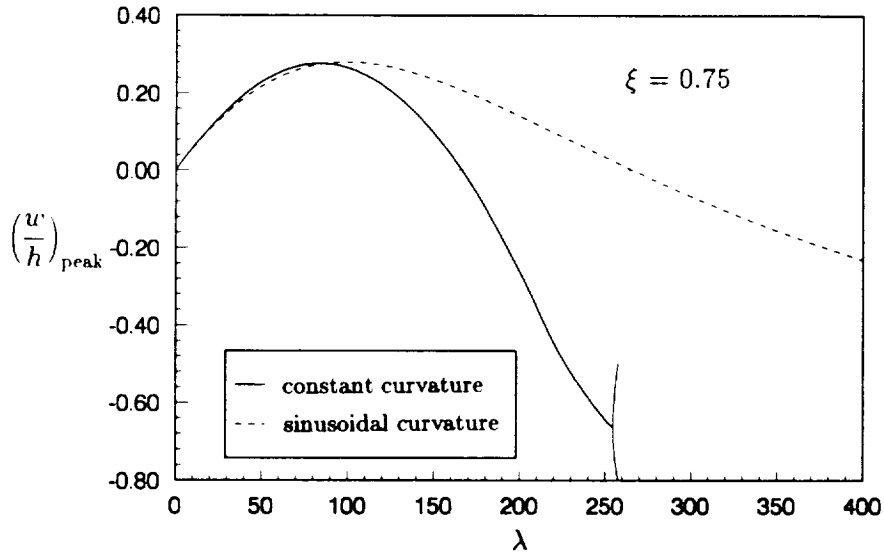

Figure 30: Bifurcation diagrams for $H/h = 2.0$.

4.6 Particle Simulation Method Application

In principle, the interaction between the structural code and the aerodynamic one can be implemented as in other recent aeroelastic applications which use Computational Fluid Dynamics (CFD). The only question that should deserve some investigation is the kind of numerical integrator to be used, since a Runge-Kutta-like algorithm can no longer be used. However, this is not expected to be a serious problem. Therefore, the major difficulty in applying a particle simulation method to the present system has to do with CPU time requirements, since these methods are very computationally intensive.

As mentioned before in Section 3.2.2, the CPU time can be assumed to be directly proportional to the number of molecules and cells in the simulated flow. Actually, the number of cells can be directly written in terms of number of time steps. In the case of the schemes implemented by McDonald [113] and Dagum [114] (Stanford Particle Simulation Method) a time step in the code is typically of the order of 1/3 of the cell size. Then, in order to obtain an estimate of the CPU time

requirements related to the present application it is useful to define a new time variable:

$$t^* = \frac{t\,U_\infty}{a} =$$

$$= \sqrt{\frac{\rho_p\,h\,a^4}{D}}\,\sqrt{\frac{U_\infty^2}{a^2}}\,t\,\sqrt{\frac{D}{\rho_p\,h\,a^4}} =$$

$$= \mathcal{T}\,\sqrt{\underbrace{\frac{\rho_p\,h}{\rho_\infty\,a}}_{1/\mu}\,\underbrace{\frac{\rho_\infty\,a^3\,U_\infty^2}{M_\infty\,D}}_{\lambda}\,M_\infty} = \sqrt{\frac{\lambda\,M_\infty}{\mu}}\,\mathcal{T}\,. \tag{88}$$

Note that t^* is a nondimensional time which measures how many panel chords have been traveled. All symbols have been defined previously and can be identified from their definitions in the Nomenclature. However, it should be recalled that $\mathcal{T}$ is the nondimensional time used during the time integration.

A reasonable value of $\mathcal{T}$ to obtain a limit cycle solution, $\mathcal{T}_{\rm sol}$, cannot be expected to be much less than 10. On the other hand, from the results previously presented in this chapter it can be seen that the smallest possible value of λ for a limit-cycle solution is of order 100. Because of restrictions on the applicability of particle simulation methods, the Mach number should not be taken much smaller than 10. Assuming a value of $\lambda\,M_\infty = 10^3$, one can obtain the total number of chords traveled in order to ensure a converged flutter solution for different values of μ, as shown in Table 1.

Table 1: Variation with μ of the number of chords traveled to achieve a limit-cycle solution: $\lambda\,M_\infty = 10^3$ and $\mathcal{T}_{\rm sol} = 10$.

μ	10^{-3}	10^{-4}	10^{-5}	10^{-6}	10^{-7}
chords traveled	10^4	3.16×10^4	10^5	3.16×10^5	10^6

The results in Table 1 can be put in terms of CPU time requirements. From Dagum's work, CPU time requirements are of 2.0 μsec/particle/timestep when one

uses the 32k processor Connection Machine, and 1.7 μsec/particle/timestep on the Cray 2. It is reasonable to assume that this time has decreased to at most 1.0 μsec/particle/timestep on the Cray YMP; possibly a Connection Machine with a larger number of processors would require similar times. The largest possible number of particles should be used in order to assure time accurate results. On the other hand, the number of cells along the panel should be large enough to avoid excessive numerical errors when obtaining the aerodynamic generalized forces. A reasonable grid could be one with 250 cells in the x direction (about 200 cells along the panel), and 50 cells in the y direction. These values reflect the considerations arrived at by Woronowicz[115] in his applications of the Stanford Method. The position of the wing leading edge, corresponding to the point where the boundary layer starts developing, should be at least a few cells ahead of the actual panel leading edge. On the other hand, the position of the wing trailing edge should be specified in such a way to allow for a sufficient number of cells after it, because of the subsonic region in the boundary layer. The extent of the grid in the y direction is necessary to avoid spurious reflections of shock waves at the upper boundary, for example. These values give a total number of 12,500 cells, and it follows that the smallest reasonable number of particles is approximately 4×10^6, which allows for approximately 300 particles/cell. In the case of about 100 cells along the panel, which is a marginally small number, the number of particles might be decreased to about 10^6 if all relative proportions are kept approximately constant. As mentioned before, a typical time step is of the order of 1/3 of the cell size. With these considerations, Tables 2 and 3 give Cray YMP CPU time requirements (in days) for the cases of 100 and 200 cells along the panel. It is clear that only the applications associated with the 100 cells case, and larger values of μ, might become feasible if a decrease of two order of magnitudes could be arranged. The values in these tables were calculated by the following formula:

$$\text{CPU time} = \frac{10^{-6}}{24 \times 3600} (\text{no. of particles}) \times \times (\text{value from Table 1}) (3 \times \text{no. cells along the panel}) . \quad (89)$$

Note that (value from Table 2)(3 × no. cells along the panel) gives the number

Table 2: Variation with μ of CPU time requirements (days) to achieve a limit-cycle solution: $\lambda M_\infty = 10^3$, $\mathcal{T}_{\text{sol}} = 10$, and 100 cells.

μ	10^{-3}	10^{-4}	10^{-5}	10^{-6}	10^{-7}
days	34.7	109.8	347.2	1098	3472

Table 3: Variation with μ of CPU time requirements (days) to achieve a limit-cycle solution: $\lambda M_\infty = 10^3$, $\mathcal{T}_{\text{sol}} = 10$, and 200 cells.

μ	10^{-3}	10^{-4}	10^{-5}	10^{-6}	10^{-7}
days	277.8	878.4	2778	8784	27778

of time steps for $\mathcal{T}_{\text{sol}} = 10$.

The first observation to be made if one is to investigate the possibility of smaller CPU times is that the values in Tables 2 and 3 are proportional to $\sqrt{\lambda M_\infty/\mu}$. This is the parameter in the estimates which may be directly affected by the panel's characteristics (material properties). However, since it is obtained from nondimensional parameters of the panel flutter problem, a change in the stiffness of the panel for example is not reflected in $\sqrt{\lambda M_\infty/\mu}$, and consequently in the CPU time requirements. Naturally, the physical time t is greatly affected. On the other hand, a lighter material makes larger values of μ more reasonable. As a limiting case, consider corkwood, which has a density of approximately 0.21 g/cm^3. This corresponds to almost a two-order-of-magnitude decrease when compared with the value of 8.20 g/cm^3 for René 41. If an altitude of 95 km is assumed instead of 110 km, which was used in the calculations shown in this chapter, a further decrease of two orders of magnitude is obtained. This makes a value of $\mu = 10^{-4}$ "reasonable", but there is little hope of managing to decrease the CPU time with a further decrease in μ and still have some physical material. Since the value of M_∞ is also "fixed" close to 10, only λ remains to be varied, that is, for smaller values of CPU time λ should

be decreased. Of all the nondimensional parameters involved in the panel flutter calculations, only four of them lead to a decrease of the linear flutter parameter for the flat panel problem. They are the Mach number, the temperature ratio, the spring parameter on the leading edge, and the applied compression parameter. By far the most strong influence is related to increasing Θ. A complete study was done in order to find conditions which would lead to smaller value of λ, but the minimum value obtained for λ_{cr} was approximately 35.[1] This is almost a decrease of one order of magnitude in λ, but it is definitely inadequate since CPU times are proportional to $\sqrt{\lambda}$.

The final conclusion of this brief investigation is that, until supercomputer speeds are increased by a factor of at least 100 it will be infeasible to carry out flutter calculations with particle-method aerodynamics.

[1] A value of the temperature ratio of 36 was used, which at the assumed altitude of 95 km means that the panel temperature is of the order of $6,780^\circ$ K $\approx 6,500^\circ$ C $\approx 11,700^\circ$ F. This is quite high to say the least.

Chapter 5

FINAL REMARKS

The main accomplishment of this work corresponds to the finding that aerodynamic shear effects are considerable in the rarefied (free-molecule) flow analyzed. Here the ratio between shear stress and pressure, for both steady and unsteady parts of the loading (up to first order), is of order of Mach number (see page 34). One consequence of including the aerodynamic shear loading is to stabilize the panel response, with an increase of the linear flutter parameter[†] of 53% relative to the pressure only value in the case of the nominal configuration specified in Section 4.1. Using results given in Section 6.5 of the book by Anderson [122], it is possible to show that in the case of a flat plate $\tau/p_\infty \sim M_\infty^2/\sqrt{\mathrm{Re}_x}$. Here τ is the value of the steady shear stress at a given point of the plate, p_∞ is the static pressure corresponding to the freestream, and Re_x is the Reynolds number based on the coordinate x measured from the leading edge of the plate. Then, depending on the position of the panel relative to the leading edge of the wing and the value of the Mach number, the ratio τ/p_∞ may be large enough to change the flutter characteristics of the panel significantly.

A convergence study regarding the number of modes to be used in the Galerkin method showed that a six-mode solution leads to converged results. Up to 12 modes were used in this research. The motion resembles continuum panel flutter,

[†]This parameter corresponds to the dynamic pressure parameter at the linear flutter boundary, that is, a limit cycle of zero amplitude.

with the distinguishing difference that the point of zero deflection (the node of the flutter mode) is closer to the center of the panel. The point of maximum deflection is also slightly farther back ($\xi \approx 0.8$). Both these changes are a direct consequence of the fact that the second mode is the dominant one, as opposed to the first mode in the case of classical panel flutter. It is believed that this happens because of the interaction between flutter and buckling in the presence of a uniformly distributed longitudinal load. Finally, it must be mentioned that the limit-cycle peak amplitudes are slightly asymmetric due to the unsteady longitudinal load.

Some key findings about the effects of the several parameters considered are as follows:

- Temperature ratio $\Theta = T_p/T_\infty$: this is the ratio of panel temperature to that of the freestream flow. The larger Θ, the larger are the aerodynamic pressures. Accordingly, the linear flutter parameter decreases with increasing Θ, all other parameters being fixed. Their relationship may be quite nonlinear.

- "Momentum accommodation coefficient" α_m: this number gives the fraction of molecules which reflects specularly upon collision with the panel. A value of 0 implies that all collisions contribute to aerodynamic shear, with the molecules being reemitted in random or "diffuse" fashion according to the temperature of the panel. Calculations show that the variation of the linear flutter parameter with α_m is close to linear if the temperature ratio is sufficiently large. In the case of the nominal configuration specified in Section 4.1, this comes about values larger than $\Theta = 3.5$.

- Mach number M_∞: the linear flutter parameter decreases monotonically with decreasing Mach number. This is contrary to the case of continuum flow if linear piston theory is used, where increasing the Mach number leads to smaller values of the linear flutter parameter.

- Spring support parameters α_{k_i}: in this analysis it is assumed that the panel is supported at leading and trailing edges by springs oriented longitudinally, with spring constants k_1 and k_2 respectively. In classical panel flutter, such

springs would affect only the supercritical limit-cycle amplitude. However, their presence also changes the linear flutter parameter in free-molecule flow because of the influence of distributed longitudinal loads representing the aerodynamic shear. The panel is strongly stabilized if only the spring at the trailing edge is considered, the effect being the opposite if only the leading edge spring constant is varied. However, the rate of decrease of the linear flutter parameter is not as large as the rate of increase in the former case.

- Applied compression parameter R_x: this quantity relates the compressive end-load to its value that gives rise to classical column buckling. It has been found that the relationship between the flutter boundary and the buckling boundary does not change much from that which is typical of continuum panel flutter. Naturally, numerical values are different from case to case.

- Pressure differential parameter P_z: this corresponds to a uniform static pressure difference between the panel's sides. An upward pressure (i.e., excess pressure in the interior) is associated with $P_z > 0$. Regardless of the direction of the force, there is an increase in the linear flutter parameter with P_z. The new feature of the free-molecule case is that the stability-boundary location is no longer symmetrical about the line $P_z = 0$, with an upward pressure causing a somewhat lower change than a downward pressure.

- Initial curvature: the amount of curvature is specified by the ratio between the panel's maximum initial height and its thickness, H/h. Both a sinusoidal and a constant (parabolic) curvature panel were considered. For small values of H/h the flutter solutions for the two different cases are very similar. However, for larger values of H/h the linear flutter parameter for the two kinds of curvature can be significantly different. This effect is already noticeable for a value of $H/h = 1$ in the cases that were studied in Chapter 4. The parabolic panel leads to smaller values of the linear flutter parameter, and so this kind of initial shape should be used in a design process if one would prefer to be on the conservative side. This last remark is made in view of the fact that the two shapes are not markedly different, with a maximum difference in their

ordinates of about 10% relative to H. Accordingly, for a very shallow curved panel (small ratio between the panel's thickness and length) it may be unrealistic to try to distinguish between one and the other due to manufacturing restrictions.

There is a substantial effect of the temperature ratio on the location of the stability boundaries for parametric studies related to the parameters α_{k_r}, R_x, and P_z. Different locations can, however, be "collapsed" onto one another by using as ordinate an appropriately normalized dynamic pressure parameter, given by equation (87). This works better for higher values of the temperature ratio. In most cases the linear flutter parameter obtained using this normalized definition decreases with increasing Θ. This implies that conservative results (smaller values) can be obtained using as an estimate the linear flutter (normalized) parameter corresponding to the highest temperature ratio to be considered, and then transforming it for each specific case of Θ.

Finally, a brief investigation was conducted on the feasibility of using a particle simulation method to obtain the aerodynamic loads. This resulted in the conclusion that such calculations can only become possible with a two orders of magnitude increase above the present speeds of supercomputers. Such a study would constitute a natural extension of the foregoing work, filling the gap between continuum and free-molecule flow. It is, therefore, recommended to a future generation of aeroelasticians.

Appendix A

GALERKIN INTEGRALS AND COEFFICIENTS

A.1 Sine and Cosine Integrals

Some of the necessary integrals in the evaluation of the Galerkin coefficients are:

1. $$I_0 = \int_0^1 \sin n\pi\xi \, \cos m\pi\xi \, dx = \begin{cases} 0 & ; \quad n = m \\ \dfrac{1}{\pi} \dfrac{n}{n^2 - m^2} \left[1 - (-1)^{m+n}\right] & ; \quad n \neq m \end{cases}$$

2. $$I_1 = \int_0^1 \xi \, \sin n\pi\xi \, \sin m\pi\xi \, dx = \begin{cases} \dfrac{1}{4} & ; \quad n = m \\ -\dfrac{2}{\pi^2} \dfrac{mn}{(n^2 - m^2)^2} \left[1 - (-1)^{m+n}\right] & ; \quad n \neq m \end{cases}$$

3. $$I_1^* = \int_0^1 \xi \, \sin n\pi\xi \, \cos m\pi\xi \, dx = \begin{cases} -\dfrac{1}{4\,n\,\pi} & ; \quad n = m \\ -\dfrac{1}{\pi} \dfrac{n}{n^2 - m^2} (-1)^{m+n} & ; \quad n \neq m \end{cases}$$

4. $$I_2 = \int_0^1 \xi^2 \sin n\pi\xi \sin m\pi\xi \, d\xi = \begin{cases} \dfrac{1}{6} - \dfrac{1}{4(n\pi)^2} & ; \quad n = m \\ \dfrac{4}{\pi^2} \dfrac{mn}{(n^2 - m^2)^2} (-1)^{m+n} & ; \quad n \neq m \end{cases}$$

5. $$I_3 = \int_0^1 \sin n\pi\xi \sin m\pi\xi \sin r\pi\xi \, d\xi =$$

$$= -\frac{2}{\pi} \frac{mnr}{(m^2 + n^2 - r^2)^2 - 4m^2n^2} \left[1 - (-1)^{m+n+r}\right]$$

6. $$I_4 = \int_0^1 \sin n\pi\xi \sin m\pi\xi \cos r\pi\xi \, d\xi =$$

$$= \frac{1}{4} \left(\delta_{n,\,m+r} + \frac{|m - r|}{m - r} \delta_{n,\,|m-r|} \right) =$$

$$= \frac{1}{4} \left(\delta_{m,\,n+r} + \frac{|n - r|}{n - r} \delta_{m,\,|n-r|} \right) =$$

$$= \frac{1}{4} \left(\delta_{r,\,|n-m|} - \delta_{r,\,n+m} \right)$$

where $$\delta_{mn} = \begin{cases} 1 & ; \quad n = m \\ 0 & ; \quad n \neq m \end{cases}$$

7. $$I_5 = \int_0^1 \sin n\pi\xi \cos m\pi\xi \cos r\pi\xi \, d\xi =$$

$$= \frac{n}{\pi} \frac{n^2 - m^2 - r^2}{(m^2 + n^2 - r^2)^2 - 4m^2n^2} \left[1 - (-1)^{m+n+r}\right]$$

A.2 Galerkin Coefficients

Assuming that the parameter p specifies the kind of initial deformation, with $p = 0$ corresponding to the constant curvature case, and $p > 0$ to the pth sine curve, the coefficients specified in equation (43) are given by

1. $$a_n = \left[(n\pi)^2 + \frac{1}{2}\left(1 - 2\frac{\alpha_k}{\alpha_{k_1}} + \alpha_k\right) P_x + R_x + \frac{\mathcal{A}_3}{2} + a_{np}\right] \frac{(n\pi)^2}{2} \quad ,$$

where

$$a_{np} = \begin{cases} \alpha_k \mathcal{A}_3 \dfrac{H}{h} \dfrac{1-(-1)^p}{p\pi} & ; \quad p > 0 \\ \dfrac{2}{3} \mathcal{A}_3 \dfrac{H}{h} \left[\alpha_k - 1 - \dfrac{3}{(n\pi)^2}\right] & ; \quad p = 0 \end{cases}$$

2. $$a^*_{nr} = 3\,\alpha_k (1-\nu^2)(r\pi)^2 \frac{(n\pi)^2}{2} \quad .$$

3. $$a^{**}_{nr} = \alpha_k \left(\mathcal{A}_3 \frac{1-(-1)^r}{r\pi} + a^{**}_{npr}\right) \frac{(n\pi)^2}{2} \quad ,$$

where

$$a^{**}_{npr} = \begin{cases} 6\dfrac{H}{h}(1-\nu^2)(r\pi)^2 \delta_{rp} & ; \quad p > 0 \\ 96\dfrac{H}{h}(1-\nu^2)\dfrac{1-(-1)^r}{r\pi} & ; \quad p = 0 \end{cases}$$

4. $$a^{***}_{nr} = -\mathcal{A}_4 \left[(1-\alpha_k) \frac{(-1)^r}{r\pi} - \alpha_k \frac{\alpha_{k_1}-1}{\alpha_{k_1}} \frac{1-(-1)^r}{r\pi} \right] \frac{(n\pi)^2}{2} \quad .$$

5. $$b_{nm} = \left(\frac{n^2+m^2}{n^2-m^2} P_x - \mathcal{A}_1 \right) \frac{mn}{n^2-m^2} \left[1-(-1)^{m+n} \right] + b_{nmp} \quad ,$$

where

$$b_{nmp} = \begin{cases} \dfrac{H}{h} \left\{ \alpha_k \mathcal{A}_3 \dfrac{1-(-1)^m}{m\pi} \dfrac{(n\pi)^2}{2} \delta_{np} + \right. \\ \qquad + 3\,\alpha_k \dfrac{H}{h} (1-\nu^2) (m\pi)^2 \delta_{mp} (n\pi)^2 \delta_{np} + \\ \qquad \left. + 2\,\mathcal{A}_3 \pi n^2 \dfrac{mnp}{(m^2+n^2-p^2)^2 - 4m^2n^2} \left[1-(-1)^{m+n+p} \right] \right\} & ; \quad p > 0 \\ 8 \dfrac{H}{h} \left\{ \mathcal{A}_3 n^2 \dfrac{m\,n}{(n^2-m^2)^2} \left[1+(-1)^{m+n} \right] \left[1-\delta_{mn} \right] + \right. \\ \qquad \left. + \alpha_k \left[\mathcal{A}_3 + 96 \dfrac{H}{h} (1-\nu^2) \right] \dfrac{1-(-1)^m}{m\pi} \dfrac{1-(-1)^n}{n\pi} \right\} & ; \quad p = 0 \end{cases}$$

6. $$b^{*}_{nmr} = \pi \mathcal{A}_3 mnr \frac{n^2+m^2-r^2}{(m^2-n^2+r^2)^2 - 4m^2r^2} \left[1-(-1)^{m+n+r} \right] \quad .$$

7. $$b^{**}_{nm} = 3\,\alpha_k \frac{H}{h} (1-\nu^2) (m\pi)^2 b^{**}_{nmp} \quad ,$$

where

$$b^{**}_{nmp} = \begin{cases} \dfrac{(n\pi)^2}{2} \delta_{np} & ; \quad p > 0 \\ 8 \dfrac{1-(-1)^n}{n\pi} & ; \quad p = 0 \end{cases}$$

8. $$c_n = -\frac{\mathcal{A}_2}{2} + \pi^2 \zeta_1 \ .$$

9. $$c_{nm} = \left(-\frac{\mathcal{A}_4}{2}\right) \frac{mn}{n^2 - m^2} \left[1 - (-1)^{m+n}\right] + \mathcal{A}_4 \frac{H}{h} c_{nmp} +$$

$$- \mathcal{A}_4 \frac{H}{h} \left[(1 - \alpha_k) \frac{(-1)^m}{m\pi} - \alpha_k \frac{\alpha_{k_1} - 1}{\alpha_{k_1}} \frac{1 - (-1)^m}{m\pi}\right] c^*_{np} \ ,$$

where

$$c_{nmp} = \begin{cases} \frac{\pi}{4} \frac{p}{m} \left[(p - m)\, \delta_{p,\, n+m} + \left(p \frac{|\, n - m\,|}{n - m} + m\right) \delta_{p,\, |n-m|}\right] & ; \quad p > 0 \\ 8\, m\, n \frac{n^2 + m^2}{(n^2 - m^2)^2} \frac{1 - (-1)^{m+n}}{(m\,\pi)^2} & ; \quad p = 0 \end{cases}$$

$$c^*_{np} = \begin{cases} \frac{(n\pi)^2}{2} \delta_{np} & ; \quad p > 0 \\ 8 \frac{1 - (-1)^n}{n\pi} & ; \quad p = 0 \end{cases}$$

10. $$c^*_{nmr} = \frac{\pi}{4} \mathcal{A}_4 \frac{m}{r} \left[(m + r)\, \delta_{n,\, m+r} + |\, m - r\,|\, \delta_{n,\, |m-r|}\right] \ .$$

11. $d_n = P_z \dfrac{1-(-1)^n}{n\pi} - \dfrac{H}{h} d_{np}$,

where

$$
d_{np} = \begin{cases}
\pi \mathcal{A}_3 \dfrac{H}{h} \dfrac{np^2}{n^2-4p^2} \left[1-(-1)^n\right] + \\
\quad + \left(\dfrac{n^2+p^2}{n^2-p^2} P_x - \mathcal{A}_1\right) \dfrac{np}{n^2-p^2} \left[1-(-1)^{n+p}\right] + \\
\quad + \left\{\dfrac{1}{2}\left(1 - 2\dfrac{\alpha_k}{\alpha_{k_1}} + \alpha_k\right) P_x + \right. \\
\qquad \left. + R_x + \mathcal{A}_3 \left[\alpha_k \dfrac{H}{h} \dfrac{1-(-1)^p}{p\pi} + \dfrac{1}{2}\right]\right\} \dfrac{(n\pi)^2}{2} \delta_{np} \qquad ; \quad p > 0 \\
4(P_x - \mathcal{A}_1) \dfrac{1+(-1)^n}{n\pi} + \dfrac{8}{n\pi} P_x + \\
\quad + 4 \left\{\left(\alpha_k - 2\dfrac{\alpha_k}{\alpha_{k_1}}\right) P_x + 2R_x + \mathcal{A}_3 + \right. \\
\qquad \left. + 4\,\mathcal{A}_3 \dfrac{H}{h} \left[\dfrac{\alpha_k}{3} + 1 - \dfrac{12}{(n\pi)^2}\right]\right\} \dfrac{1-(-1)^n}{n\pi} \qquad ; \quad p = 0
\end{cases}
$$

Appendix B

LONGITUDINAL SPRINGS EFFECTS

The influence of the longitudinal springs on the linear flutter parameter is given by the term multiplying P_x on the expression for a_n in Appendix A, which is

$$\mathcal{F} = \left(1 - 2\frac{\alpha_k}{\alpha_{k_1}} + \alpha_k\right) \quad .$$

Assume $\alpha_{k_1}/\alpha_{k_2} = \mathcal{C}$. Then α_k can be rewritten as

$$\alpha_k = \frac{\alpha_{k_1}}{\mathcal{C} + 1 - \alpha_{k_1}} = \tag{90}$$

$$= \frac{\alpha_{k_2}}{\mathcal{C}^* + 1 - \alpha_{k_2}} , \tag{91}$$

where $\mathcal{C}^* = 1/\mathcal{C}$. $\mathcal{F}$ can then be expressed in terms of α_{k_1} or α_{k_2} alone:

$$\mathcal{F} = \frac{\mathcal{C} - 1}{\mathcal{C} + 1 - \alpha_{k_1}} = \tag{92}$$

$$= \frac{1 - \mathcal{C}^*}{\mathcal{C}^* + 1 - \alpha_{k_2}} \tag{93}$$

First thing to note is how $\mathcal{F}$ and α_k vary when the value of $\mathcal{C}$ changes. Then

1. $\mathcal{C} > 1 \Rightarrow \alpha_{k_1} > \alpha_{k_2}$. Then: $0 < \mathcal{F} < 1$ and $\alpha_k < \alpha_{k_1}$.

2. $\mathcal{C} < 1 \Rightarrow \alpha_{k_2} > \alpha_{k_1}$. Then: $-1 < \mathcal{F} < 0$ and $\alpha_k < \alpha_{k_2}$.

Secondly, the value of λ_{cr} for an arbitrary combination α_{k_1}, α_{k_2} can be found by considering one of the limiting cases $\overline{\alpha}_{k_1} = 1, \overline{\alpha}_{k_2} < 1$ or $\overline{\alpha}_{k_2} = 1, \overline{\alpha}_{k_1} < 1$, depending whether $\alpha_{k_1} > \alpha_{k_2}$ or not. Here $(\bar{\cdot})$ indicates an equivalent problem with different values for α_{k_i}.

1. $\alpha_{k_1} > \alpha_{k_2} \Rightarrow \overline{\alpha}_{k_1} = 1$, $\overline{\alpha}_{k_2} = 1/\overline{\mathcal{C}}$

   The value of $\overline{\mathcal{C}}$ can be found by equating $\mathcal{F}$ and $\overline{\mathcal{F}}$, that is,

$$\frac{\mathcal{C} - 1}{\mathcal{C} + 1 - \alpha_{k_1}} = \frac{\overline{\mathcal{C}} - 1}{\overline{\mathcal{C}}} \quad .$$

   Then

$$\overline{\alpha}_{k_2} = -\frac{\alpha_{k_1} - 2}{\mathcal{C} + 1 - \alpha_{k_1}} \quad . \tag{94}$$

   It can also be shown that $\alpha_k < \overline{\alpha}_k$, which implies that the limit-cycle amplitude for the pair α_{k_1}, α_{k_2} is larger than the one corresponding to $\overline{\alpha}_{k_1}$, $\overline{\alpha}_{k_2}$ if λ is held constant.

2. $\alpha_{k_1} < \alpha_{k_2} \Rightarrow \overline{\alpha}_{k_2} = 1$, $\overline{\alpha}_{k_1} = 1/\overline{\mathcal{C}}^*$

   The value of $\overline{\alpha}_{k_1}$ can be found as in the previous case, except that now $\mathcal{F}$ and $\overline{\mathcal{F}}$ should be written in terms of α_{k_2}. Then

$$\overline{\alpha}_{k_1} = -\frac{\alpha_{k_2} - 2}{\mathcal{C}^* + 1 - \alpha_{k_2}} \quad . \tag{95}$$

   Again it can be shown that the limit cycle amplitude for the pair α_{k_1}, α_{k_2} is larger than the one corresponding to $\overline{\alpha}_{k_1}$, $\overline{\alpha}_{k_2}$ if λ is held constant.

BIBLIOGRAPHY

[1] Dowell, E.H. - *Aeroelasticity of Plates and Shells*, Noordhoff International Publishing, Leyden, The Netherlands, 1975.

[2] Reed, W.H., III, Hanson, P.W., and Alford, W.J., Jr. - "Assessment of Flutter Model Testing Relating to the National Aero-Space Plane", NASA Langley Research Center, NASP CR 1002, Hampton, VA, July, 1987.

[3] Fung, Y.C. - "A Summary of the Theories and Experiments on Panel Flutter", *AGARD — Manual on Aeroelasticity*, Part III, Chapter 7, Feb., 1961.

[4] Bisplinghoff, R.L. and Ashley, H. - *Principles of Aeroelasticity*, Dover Publications, Inc., New York, Chapter 8, 1962.

[5] Bolotin, V.V. - *Nonconservative Problems of the Theory of Elastic Stability*, MacMillan Company, New York, Chapter 4, 1963.

[6] Bohon, H.L. and Dixon, S.C. - "Some Recent Developments in Flutter of Flat Panels", *Journal of Aircraft*, Vol. 1, Sept.-Oct., 1964, pp. 280-288.

[7] Johns, D.J. - "A Panel Flutter Review", *AGARD — Manual of Aeroelasticity*, Part III, Chapter 7, Supplement, May, 1969.

[8] Dowell, E.H. - "Panel Flutter: A Review of the Aeroelastic Stability of Plates and Shells", *AIAA Journal*, Vol. 8, March, 1970, pp. 385-399.

[9] Dowell, E.H. - "Panel Flutter, NASA Space Vehicle Design Criteria", *NASA SP-8004*, June, 1972.

[10] Jordan, P.F. - "The Physical Nature of Panel Flutter", *Aero Digest*, Vol. 72, Feb., 1956, pp. 34-38.

[11] Gislason, T., Jr. - "Experimental Investigation of Panel Divergence at Subsonic Speeds", *AIAA Journal*, Vol. 9, Nov., 1971, pp. 2252-2258.

[12] Dugundji, J., Dowell, E.H., and Perkin, B. - "Subsonic Flutter of Panels on Continuous Elastic Foundations", *AIAA Journal*, Vol. 1, May, 1963, pp. 1146-1154.

[13] Dowell, E.H. and Voss, H.M. - "Theoretical and Experimental Panel Flutter Studies in the Mach Number Range 1.0 to 5.0", *AIAA Journal*, Vol. 3, Dec., 1965, pp. 2292-2304.

[14] Olson, M.D. and Fung, Y.C. - "Supersonic Flutter of Circular Cylindrical Shells Subjected to Internal Pressure and Axial Compression", *AIAA Journal*, Vol. 4, May, 1966, pp. 858-864.

[15] Shideler, J.L., Dixon, S.C., and Shore, C.P. - "Flutter at Mach 3 Thermally Stressed Panels and Comparison with Theory for Panels with Edge Rotational Restraint", *NASA TN D-3498*, Aug., 1966.

[16] Muhlstein, L., Jr., Gaspers, P.A., Jr., and Riddle, D.W. - "An Experimental Study of the Influence of the Turbulent Boundary Layer on Panel Flutter", *NASA TN D-4486*, March, 1968.

[17] Hess, R.W. - "Experimental and Analytical Investigation of the Flutter of Flat Build-up Panels under Streamwise In-Plane Load", *NASA TR R-330*, Feb., 1970.

[18] Gaspers, P.A., Jr., Muhlstein, L., Jr., and Petroff, D.N. - "Further Experimental Results on the Influence of the Turbulent Boundary Layer on Panel Flutter", *NASA TN D-5798*, May, 1970.

[19] Kappus, H.P., Lemley, C.E., and Zimmerman, N.H. - "An Experimental Investigation of High Amplitude Panel Flutter", *NASA CR-1837*, May, 1971.

[20] Dowell, E.H. - "Fatigue Life Estimation of Fluttering Panels", *AIAA Journal*, Vol. 8, Oct., 1970, pp. 1879-1881.

[21] Xue, D.Y. and Mei, C. - "Finite Element Nonlinear Flutter and Fatigue Life of 2-D Panels with Temperature Effects", *Proceedings of the AIAA/ASME/-ASCE/AHS/ASC 32nd Structures, Structural Dynamics, and Materials Conference*, Baltimore, MD, April, 1991, pp. 1981-1991.

[22] Hedgepeth, J.M. - "On the Flutter of Panels at High Mach Numbers", *Journal of the Aeronautical Sciences*, Vol. 23, June, 1956, pp. 609-610.

[23] Hedgepeth, J.M. - "Flutter of Rectangular Simply Supported Panels at High Supersonic Speeds", *Journal of the Aeronautical Sciences*, Vol. 24, Aug., 1957, pp. 563-573,586.

[24] Erickson, L.L. and Anderson, M.S. - "Supersonic Flutter of Simply Supported Isotropic Sandwich Panels", *NASA TN D-3171*, April, 1966.

[25] Marafioti, F.A. and Johnston, E.R., Jr. - "Effects of Rotary Inertia on the Supersonic Flutter of Sandwich Panels", *AIAA Journal*, Vol. 9, Feb., 1971, pp. 245-249. See also Erickson, L.L. "Comments on 'Effects of Rotary Inertia on the Supersonic Flutter of Sandwich Panels' ", *AIAA Journal*, Vol. 9, Oct., 1971, pp. 2110-2112.

[26] Erickson, L.L. - "Supersonic Flutter of Sandwich Panels: Effects of Face Sheet Bending Stiffness, Rotary Inertia, and Orthotropic Core Shear Stiffnesses", *NASA TN D-6427*, July, 1971.

[27] Meirovitch, L. - *Dynamics and Control of Structures*, John Wiley & Sons, New York, 1990, pp. 298-300.

[28] Ellen, C.H. - "Approximate Solutions of the Membrane Flutter Problem", *AIAA Journal*, Vol. 3, June, 1965, pp. 1186-1187.

[29] Dowell, E.H. and Voss, H.M. - "The Effect of a Cavity on Panel Vibration", *AIAA Journal*, Vol. 1, Feb., 1963, pp. 476-477.

[30] Eisley, J.G. and Luessen, G. - "Flutter of Thin Plates under Combined Shear and Normal Edge Forces", *AIAA Journal*, Vol. 1, March, 1963, pp. 620-626.

[31] Kobayashi, S. - "Supersonic Panel Flutter of Unstiffened Circular Cylindrical Shells Having Simply Supported Ends", *Transactions of the Japan Society for Aeronautical and Space Sciences*, Vol. 6, 1963, pp. 27-35.

[32] Voss, H.M. and Dowell, E.H. - "Effect of Aerodynamic Damping on Flutter of Thin Panels", *AIAA Journal*, Vol. 2, Jan., 1964, pp. 119-120.

[33] McElman, J.A. - "Flutter of Two Parallel Flat Plates Connected by an Elastic Medium", *AIAA Journal*, Vol. 2, Feb., 1964, pp. 377-379.

[34] Kornecki, A. - "A Note on the Supersonic Panel Flutter of Oblique Clamped Plates", *Journal of the Royal Aeronautical Society*, Vol. 68, April, 1964, pp. 270-271.

[35] Bohon, H.L. and Anderson, M.S. - "Role of Boundary Conditions on Flutter of Orthotropic Panels", *AIAA Journal*, Vol. 4, July, 1966, pp. 1241-1248.

[36] Dugundji, J. - "Theoretical Considerations of Panel Flutter at High Supersonic Mach Numbers", *AIAA Journal*, Vol. 4, July, 1966, pp. 1257-1266. See also Dugundji, J. - "Errata and Addenda: 'Theoretical Considerations of Panel Flutter at High Supersonic Mach Numbers' ", *AIAA Journal*, Vol. 7, Aug., 1969, pp. 1663-1664.

[37] Durvasula, S. - "Flutter of Simply Supported, Parallelogrammic, Flat Panels in Supersonic Flow", *AIAA Journal*, Vol. 5, Sept., 1967, pp. 1668-1673.

[38] Olson, M.D. and Fung, Y.C. - "Comparing Theory and Experiment for the Supersonic Flutter of Circular Cylindrical Shells", *AIAA Journal*, Vol. 5, Oct., 1967, pp. 1849-1856.

[39] Dixon, S.C. and Hudson, M.L. - "Flutter Boundary for Simply Supported Unstiffened Cylinders", *AIAA Journal*, Vol. 7, July, 1969, pp. 1390-1391.

[40] Kamal,K. and Durvasula, S. - "Flutter of Laminated Composite Skew Panels in Supersonic Flow", *Developments in Mechanics - Proceedings of the 19th Midwestern Mechanics Conference*, Vol. 13, 1985, pp. 440-441.

[41] Dowell, E.H. - "Flutter of Infinitely Long Plates and Shells. Part I: Plate", *AIAA Journal*, Vol. 4, Aug., 1966, pp. 1370-1377.

[42] Dowell, E.H. - "Flutter of Infinitely Long Plates and Shells. Part II: Cylindrical Shell", *AIAA Journal*, Vol. 4, Sept., 1966, pp. 1510-1518.

[43] Kobayashi, S. - "Two-Dimensional Panel Flutter. I. Simply Supported Panel", *Transactions of the Japan Society for Aeronautical and Space Sciences*, Vol. 5, 1962, pp. 90-102.

[44] Kobayashi, S. - "Two-Dimensional Panel Flutter. II. Clamped Panel", *Transactions of the Japan Society for Aeronautical and Space Sciences*, Vol. 5, 1962, pp. 103-118.

[45] Eastep, F.E. and McIntosh, S.C., Jr. - "Analysis of Nonlinear Panel Flutter and Response Under Random Excitation or Nonlinear Aerodynamic Loading", *AIAA Journal*, Vol. 9, March, 1971, pp. 411-418.

[46] Kuo, C.-C., Morino, L., and Dugundji, J. - "Perturbation and Harmonic Balance Methods for Nonlinear Panel Flutter", *AIAA Journal*, Vol. 10, Nov., 1972, pp. 1479-1484.

[47] Yuen, S.W. and Lau, S.L. - "Effects of In-Plane Load on Nonlinear Panel Flutter by Incremental Harmonic Balance Method", *AIAA Journal*, Vol. 29, Sept., 1991, pp. 1472-1479.

[48] Morino, L. - "A Perturbation Method for Treating Nonlinear Panel Flutter Problems", *AIAA Journal*, Vol. 7, March, 1969, pp. 405-411.

[49] Dowell, E.H. - "Nonlinear Oscillations of a Fluttering Plate", *AIAA Journal*, Vol. 4, July, 1966, pp. 1267-1275.

[50] Dowell, E.H. - "Nonlinear Oscillations of a Fluttering Plate. II", *AIAA Journal*, Vol. 5, Oct., 1967, pp. 1856-1862.

[51] Dowell, E.H. - "Theoretical-Experimental Correlation of Plate Flutter Boundaries at Low Supersonic Speeds", *AIAA Journal*, Vol. 6, Sept., 1968, pp. 1810-1811.

[52] Dowell, E.H. - "Nonlinear Flutter of Curved Plates", *AIAA Journal*, Vol. 7, March, 1969, pp. 424-431.

[53] Dowell, E.H. - "Nonlinear Flutter of Curved Plates. II", *AIAA Journal*, Vol. 8, Feb., 1970, pp. 259-261.

[54] Dowell, E.H. - "Flutter of Buckled Plates at Zero Dynamic Pressure", *AIAA Journal*, Vol. 8, March, 1970, pp. 583-584.

[55] Ventres, C.S. and Dowell, E.H. - "Comparison of Theory and Experiment for Nonlinear Flutter of Loaded Plates", *AIAA Journal*, Vol. 8, Nov., 1970, pp. 2022-2030.

[56] Ventres, C.S. - "Flutter of a Buckled Plate Exposed to a Static Pressure Differential", *AIAA Journal*, Vol. 9, May, 1971, pp. 958-960.

[57] McIntosh, S.C., Jr. - "Effect of Hypersonic Nonlinear Aerodynamic Loading on Panel Flutter", *AIAA Journal*, Vol. 11, Jan., 1973, pp. 29-32.

[58] Dowell, E.H. - "Aerodynamic Boundary Layer Effects on Flutter and Damping of Plates", *Journal of Aircraft*, Vol. 10, Dec., 1973, pp. 734-738.

[59] Dowell, E.H. and Ilgamov, M. - *Studies in Nonlinear Aeroelasticity*, Springer-Verlag, New York, Chapter V, 1988.

[60] Sipcic, S.R. and Morino, L. - "Dynamic Behavior of Fluttering Two-Dimensional Panels on an Airplane in Pull-Up Maneuver", *AIAA Journal*, Vol. 29, Aug., 1991, pp. 1304-1312.

[61] Weiliang, Y. and Dowell, E.H. - "Limit Cycle Oscillation of a Fluttering Cantilever Plate", *AIAA Journal*, Vol. 29, Nov., 1991, pp. 1929-1936.

[62] Przemieniecki, J.S. - *Theory of Matrix Structural Analysis*, Dover Publications, Inc., New York, 1985.

[63] Olson, M.D. - "Finite Elements Applied to Panel Flutter", *AIAA Journal*, Vol. 5, Dec., 1967, pp. 2267-2270.

[64] Sarma, B.S. and Varadan, T.K. - "Certain Discussions in the Finite Element Formulation of Nonlinear Vibration Analysis", *Computers and Structures*, Vol. 15, Nov.-Dec., 1982, pp. 643-646.

[65] Kariappa and Somashekar, B.R. - "Application of Matrix Displacement Methods in the Study of Panel Flutter", *AIAA Journal*, Vol. 7, Jan., 1969, pp. 50-53.

[66] Olson, M.D. - "Some Flutter Solutions Using Finite Elements", *AIAA Journal*, Vol. 8, April, 1970, pp. 747-752.

[67] Kariappa, V. and Somashekar, B.R. - "Flutter of Skew Panels by the Matrix Displacement Approach", *Journal of the Royal Aeronautical Society*, Vol. 74, Aug., 1970, pp. 672-675.

[68] Kariappa, Somashekar, B.R., and Shah, C.G. - "Discrete Element Approach to Flutter of Skew Panels with In-Plane Forces under Yawed Supersonic Flow", *AIAA Journal*, Vol. 8, Nov., 1970, pp. 2017-2022.

[69] Sander, G., Bon, C., and Geradin, M. - "Finite Element Analysis of Supersonic Panel Flutter", *International Journal for Numerical Methods in Engineering*, Vol. 7, 1973, pp. 379-394.

[70] Bismarck-Nasr, M.N. - "Finite Element Method Applied to the Supersonic Flutter of Circular Cylindrical Shells", *International Journal for Numerical Methods in Engineering*, Vol. 10, 1976, pp. 423-435.

[71] Bismarck-Nasr, M.N. - "Finite Element Method Applied to the Flutter of Two Parallel Elastically Coupled Flat Plates", *International Journal for Numerical Methods in Engineering*, Vol. 11, 1977, pp. 1188-1193.

[72] Srinivasan, R.S. and Babu, B.J.C. - "Free Vibration and Flutter of Laminated Quadrilateral Plates", *Computers and Structures*, Vol. 27, 1987, pp. 297-304.

[73] Lee, I. and Cho, M.-H. - "Flutter Analysis of Composite Panels in Supersonic Flow", *Proceedings of the AIAA/ASME/ASCE/AHS/ASC 31st Structures, Structural Dynamics, and Materials Conference*, Long Beach, CA, April, 1990, pp. 1540-1550.

[74] Argyris, J.H. - "Matrix Displacement Analysis of Plates and Shells", *Ingenieur Archiv*, Vol. 35, June, 1966, pp. 102-142.

[75] Mei, C. - "A Finite-Element Approach for Nonlinear Panel Flutter", *AIAA Journal*, Vol. 15, Aug., 1977, pp. 1107-1110. See also Prathap, G. - "Comment on 'A Finite-Element Approach for Nonlinear Panel Flutter' ", *AIAA Journal*, Vol.16, Aug., 1978, pp. 863-864.

[76] Rao, K.S. and Rao, G.V. - "Large Amplitude Supersonic Flutter of Panels with Ends Elastically Restrained Against Rotation", *Computers and Structures*, Vol. 11, March, 1980, pp. 197-201.

[77] Rao, K.S. and Rao, G.V. - "Nonlinear Supersonic Flutter of Panels Considering Shear Deformation and Rotary Inertia", *Computers and Structures*, Vol. 17, March, 1983, pp. 361-364.

[78] Han, A.D. and Yang, T.Y. - "Nonlinear Panel Flutter Using High-Order Triangular Finite Elements", *AIAA Journal*, Vol. 21, Oct., 1983, pp. 1453-1461.

[79] Rao, G.V. and Rao, K.S. - "Supersonic Flutter of Short Panels on an Elastic Foundation", *AIAA Journal*, Vol. 22, June, 1984, pp. 856-857.

[80] Sarma, B.S. and Varadan, T.K. - "Nonlinear Panel Flutter by Finite-Element Method", *AIAA Journal*, Vol. 26, May, 1988, pp. 566-574.

[81] Mei, C. and Gray, C.E. - "A Finite-Element Method for Large-Amplitude, Two-Dimensional Panel Flutter at Hypersonic Speeds", *Proceedings of the AIAA/ASME/ASCE/AHS/ASC 30th Structures, Structural Dynamics, and Materials Conference*, Mobile, AL, April, 1989, pp. 37-51.

[82] Xue, D.Y., Mei, C., and Shore, C.P. - "Finite-Element Two-Dimensional Panel Flutter at High Supersonic Speeds and Elevated Temperature", *Proceedings of the AIAA/ASME/ASCE/AHS/ASC 31th Structures, Structural Dynamics, and Materials Conference*, Long Beach, CA, April, 1990, pp. 1464-1475.

[83] Liaw, D.G. and Yang, H.T.Y. - "Nonlinear Supersonic Flutter and Reliability of Uncertain Laminated Plates", *Proceedings of the AIAA/ASME/ASCE/-AHS/ASC 32nd Structures, Structural Dynamics, and Materials Conference*, Baltimore, MD, April, 1991, pp. 1964-1970.

[84] Dixon, I.R. and Mei, C. - "Finite Element Analysis of Nonlinear Flutter of Composite Panels", *Proceedings of the AIAA/ASME/ASCE/AHS/ASC 32nd Structures, Structural Dynamics, and Materials Conference*, Baltimore, MD, April, 1991, pp. 2002-2010.

[85] Mei, C. and Rogers, J.L., Jr. - "NASTRAN Nonlinear Vibration Analysis of Beam and Frame Structures", *NASA TM X-3278*, Sept., 1975, pp. 259-284.

[86] Bergan, P.G. and Clough, R.W. - "Convergence Criteria for Iterative Processes", *AIAA Journal*, Vol. 10, Aug., 1972, pp. 1107-1108.

[87] Meirovitch, L. - *Elements of Vibration Analysis*, McGraw-Hill Book Company, New York, 1986, pp. 374-380.

[88] Parks, P.C. - "A Stability Criterion for Panel Flutter via the Second Method of Liapunov", *AIAA Journal*, Vol. 4, Jan., 1966, pp. 175-177.

[89] Webb, G.R. *et al.* - "Further Study on 'A Stability Criterion for Panel Flutter via the Second Method of Liapunov' ", *AIAA Journal*, Vol. 5, Nov., 1967, pp. 2084-2085.

[91] Chia, C.-Y. - *Nonlinear Analysis of Plates*, McGraw-Hill International Book Company, New York, Chapter 1, 1987.

[92] Ellen, C.H. - "Influence of Structural Damping on Panel Flutter", *AIAA Journal*, Vol. 6, Nov., 1968, pp. 2169-2174.

[93] Lottati, I. - "The Role of Damping on Supersonic Panel Flutter", *AIAA Journal*, Vol. 23, Oct., 1985, pp. 1640-1642. See also Flax, A.H. - "Comment on 'The Role of Damping on Supersonic Panel Flutter' ", *AIAA Journal*, Vol. 24, Nov., 1986, pp. 1886-1887.

[94] Edberg, D.L. - *Measurement of Material Damping in a Simulated Space Environment*, Ph.D. Thesis, Dept. of Aeronautics and Astronautical, Stanford University, Dec., 1984.

[95] Ashley, H. and Zartarian, G. - "Piston Theory — A New Aerodynamic Tool for the Aeroelastician", *Journal of the Aeronautical Sciences*, Vol. 23, Dec., 1956, pp. 1109-1118.

[96] Ashley, H. - "Applications of the Theory of Free Molecule Flow to Aeronautics", *Journal of the Aeronautical Sciences*, Vol. 16, Feb., 1949, pp. 95-104.

[97] Kennard, E.H. - *Kinetic Theory of Gases*, McGraw-Hill Book Company, Inc., New York, 1938.

[98] Vincenti, W.G. and Kruger, C.H., Jr. - *Introduction to Physical Gas Dynamics*, Robert E. Krieger Publishing Company, Malabar, Florida, 1986.

[99] Muntz, E.P. - "Rarefied Gas Dynamics", *Annual Review of Fluid Mechanics*, Vol. 21, 1989, pp. 387-417.

[100] Goodman, F.O. and Wachman, H.Y. - *Dynamics of Gas-Surface Scattering*, Academic Press, New York, 1976.

[101] Hurlbut, F.C. - "Gas/Surface Scattering Models for Satellite Applications", *Progress in Astronautics and Aeronautics*, Vol. 103, 1986, pp. 97-119.

[102] Hurlbut, F.C. - "Particle Surface Interaction in the Orbital Context: A Survey", *Progress in Astronautics and Aeronautics*, Vol. 116, 1989, pp. 419-450.

[103] Thomas, L.B., Krueger, C.L., and Loyalka, S.K. - "Studies of Thermal Accommodation and Conduction in the Transition Regime", *Progress in Astronautics and Aeronautics*, Vol. 116, 1989, pp. 502-516.

[104] Bird, G.A. - *Molecular Gas Dynamics*, Clarendon Press, Oxford, 1976.

[105] Hurlbut, F.C. and Sherman, F.S. - "Application of the Nocilla Wall Reflection Model to Free-Molecule Kinetic Theory", *The Physics of Fluids*, Vol. 11, March, 1968, pp. 486-496.

[106] Pandolfi, M. and Zavattaro, M.G. - "Upper Atmosphere Aerodynamics: Gas-Surface Interaction and Comparison with Wind-Tunnel Experiments", *Progress in Astronautics and Aeronautics*, Vol. 116, 1989, pp. 476-486.

[107] Shidlovskiy, V.P. - *Introduction to the Dynamics of Rarefied Gases*, American Elsevier Publishing Company, Inc., New York, Chapter 2, 1967.

[108] Cercignani, C. - *The Boltzmann Equation and Its Applications*, Springer-Verlag, New York, 1988.

[109] Bird, G.A. - "Monte Carlo Simulation of Gas Flows", *Annual Review of Fluid Mechanics*, Vol. 10, 1978, pp. 11-31.

[110] Bird, G.A. - "Low-Density Aerothermodynamics", *Progress in Astronautics and Aeronautics*, Vol. 103, 1986, pp. 3-24.

[111] Bird, G.A. - "Direct Simulation of Gas Flows at the Molecular Level", *Communications in Applied Numerical Methods*, Vol. 14, 1988, pp. 165-172.

[112] Baganoff, D. and McDonald, J.D. - "A Collision-Selection Rule for a Particle Simulation Method Suited to Vector Computers", *Physics of Fluid A*, Vol. 2, July, 1990, pp. 1248-1259.

[113] McDonald, J.D. - *A Computationally Efficient Particle Simulation Method Suited to Vector Computer Architectures*, Ph.D. Thesis, Dept. of Aeronautics and Astronautics, Stanford University, Dec., 1989.

[114] Dagum, L. - *On the Suitability of the Connection Machine for Direct Particle Simulation*, Ph.D. Thesis, Dept. of Aeronautics and Astronautics, Stanford University, June, 1990.

[115] Woronowicz, M.S. - *Application of a Vectorized Particle Simulation to the Study of Plates and Wedges in the High-Speed Rarefied Flow*, Ph.D. Thesis, Dept. of Aeronautics and Astronautics, Stanford University, June, 1991.

[116] Lumpkin, F.E., III, and Chapman, D.R. - "Accuracy of the Burnett Equations for Hypersonic Real Gas Flows", *AIAA Paper 91-0771*, Jan., 1991.

[117] Celenligil, M.C., Bird, G.A., and Moss, J.N. - "Direct Simulation of Three-Dimensional Hypersonic Flow About Intersecting Blunt Wedges", *AIAA Journal*, Vol. 27, Nov., 1989, pp. 1536-1542.

[118] Press, W.H. *et al* - *Numerical Recipes: The Art of Scientific Computing*, Cambridge University Press, Cambridge, Chapter 15, 1987.

[119] Anonymous - *U.S. Standard Atmosphere, 1976*, U.S. Government Printing Office, Washington, D.C., Oct., 1976.

[120] Williams, R.M. - "National Aero-Space Plane: Technology for America's Future", *Aerospace America*, Vol. 24, Nov., 1986, pp. 18-22.

[121] Shih, P.K. *et al.* - "Structures for Hypervelocity Flight", *Aerospace America*, Vol. 27, May, 1989, pp. 28-31.

[122] Anderson, J.D., Jr. - *Hypersonic and High Temperature Gas Dynamics*, Part II, McGraw-Hill Book Company, New York, 1989.

*U.S. GOVERNMENT PRINTING OFFICE: 1993-728-150/60039

REPORT DOCUMENTATION PAGE

Form Approved
OMB No. 0704-0188

1. AGENCY USE ONLY (*Leave blank*)	2. REPORT DATE	3. REPORT TYPE AND DATES COVERED
	May 1993	Contractor Report

4. TITLE AND SUBTITLE
Hypersonic Panel Flutter in a Rarefied Atmosphere

5. FUNDING NUMBERS
G NGL-05-020-243
WU 505-63-50

6. AUTHOR(S)
Hugo B. Resende

7. PERFORMING ORGANIZATION NAME(S) AND ADDRESS(ES)
Stanford University
Department of Aeronautics and Astronautics
Stanford, California 94305

8. PERFORMING ORGANIZATION REPORT NUMBER
SUDAAR 614

9. SPONSORING / MONITORING AGENCY NAME(S) AND ADDRESS(ES)
National Aeronautics and Space Administration
Langley Research Center
Hampton, VA 23681-0001

10. SPONSORING / MONITORING AGENCY REPORT NUMBER
NASA CR-4514

11. SUPPLEMENTARY NOTES
Langley Technical Monitor: John W. Edwards

12a. DISTRIBUTION / AVAILABILITY STATEMENT
Unclassified-Unlimited
Subject Category 02

12b. DISTRIBUTION CODE

13. ABSTRACT (*Maximum 200 words*)

Panel flutter is a form of dynamic aeroelastic instability resulting from the interaction between motion of a aircraft structural panel and the aerodynamic loads exerted on that panel by air flowing past one of the faces. The present investigation studies panel flutter in an aerodynamic regime known as "free molecule flow", wherein intermolecular collisions can be neglected and loads are caused by interactions between individual molecules and the bounding surface. After collision with the panel, molecules may be reflected specularly or reemitted in diffuse fashion. Two parameters characterize this process: the "momentum accommodation coefficient", which is the fraction of the specularly reflected molecules; and the ratio between the panel temperature and that of the free airstream. This model is relevant to the case of hypersonic flight vehicles traveling at very high altitudes and especially for panels oriented parallel to the airstream or in the vehicle's lee. Several parametric studies are presented. They include the effects of 1) temperature ratio; 2) momentum accommodation coefficient; 3) spring parameters, which are associated with how the panel is connected to adjacent structures; 4) a parameter which relates compressive end load to its value which would cause classical column buckling; 5) a parameters proportional to the pressure differential between the front and back faces; and 6) initial curvature. The research is completed by an investigation into the possibility of accounting for molecular collisions, which proves to be infeasible given the speeds of current mainframe supercomputers.

14. SUBJECT TERMS
Flutter
Panel flutter
Nonlinear dynamics

15. NUMBER OF PAGES
116

16. PRICE CODE
A06

17. SECURITY CLASSIFICATION OF REPORT	18. SECURITY CLASSIFICATION OF THIS PAGE	19. SECURITY CLASSIFICATION OF ABSTRACT	20. LIMITATION OF ABSTRACT
Unclassified	Unclassified	Unclassified	

NSN 7540-01-280-5500

Standard Form 298 (Rev. 2-89)
Prescribed by ANSI Std. Z39-18
298-102

National Aeronautics and
Space Administration
Code JTT
Washington, D.C.
20546-0001
Official Business
Penalty for Private Use, $300

BULK RATE
POSTAGE & FEES PAID
NASA
Permit No. G-27

NASA

POSTMASTER: If Undeliverable (Section 158 Postal Manual) Do Not Return